Palaeogeography, Palaeoclimatology, Palaeoecology 580 (2021) 110527

Contents lists available at ScienceDirect

Palaeogeography, Palaeoclimatology, Palaeoecology

journal homepage: www.elsevier.com/locate/palaeo

Environmental conditions during the late Oligocene transgression in the North Alpine Foreland Basin (Eferding Formation, Egerian) – A multidisciplinary approach

Thomas Filek [a,*], Felix Hofmayer [b,h], Iris Feichtinger [c], Björn Berning [d], Jürgen Pollerspöck [e], Jennifer Zwicker [f], Daniel Smrzka [f], Jörn Peckmann [g], Matthias Kranner [c], Oleg Mandic [c], Bettina Reichenbacher [h], Andreas Kroh [c], Alfred Uchman [i], Reinhard Roetzel [b], Mathias Harzhauser [c]

[a] Department of Paleontology, University of Vienna, Althanstraße 14, 1090 Vienna, Austria
[b] Department of Sedimentology, Geologische Bundesanstalt, Neulinggasse 38, 1030 Vienna, Austria
[c] Geological-Palaeontological Department, Natural History Museum Vienna, Burgring 7, 1010 Vienna, Austria
[d] Geoscience Collections, Oberösterreichische Landes-Kultur GmbH, Welser Str. 20, 4060 Leonding, Austria
[e] Bavarian State Collection of Zoology, Münchhausenstraße 21, 81247 Munich, Germany
[f] Department of Geology & Palaeontology, University of Vienna, Althanstraße 14, 1090 Vienna, Austria
[g] Institute for Geology, Center for Earth System Research and Sustainability, University Hamburg, Bundesstraße 55, 20146 Hamburg, Germany
[h] Department of Earth and Environmental Sciences, Ludwig-Maximilians-University, Richard-Wagner-Str. 10, 80333 Munich, Germany
[i] Institute of Geological Sciences, Faculty of Geography and Geology, Jagiellonian University, Gronostajowa 3a, 30-387 Kraków, Poland

ARTICLE INFO

Editor: A Dickson

Keywords:
Central Paratethys
Palaeoecology
Palaeogeography
Palaeoclimatology
Eutrophication
Stratigraphy

ABSTRACT

The North Alpine Foreland Basin (NAFB) comprises one of the most complete sedimentary records of the Oligocene and Miocene, driven by global sea-level fluctuations, vast sedimentary influx and tectonic movement. The locality of Unterrudling near Eferding (Upper Austria) exposes the largest succession of sedimentary deposits from the late Oligocene in the eastern NAFB. Additionally, this section shows the facies transition from the shallow-water Linz-Melk Formation to the deep-water Eferding Formation. In this work, the fossil fauna and flora of the Eferding Formation as well as its lithology are re-evaluated using a multidisciplinary approach to gain new insights into the palaeoenvironment, palaeoclimate, and palaeoecology. A transgressive sequence is documented using sedimentological and ichnological data. Furthermore, a correlation to the late Chattian transgressive Ch-3 sequence is suggested. The impact of rising sea-level on marine biota is shown in detail by analysing various groups (Bivalvia, Echinodermata, Anthozoa, Foraminifera, Chondrichthyes and Osteichthyes), with several newly reported species for the Eferding Formation. Moreover, washed in plant material was analysed for the interpretation of the terrestrial climate indicating mainly humid subtropical conditions. Finally, the presence of phosphatic nodules indicates eutrophication on the shelf environment and the possibility of upwelling currents.

1. Introduction

The North Alpine Foreland Basin (NAFB) (Fig. 1A) is a prominent archive for the Oligocene and Miocene of Europe. The thick and commonly fossiliferous sedimentary successions accumulated during this interval provide invaluable insights into the geological development of the foreland basin and changes in environmental conditions (Lemcke, 1988; Schlunegger et al., 2001; Kuhlemann and Kempf, 2002; Böhme, 2003). Palaeogeographic interpretations of the NAFB are well established (Lemcke, 1988; Bachmann and Müller, 1992; Doppler et al., 1996; Rögl, 1998; Kuhlemann and Kempf, 2002; Kovác et al., 2017) and improved by taking evolutionary dynamics of biota into account (Harzhauser and Mandic, 2008; Pippèrr and Reichenbacher, 2017). These large-scale reconstructions rely on constrained age models and environmental interpretations at a regional scale. Therefore, lithostratigraphic studies were carried out (Wagner, 1998; Doppler et al.,

* Corresponding author.
E-mail address: thomas.filek@univie.ac.at (T. Filek).

https://doi.org/10.1016/j.palaeo.2021.110527
Received 29 March 2021; Received in revised form 27 May 2021; Accepted 9 June 2021
Available online 2 July 2021

2005; Pirkenseer et al., 2018) and supported by biostratigraphic schemes (Hochuli, 1978; Reichenbacher, 1993; Berggren et al., 1995; Cicha et al., 1998; Steininger, 1999; Piller et al., 2007; Hilgen et al., 2012). More recently magnetostratigraphy (Sant et al., 2017; Van der Boon et al., 2018), 3D modelling (Hofmayer et al., 2019), sequence stratigraphy (Haq et al., 1988; Vakarcs et al., 1998; Grunert et al., 2013; Kalifi et al., 2020), cyclostratigraphy (Harzhauser et al., 2013; Grunert et al., 2014) and chemostratigraphy (Grunert et al., 2015; Teschner and Reichenbacher, 2017; Hülscher et al., 2019) were added to the toolset. However, these previous studies focused mainly on a single aspect, without considering all available data, although integrative approaches to stratigraphy are getting increasingly more attention (Berger et al., 2005; Kälin and Kempf, 2009; Grunert et al., 2010a, 2010b; Sachsenhofer et al., 2010; Houben et al., 2012; Roetzel et al., 2014; Palzer-Khomenko et al., 2018; Pippèrr et al., 2018; Mandic et al., 2019a, 2019b). Palaeoenvironmental and palaeoecological interpretations, on the other hand, are still based on single groups of organisms only, such as plants (Böhme et al., 2007; Kovar-Eder et al., 2008), molluscs (Schneider and Prieto, 2011; Nebelsick et al., 2019; Mandic et al., 2020), sharks (Pollerspöck and Straube, 2017), trace fossils (Uchman and Krenmayr, 2004), ostracods (Brinkmann et al., 2019), and foraminifera (Pippèrr, 2011; Pippèrr and Reichenbacher, 2017), or on sedimentology and geochemistry alone (Roetzel et al., 1983; Faupl and Roetzel, 1990; Kocsis et al., 2008).

In addition, the available literature on the Oligocene strata of the eastern NAFB is often outdated (Rögl and Steininger, 1969; Roetzel et al., 1983; Dohmann and Braunstein, 1993; Wagner, 1996) and recent studies covering this time period are scarce (Rupp and Ćorić, 2012; Grunert et al., 2010a, 2010b, 2015; Knierzinger et al., 2019). Moreover, the recently formalized stratigraphic framework of the upper Oligocene,

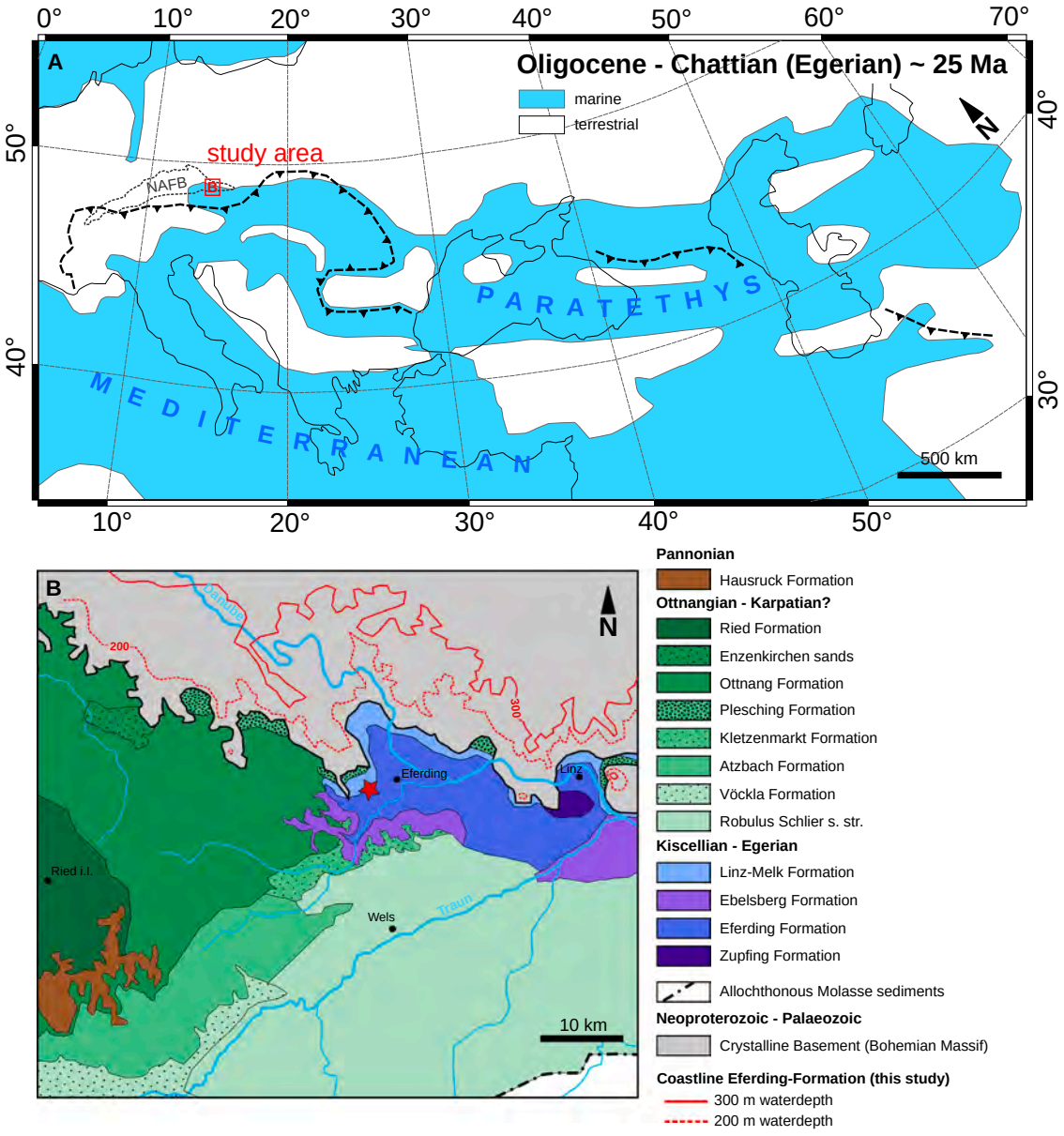

Fig. 1. Study area.
(A) Palaeogeographic map of the Egerian Paratethys stage, lasting from 27.5 to 21.5 Ma (Piller et al., 2007), modified after Kuhlemann and Kempf (2002) and Rögl (1998); dashed lines represent the recent Alpine, Carpathian and Caucasian thrust fronts. (B) Simplified geological map of the Oligocene to Miocene formations of Upper Austria at a scale of 1:200,000 (Rupp et al., 2011); the study site Unterrudling is marked with a red star. Interpreted coastlines during deposition of the Eferding Formation (red lines) are inferred from the reconstructed palaeodepths of 300 m and 200 m discussed in this study. For the isolines the recent topography is used. (For interpretation of the references to colour in this figure legend, the reader is referred to the web version of this article.)

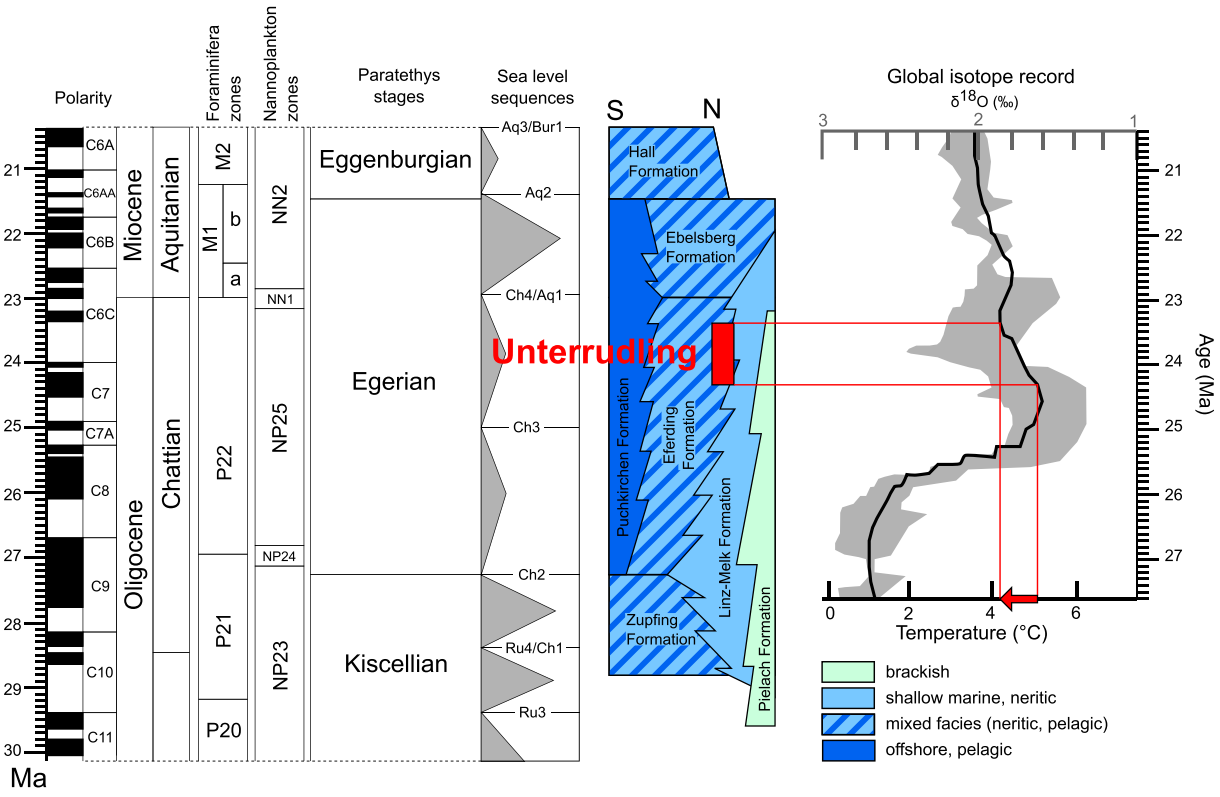

Fig. 2. Stratigraphy.
Stratigraphic chart of Central and Western Paratethys regional stages according to Piller et al. (2007). The correlation of the formations in Upper Austria follows Rupp et al. (2011) and Hofmayer et al. (2019); The stratigraphic position of the outcrop Unterrudling (red bar) follows Rupp and Ćorić (2015). Global deep-sea isotope record taken from Zachos et al. (2001a, 2001b), the temperature represents deep-sea benthic values. Colours of the different formations according to Piller et al. (2007). Calcareous nannoplankton zonation according to Martini (1971), planktonic foraminifera zonation according to Gradstein et al. (2020). (For interpretation of the references to colour in this figure legend, the reader is referred to the web version of this article.)

and in particular the Eferding Formation (Rupp and Ćorić, 2015), was only sparingly integrated in further studies (Feichtinger et al., 2019a, 2019b; Grunert et al., 2010a, 2010b). Even though, a large potential for palaeoenvironmental implications was shown for the Eferding Formation at the locality of Unterrudling (Kovar-Eder and Berger, 1987). This site in Upper Austria exposes a fossiliferous upper Oligocene sedimentary succession, comprising the Linz-Melk Formation and the Eferding Formation (Figs. 2, 3) (Rupp and Ćorić, 2015; Kovar-Eder and Berger, 1987; Feichtinger et al., 2019a, 2019b, 2020). This site is the largest and most complete section of Oligocene deposits exposed in the eastern NAFB and the dark marls of the Eferding Formation proved to be very fossiliferous (Kovar-Eder and Berger, 1987; Feichtinger et al., 2019a, 2019b, 2020).

Within this study a revised interpretation of environmental conditions and ecological networks of the Eferding Formation is presented to provide new constraints on palaeogeographic changes and climatic conditions during the Egerian (late Oligocene) in the NAFB. A comprehensive multidisciplinary approach including high resolution sedimentology, micro- and macro-palaeontology, palaeobotany, ichnology, geochemistry, and sedimentary petrography is used to interpret sea-level changes, ecological networks, as well as marine and terrestrial conditions, and to resolve stratigraphic and palaeogeographic issues for the Egerian in the NAFB.

2. Geological setting

2.1. General background

The disintegration of the Tethys Ocean, which began in the late Eocene (Rögl, 1998), led to the formation of the Paratethys Sea (Fig. 1A; Rögl and Steininger, 1983; Steininger and Wesseley, 2000). During the Egerian stage, the NAFB experienced large-scale sedimentary discharge from the Alps (Kuhlemann et al., 2002) and tectonic uplift (Doppler et al., 1996). This interplay caused the development of extensive terrestrial environments to evolve across most of the NAFB, whereby only the eastern part remained marine (Fig. 1A) (Kuhlemann and Kempf, 2002). The Paratethys has been subdivided into the western, central and eastern parts, which prompted the introduction of regional stages for each realm (Rögl, 1996; Reichenbacher, 1999). In the Central Paratethys, the upper Oligocene is represented by the Egerian regional stages (Fig. 2; Báldi and Seneš, 1975), which ranges from the Chattian to the Aquitanian global stage with an age of 27.3–21.5 Ma (Piller et al., 2007). This time period was characterized by drastic palaeogeographic and palaeoenvironmental changes (e.g., Lemcke, 1988; Rögl, 1998; De Ruig and Hubbard, 2006; Harzhauser and Piller, 2007), particularly affecting the westernmost part of the Paratethys Sea, the North Alpine Foreland Basin (NAFB) (Fig. 1B; Kuhlemann and Kempf, 2002). The NAFB is a classical foreland basin (Bachmann and Müller, 1992) formed by the subduction of the European Plate under the African-Adriatic Plate (Ratschbacher et al., 2004). The deposits (Figs. 1B, 2) of the NAFB are generally termed “Molasse”, which refers to their soft, often unlithified character (Fig. 3). Most of these deposits originate from the exhumation and weathering of the Alps as well as from the Franconian Platform and the Bohemian Massif (Ortner and Stingl, 2001). The area of the Northern Calcareous Alps was still rather flat during most of the Oligocene and covered by the fluvial gravelly facies of the Augenstein Formation (Fritsch et al., 2001).

In the western part, previously existing seaways to the Mediterranean and the North Sea were closed (Grunert et al., 2012; Hilgen et al., 2012). Knierzinger et al. (2019) even postulated a partial isolation to

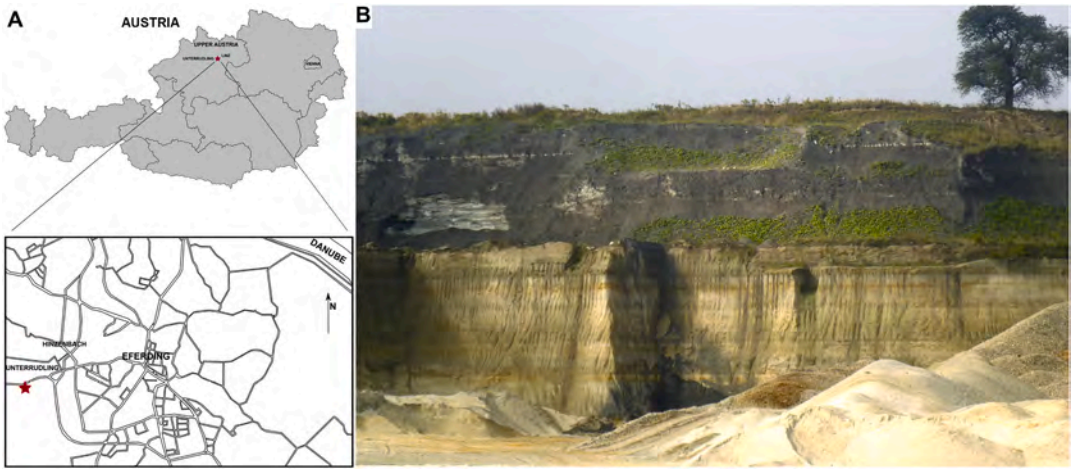

Fig. 3. Study site.
Locality: (A) Location of the Unterrudling sand pit. (B) Photograph showing the exposed formations (Linz-Melk Formation (base), Eferding Formation (top)).

the east by a tectonically induced ridge. Most of the sedimentary material was transported by large river systems eastwards into the marine realm (Doppler et al., 1996; Pirkenseer et al., 2018), resulting in turbiditic depositis and the formation of deep-sea channels parallel to the orogenic belt (Masalimova et al., 2015; Sharman et al., 2018) and various marine diachronous facies (Figs. 1B, 2) (Rupp et al., 2011). Several river systems drained the Bohemian Massif from the north, represented by the beds of Freistadt-Kefermarkt north of Linz (Chábera and Huber, 2000), and the St. Marein-Freischling Formation north of Krems (Nehyba and Roetzel, 2010).

2.2. Locality and associated deposits

The locality of Unterrudling (WGS84: 48°18′09.9″N 13°59′35.9″E) (Fig. 3) in the eastern NAFB is located close to the northern mainland of the Bohemian Massif. It is dated to the middle Egerian (~25.6 Ma) using nannoplankton (Zone NP25) and it represents the transition of a shallow marine to a deep-sea environment during the Egerian (Fig. 2; Rupp and Ćorić, 2015). Several different depositional environments persisted in close proximity during that time (Kuhlemann and Kempf, 2002). Local intertidal zones in estuarine environments existed along the coast of the Bohemian Massif (Roetzel et al., 1983; Harzhauser and Mandic, 2001). These brackish deposits (Pielach Formation; Wagner, 1996) are preserved as small patches or as intercalations in coastal sands (Ćorić et al., 2013), indicating a regressive phase in some areas (Roetzel et al., 1983). The Linz-Melk Formation represents the marine nearshore facies up to the shelf-zone (Figs. 1B, 2; Roetzel et al., 1983; Krenmayr and Roetzel, 2000b). These shallow marine deposits display a large lithological variety along the margin of the Bohemian Massif (Rupp et al., 2011). The facies range from coarse-grained, breaker-zone sands (Roetzel et al., 1983) to massive, poorly sorted and strongly bioturbated shoreface sands. Furthermore, up to several metres thick mega-scale cross-stratified sandwaves have been reported (Krenmayr and Roetzel, 2000a). The dominance of quartz and minor clastic feldspar in a kaolinitic matrix is typical for the Linz-Melk Formation (Roetzel et al., 1983), and the strata are known for their remains of marine vertebrates such as cetaceans and sirenians (Marx et al., 2011; Voss et al., 2016). The shelf deposits, formerly termed "Älterer Schlier" were recently formalized and comprise the Eferding Formation (Rupp and Ćorić, 2015) as well as the overlying Ebelsberg Formation (Rupp and Ćorić, 2012; Figs. 1, 2). Both are composed of dark grey, partly laminated silts to clays. These strata are locally rich in well-preserved fossils, possibly due to anoxic bottom water conditions (Kovar-Eder and Berger, 1987; Grunert et al., 2010a, 2010b; Rupp and Ćorić, 2015). At the southern margin of the NAFB in the vicinity of the ancient thrust front, the basin was at its deepest and characterized by coarse-grained turbiditic deposits and deep-sea canyons (Wagner, 1998; De Ruig and Hubbard, 2006), with estimated palaeodepths of 1000–1500 m (Kuhlemann and Kempf, 2002; Grunert et al., 2010a, 2010b). These deposits are assigned to the Puchkirchen Formation (Fig. 2; Wagner, 1996; Pytlak et al., 2017).

3. Material and methods

A 41-m-thick geological profile of the Unterrudling section was studied for the sedimentological, palaeontological and geochemical interpretations. Different lithological horizons were identified and separated into several beds (Fig. 4). Abbreviations 'LM' for the Linz-Melk Formation, and 'E' for the Eferding Formation are used. Samples were collected from several horizons (Fig. 4, Table 1) for the analyses of fossil taxa and thin section petrography. A compilation of the collected material in Unterrudling is given in Table 1.

3.1. Sedimentology and granulometry

Fifteen samples for representative granulometric analysis were taken (Table 1). Grain size analyses were carried out at the Austrian Geological Survey using a combination of wet sieving in ½ Phi steps and Sedigraph for grain sizes <0.032 mm. The sieve analysis data and the data generated from the Micromeritics SediGraph 5100 were subsequently calculated and displayed with the software program SedPakWin (Reitner et al., 2005).

3.2. Thin section petrography and X-ray diffraction

Petrography of phosphatic concretions was analysed on thin sections of standard size using a Leica DM 4500 P polarization microscope coupled to a Leica DFC 450C camera, using the Leica Application Suite 4.4.0 for image analysis and camera control (Table 1, Fig. 5). The phosphatic concretions were separated into 6 piles of 6 to 10 individual concretions based on size and morphology. Sample piles for X-ray diffraction were crushed using a rock hammer and further processed to fine powder using an agate mortar and pestle. The powdered samples were analysed using a Philips X'Pert 3710 mpd diffractometer at the Department of Mineralogy and Crystallography of the University of Vienna. X-ray diffraction patterns and mineral identification was conducted using the Bruker-AXS Eva 13.0.0.3 software package. The Bruker TOPAS 3 software using the crystallographic open database (COD) was used for structural identification and refinement of minerals.

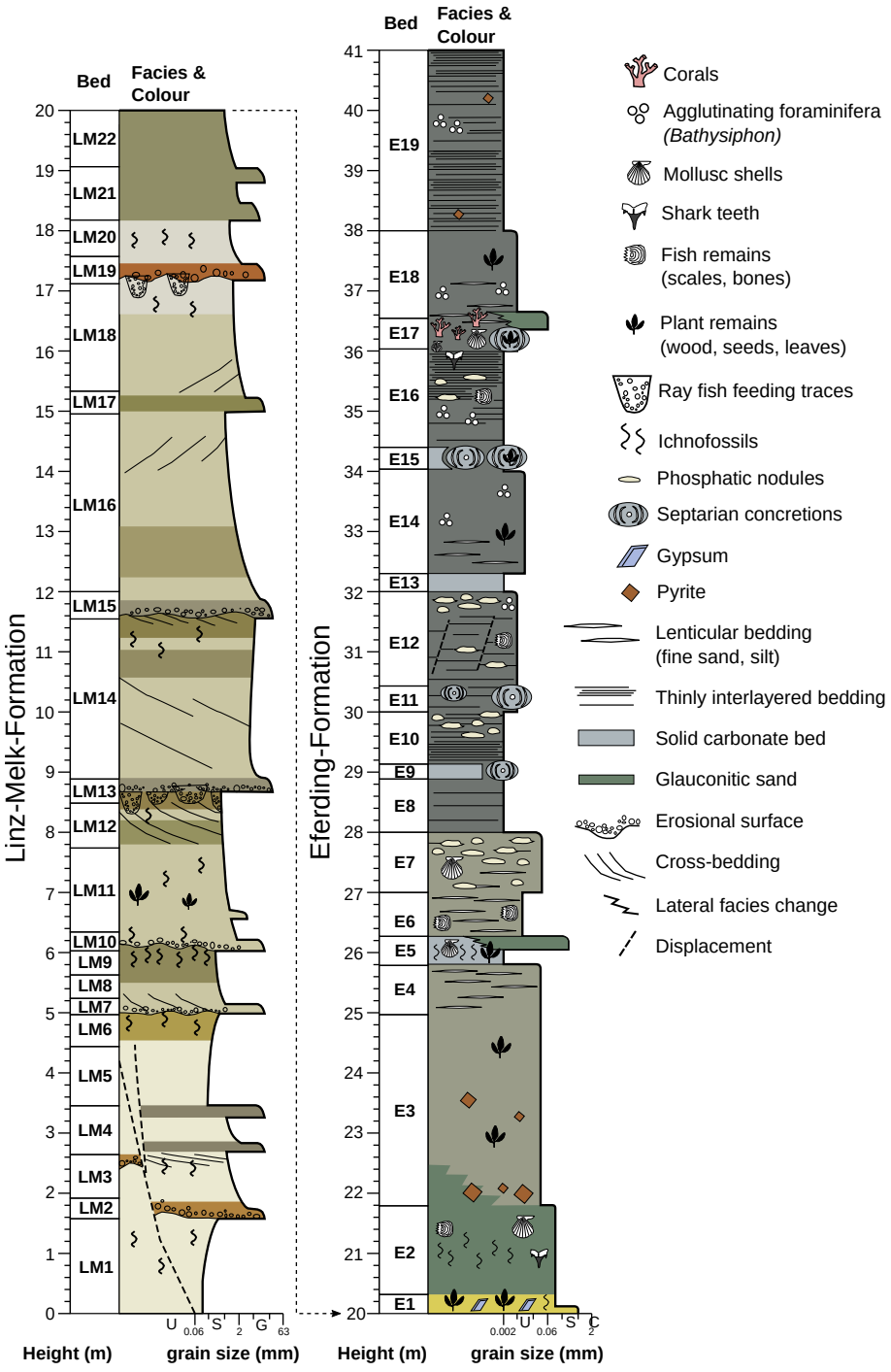

Fig. 4. Geological profile.
Geological profile of the section Unterrudling. Different beds are separated into Linz-Melk Formation (LM) and Eferding Formation (E).

3.3. Ichnology

Trace fossils, mainly burrows, were prepared in the field, either by cutting clean sections through the burrow, or by uncovering larger burrows with scraping tools. The environmental and ecological interpretations are following the current literature summarized in text books in the larger part (e.g., Bromley, 1996; Pemberton et al., 2001; Miller, 2007; Buatois and Mángano, 2011; Bromley and Knaust, 2012; Knaust, 2017; and references therein).

3.4. Palynology and palaeobotany

Sediment samples (concretions and surrounding sediments, c. 60 g) (Table 1) were prepared following the method of Halbritter et al. (2018) for pollen extraction. The remaining material was mixed with glycerol and stored in small sample tubes. The identification of the pollen follows the single grain technique (cf. Zetter, 1998; Hesse et al., 2009), where the same pollen grain analysed with light microscopy (LM) is used for scanning electron microscopy (SEM). The resulting images (Figs. S4, S5) were used for detailed descriptions and affiliations with extant botanical families and genera (= next living relatives). The distributions of the nearest

Table 1
Analysed material from the Eferding Formation and its allocation and abundances through the profile.

Taxon/Sample	Total number of samples (individuals)	Beds (see Fig.3)	Field work	Analysed by	Deposited in
Granulometry	15	LM2, LM3, LM5, LM7, LM11, LM14, LM15, LM16, LM18, E3(2×), E4, E5, E7, E10	2001	Roetzel	GBA
Phosphatic concretions	50	E16	2020	Smrzka, Zwicker	IPUW
Ichnofossils	8	LM9, LM11, LM13, E1, E2, E17, LM7-LM12	2001, 2020	Uchman	
Pollen & Leaves	4 & 7	E7, E10, E12, E16	2019	Filek	NHMW, OLL, IPUW
Bivalvia	9 (42)	E2, E3, E16, E17	2018, 2020	Mandic	NHMW
Osteichthyes	1 (43)	E17	2020	Reichenbacher	NHMW
Chondrichthyes	4 (102)	E1-E8 (mixed sample), E2, E16, E17	2020	Pollerspöck, Feichtinger	NHMW, OLL
Echinodermata	2	E16, E17	2020	Kroh	NHMW
Foraminifera	2	E16, E12-E19	2020	Kranner	IPUW
Foraminifera (Rupp and Ćorić, 2015)	18	E3(3×), E4, E5, E7, E8, E9, E10, E12(2×), E14(2×), E16, E17, E18, E19	2015	Rupp, Kranner	GBA
Corals	1	E17	2020	Berning	NHMW

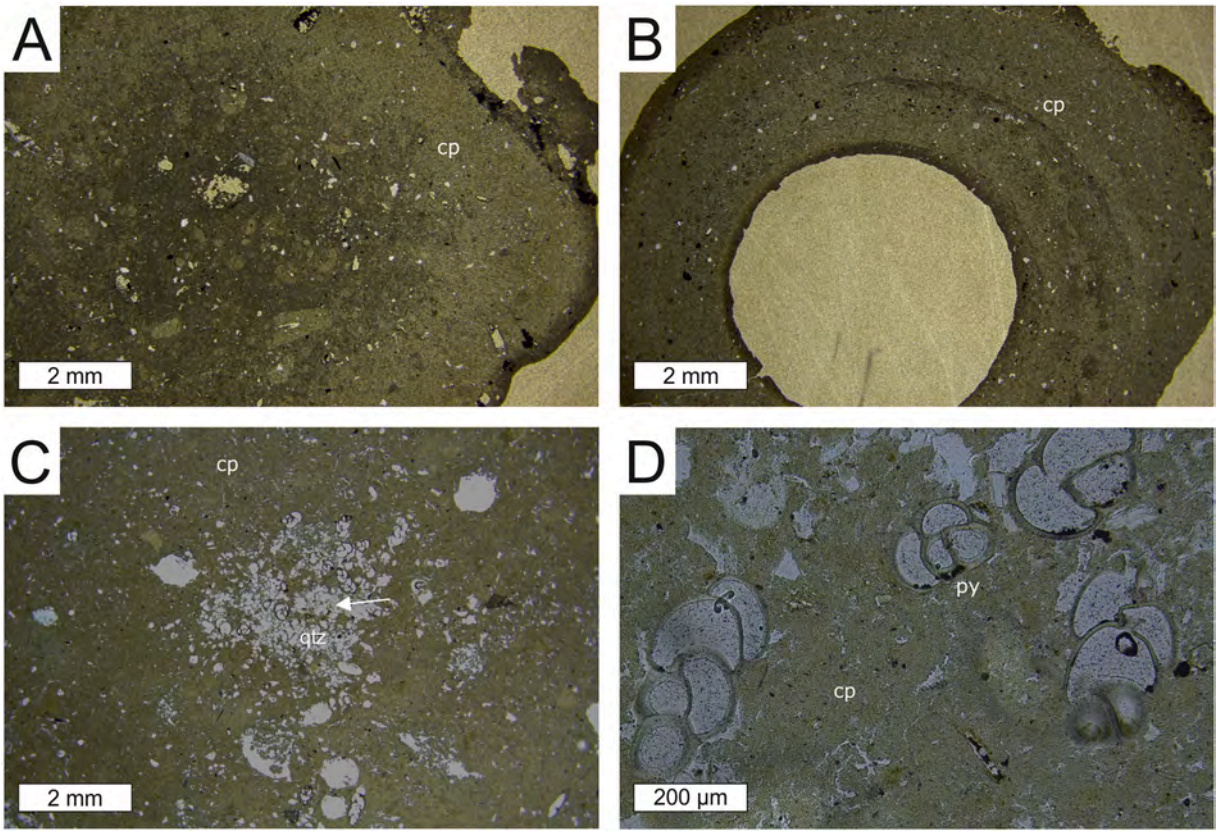

Fig. 5. Petrography of phosphatic nodules.
Thin section micrographs of Unterrudling phosphatic concretions, cp – cryptocrystalline phosphate, qtz – quartz, py – pyrite. (A) Spherical to oval concretion with dispersed detrital grains within a matrix of cryptocrystalline phosphate. (B) Tubular concretions with zonation composed of cryptocrystalline phosphate. (C) Accumulation of detrital and biogenic particles within a spherical concretion featuring angular quartz grains, glauconite (arrow), and foraminifera. (D) Benthic foraminifera (*Bulimina* sp.) in the centre of a spherical concretion within a cryptocrystalline phosphate matrix. Foraminifera shells are partly replaced by cryptocrystalline phosphate and feature framboidal pyrite.

living relatives of newly identified taxa were selected for the reconstruction of the climate during the late Oligocene period. For the distribution of next living relatives, the databases international plant name index (IPNI, 2020), Tropicos and Plants of the World (POWO, 2019) and the Köppen Geiger Classification (Kottek et al., 2006) were used.

Newly described fossilized leaves combined with descriptions of Kovar-Eder and Berger (1987) from the Eferding Formation were used to interpret the palaeoclimate using Climate Leaf Analysis Multivariate Program (CLAMP), after Soysal et al., 2017). Fossil taxa described by Kovar-Eder and Berger (1987) are housed in the following museums (Natural History Museum, NHMW), Oberösterreichische Landes-Kultur GmbH (formerly Oberösterreichisches Landesmuseum Linz, OLL), Stadtmuseum Linz Nordico, Bavarian State Collection of Palaeontology and Geology (BSPG), and were not all reviewed as parts of the collections were missing. Only a small number of taxa (10 in total) could be used for the CLAMP analysis and so only an approximation of the climate

was interpreted.

3.5. Anthozoa

Numerous specimens of scleractinian coral skeletons were recovered from layer E17, among them a 40 × 30 cm slab with several colonies preserved in it. The colonies were excavated from the clayey sediment and the friable skeletons hardened. For identification, the works on scleractinia (Zibrowius, 1980) and deep-coral growth (Taviani et al., 2005) were used.

3.6. Bivalvia

Bivalve samples were collected in 2020 from beds E16 and E17 (Fig. S6 A–D, F–J; Table 1). Additional specimens were photographed on site in 2018 from beds E2 and E3 (Fig. S6 E, Table 1). Washing and sieving has not been applied to the collected bulk sediment samples, as the incorporated shell remains strongly tend to disintegrate. The preparation of available shells was carried out under the stereomicroscope, in respect to their small general size and extreme fragility. Treatment included fixation by a diluted vinyl acetate aqueous dispersion (i.e. Mowilith) to prevent further shell disintegration after drying. Laboratory photographs were made by Nikon D5200. All study material is in the collection of the Natural History Museum Vienna (NHMW 2020/0140).

3.7. Echinodermata, Chondrichthyes and Osteichthyes

Small elasmobranch teeth, otoliths and remains of echinoderms were extracted exclusively from 100 kg sediment derived from the coral layer (E17). The sediment was dried, dissolved using diluted hydrogen peroxide and screen washed (mesh sizes 500, 250, and 125 μm). For preparing Scanning Electron Microscope images, the ichthyoliths were mounted on stubs and coated with a gold alloy for photography using a JEOL JSM Neoscope at the Geological-Palaeontological Department of the Natural History Museum (NHMW) in Vienna. Isolated larger elasmobranch teeth were collected from various horizons directly in the quarry (Table 1; see Figs. S7, S8).

All material is housed at the NHMW in Vienna, the Department of Palaeontology University of Vienna (IPUW) or the OLL. Collection numbers for all taxa are given in Appendix 1.

3.8. Foraminifera

Thin sections of the phosphatic nodules, produced for petrographic examinations yielded clumped foraminifera. These were identified and assigned at the genus level (Table 3). The foraminifera samples from Rupp and Ćorić (2015), which were taken in 1 m resolution, were re-evaluated. The sample acronyms of Rupp and Ćorić (2015) correspond thenew samples: UR2–UR4 = E1–E3, UR5–UR12 = E4–E11 and UR13–UR19 = E12–E18. The samples are correlated to the geological profile of this study (Table 1, Fig. 4), environmental and ecological interpretations are based on published ranges of extant foraminifera (Murray, 1991, 2006; Sgarrella and Moncharmont Zei, 1993; Kaiho, 1994; Altenbach et al., 2003; Rögl and Spezzaferri, 2003; Hohenegger, 2005; Kaminski and Gradstein, 2005; Rasmussen, 2005; Spezzaferri and Tamburini, 2007; Báldi and Hohenegger, 2008; Sen Gupta et al., 2009; Grunert et al., 2010a, 2010b; Pippèrr and Reichenbacher, 2010; Milker and Schmiedl, 2012; Holcová et al., 2015, 2018; Székely et al., 2017).

These range values were used as limits in the calculations of Hohenegger (2005) and Báldi and Hohenegger (2008) to determine palaeobathymetry. For calculating salinity and bottom water temperature the limits of these parameters were used as "l_j" and hence all parameters were calculated with the following formula (Eq. (1)) developed by Hohenegger (2005) and extended by Báldi and Hohenegger (2008) with a 95% confidence interval:

$$depth = \sqrt{\frac{\sum_{j=1}^{m} l_j a_j d_j^{-1}}{\sum_{j=1}^{m} a_j d_j^{-1}}} \quad (1)$$

Where l_j stands for the location parameter (depth, salinity or bottom water temperature) represented by the geometric mean ($\sqrt{xjmin*xjmax}$), whereas the weighting factor d_j in this equation was calculated with (x_{jmax} - x_{jmin}) and a_j represents the relative abundance of the species. For more detailed information see Hohenegger (2005 and Báldi and Hohenegger (2008).

Further palaeowater depth calculations using the P/B ratio are conducted taking into account planktonic (P) and benthic (B) foraminifera as well as stress markers (S) by using the formula of Van der Zwaan et al. (1990): $P(\%) = \frac{P}{(P+B-S)}$, $Depth(m) = e^{3.58718} + 0.03534 * P(\%)$.

In the following paragraphs calculated absolute values are rounded to the nearest ten (for depth calculations) or to the integer (temperature and salinity) are listed and represent only approximations.

Bathymetric categories defined by Adegoke et al. (2017): inner neritic = shoreface down to ca. 40 m, middle neritic = 40–100 m, outer neritic = 100–200 m, bathyal = below 200 m were applied.

The ecological parameters "Feeding Type", "Mode of life" and "Oxygenation" were plotted in a ternary diagrams (Fig. 8A–C) combined with a density map. For the ternary plots (Fig. 8A–C), the absolute values were transferred in percentages per sample; purple colours indicate absence, light blue low abundance, green and yellow moderate abundance and orange to red indicate high values. The definition of oxygenation follows Kaiho (1994). Hence, we distinguish between oxic, suboxic and dysoxic indicators and high oxic, low oxic, suboxic and dysoxic conditions. Quantitative analyses have been conducted using the software PAST (Paleontological Statistics, version 4.03; Hammer et al., 2001) and were illustrated using CorelDraw X8.

4. Results

All newly collected fossils and ecological interpretations are given in Tables 2 and 3. Representative fossils from the Eferding Formation are shown in Fig. 7. Representative sedimentological facies are depicted in Fig. S1 (Linz-Melk Formation) and S2 (Eferding Formation) and a detailed overview of the identified taxa is provided in Figs. S3–S8.

4.1. Lithology

The outcrop shows a 41 m-thick section comprising 20 m of the sandy Linz-Melk Formation overlain by 21 m of the silty-clayey Eferding Formation (Fig. 3).

4.1.1. Linz-Melk Formation

The basal part of the section (Fig. 4) features a 4.5 m-thick whitish to pale coloured medium to fine-grained and strongly bioturbated sand, which is subdivided by three gravelly and two fining upwards intercalations (LM2-LM5). The grain sorting at the base (LM1) is quite poor (Fig. 6). Normal faults with displacements of about 1 m were observed in this interval. The gravelly layer LM7 shows a clear erosional base cutting into a several cm thick bioturbated layer (LM6, Fig. S1). This sequence is repeated after 1 m (LM8–10), whereas LM9 exhibits abundant trace fossils (Fig. S1). Between 6.4 m and 7.8 m (LM11), the well sorted, medium sand contains wood fragments as well as trace fossils such as >50 cm long branching burrows (Fig. S1). The sediment appears massive and shows evidence of dense bioturbation structures. Cross-bedding can be observed in the 1-m-thick bed LM12 (Fig. 4). From a gravel layer at the top (LM13), burrows and up to 50 cm deep gravel filled pockets disturb the cross-bedded sand below (Fig. S1). From 9 to 20 m, where several gravelly layers (LM15, LM17, LM19, LM21) with erosional base interrupt the partly cross-bedded fine gravelly and coarse sands (LM14, LM16, LM18, LM20, LM22) (Figs. 4, S1), a general

Table 2
Table of the examined fossil leaves and pollen taxa from the Eferding formation.

CLAMP

MAT	WMMT	CMMT	GROWSEAS	GSP	MMGSP
20.6	28.2	10.7	11.1	169.3	16.2

3-WET	3-DRY	RH	SH	ENTHAL
83.2	12.4	68	11.3	33.8

Parent taxon	Taxa	Stratigraphy	Genus distribution	Decidious	Evergreen	Identified by/Figure
Magnoliophyta	*Dicotylophyllum*	Cretaceous-Oligocene				Kovar-Eder and Berger (1987)
Myricaceae	*Myrica lignitum*	Eocene-Miocene	cosmopolitan	+	+	Kovar-Eder and Berger (1987)
Fagaceae	aff. *Quercus sprengeli*, *Quercus vel Castanea* sp.	Cretaceous-today	N-Hemisphere	+	+	Kovar-Eder and Berger (1987)
Platanaceae	*Platanus neptuni*	Oligocene-Miocene	SE-As, Eu, N-Am	+		Kovar-Eder and Berger (1987)
Lauraceae	*Lauraceae* gen. et sp. indet					Kovar-Eder and Berger (1987)
	Daphnogene cinnamomifolia	Eocene-Miocene			+	this study, Kovar-Eder and Berger (1987), Fig. S5 (G, I)
Mycophyta	*Mycophyta* indet.					this study, Kovar-Eder and Berger (1987), Fig. S5 (J)

POLLEN

Taxa	Abundancies	Stratigraphy	Köppen-Geiger Classification	Recent Distribution	Figure
Fagaceae indet.	X	recent	Cfa, Cfb, Cfc, Csa, Csb, Csc, Cwa, Cwb, CWc, Dfa, Dfb	N-Hemisphere	S5 (A)
Pinus sp. (haploxylon & dyploxylon type)	X X X	recent	As, BWk, BWh, BSk, BSh, Cfa, Cfb, Cfc, Csa, Csb, Csc, Cwa, Cbb, Cwc, Dfa, Dfb, Dfc, Dfd, Dsa, Dsb, Dsc, Dwa, Dwb	Am, Eu, N-Af, As	
Picea sp.	X X X	recent	Cfa, Cfb, Cfc, Csa, Csb, Csc, Cwa, Cwb, CWc, Dfa, Dfb, Dfc, Dfd, Dsa, Dsb, Dsc, Dwb, Dwc, Dwd, ET	N-Am, Eu, As	S4 (C)
Cathaya sp.	X X X	recent	Cfa, Cwb	SE-As	S4 (A)
Tsuga sp.	X X	recent	Bsk, Cfa, Cfb, Cfc, Csa, Csb, Dfb, Dfc, Dwb, Dwc, ET	Am, As	S4 (B)
Cupressaceae indet.	X X X	recent	BSk, BSh, Cfa, Csa, Csb, Cwa, Cwb	cosmopolitan	S4 (D)
Sparganium sp.	X	recent	Cfa, Cfb, Csa, Csb, Cwa, Cwb, Dfb, Dsb	Am, Eu, N-Af, As, E-Aus	S4 (E)
Platanus sp.	X	recent	Am, As, BSh, BSk, Bwh, Bwk, Cfa, Cfb, Csa, Cwa, Dfa, Dfb, Dfc, Dsa, Dsb	N-Am, Eu, SE-As	S4 (F)
Cedrelospermum sp.	X X	Eocene-Oligocene	–	N-Am, Eu, As	S4 (G)
Zelkova sp.	X X	recent	Cfa, Cwa, Cwb, Csa, Csb	As	S4 (H)
Eotrigonobalanopsis sp.	X X	Oligocene-Miocene	–	Eu	
Trigonobalanopsis sp.	X X	Oligocene-Miocene	–	Eu	S5 (B)
Quercus sp.	X	recent	Af, BWh, BSk, Cfa, Cfb, Cfc, Csa, Csb, Csc, Cwa, Cwb, CWc, Dfa, Dfb, Dwa, Dwb, Dwc	Am, Eu, N-Af, SE-As	S5 (C)
Carpinus sp.	X X	recent	Am, Aw, Cfa, Cfb, Cwb, Dfa, Dfb, Dfc	Am, Eu, As	S4 (M)
Betula sp.	X	recent	Am, As, BWk, BWh, BSk, Cfa, Cfb, Cfc, Csa, Csb, Csc, Cwa, Cwb, CWc, Dfa, Dfb, Dfc, Dfd, Dsa, Dsb, Dsc, Dwa, Dwb, Dwc, Dwd, EF, ET	N-Hemisphere	S5 (D)
Engelhardia sp.	X X X	recent	Af, Am, As, Aw, Cfa, Cfb, Csa, Cwa, Cwb,	SE-As	S4 (O)
Carya sp.	X X	recent	As, Aw, BSh, Bsk, Cfa, Cfb, Cwa, Cwb, Dfa, Dfb, Dfc	N-Am, SE-As	S4 (N), S5 (E, F)
Euphorbia sp.	X X	recent	Af, Am, As, Aw, BWk, BWh, BSk, BSh, Cfa, Cfb, Cfc, Csa, Csb, Csc, Cwa, Cwb, CWc, Dfa, Dfb, Dfc, Dfd, Dsa, Dsb, Dsc, Dwa, Dwb, Dwc, Dwd	Am, Eu, Af, As, Aust	S4 (I)
Rhederodendron sp.	X X X	recent	Cfa, Cwb	SE-As	S4 (J)
Vitellariopsis cf. *marginata*	X X	recent	Aw, Bsk, Cfa, Cfb, Csa, Csb, Cwa, Cwb, Bsh	S-Af	S4 (K)
Symplocos sp.	X	recent	Af, Am, As, Aw, Cfa, Cfb, Cwa, Cwb	Am, SE-As, E-Aust	S4 (L)
Phillyrea sp.	X X	recent	Cfa, Cfb, Csa, BWk, BWh, BSk	S-Eu, Af	S4 (P)

Footnote: Indications about climate (CLAMP) and environment through the affiliations to extant taxa. Geographical occurrences of the extant taxa and climatic conditions of these areas follow the Koeppen and Geiger classification (Kottek et al., 2006). Abbreviations: N – North, S – South, SE – Southeast, Af – Africa, As – Asia, Am – America, Aust – Australia, Eu – Europe.

Table 3
Detailed taxa list of the Eferding Formation and their palaeoecological implication. Abundancies are indicated as X (rare), XX (frequent), and XXX (very frequent).

	Abundance	Bed	Ecological Implications	Figure
Ichnofossils				
Dactyloidites cf. *peniculus*	xx	LM7-LM12	shoreface	
Bornichnus tortuosus	xx	LM7-LM12	intertidal-shelf	
Macaronichnus segregatis	xxx	LM11	shallow-marine, oxygenated	Fig. S3 (D)
Ophiomorpha cf. *annulata*	x	LM11	shallow-marine, lower foreshore - upper shoreface	Fig. S3 (B)
cf. *Ophiomorpha irregulaire*	xx	E2		Fig. S3 (C)
Ophimorpha isp.	x	LM11		Fig. S3 (A)
Piscichnus waitemata	xxx	LM13	intertidal, fair weather wave base	Fig. S3 (F)
?*Teichichnus* isp.	x	E2	marine, lagoonal	Fig. S3 (E)
Thalassinoides isp.	xxx	LM9	shallow-marine	Fig. S3 (G)
Teredolites clavatus	xx	E1	wood-boring, shallow-marine, transgressive	Fig. S3 (H)
Apectoichnus longissimus	xx	E1	wood-boring bivalve	Fig. S3 (H)
Asthenopodichnium isp.	x	E17	mayfly boring	Fig. S3 (I)
Bivalvia				
Delectopecten vitreus	x	E2, E3, E17	50-4255 m depth, cold water, coral-association	Fig. S6 (F-H)
Neopycnodonte navicularis	xx	E2, E16, E17	45-250 m depth, cementing, cold water, coral-association	Fig. S6 (A-D)
Propeamussium semiradiatum	x	E2	100-5000 m depth, cold water, active swimmer, carnivorous	Fig. S6 (E)
Ctenoides aff. eximia	xxx	E17	0-50 m depth, warm water	Fig. S6 (I, J)
Anthozoa				
Madropora cf. *ocoulata*	xx	E17	deeper water	
Foraminifera				
Bathysiphon spp.	xx	E12-E19	infaunal, cold, upper bathyal	
Uvigerinidae indet.	xx	E16	cold, 100-4500m depth	Fig. 5 (D)
Buliminidae indet.	xx	E16	infaunal, cold, shelf-bathyal	Fig. 5 (D)
Echinoidea				
Spatangoida indet.		E16, E17	endobenthic	
Cidardoida indet.		E16, E17		
Chondrichthyes				
Etmopterus sp.	xxx	E17	deeper water	Fig. S7 (A-B)
Palaeocentroscymnus sp. (OLL)	xxx	not known	deeper water	
Palaeocentroscymnus sp.	xxx	E17	deeper water	Fig. S7 (C-D)
Dalatidae nov. gen. nov. sp (OLL)	xxx	not known	deeper water	
Dalatidae nov. gen. nov. sp.	xxx	E17	deeper water	Fig. S7 (E-F)
Centroselachus sp.	x	E17	deeper water	Fig. S7 (G-H)
?*Centroselachus* sp.	x	E17	deeper water	
Heptranchias sp.	x	E17	down to 1000m	Fig. S7 (N-O)
Echinorhinus sp.	x	E17	down to 900m, benthic	
Echinorhinus sp.	x	not known	down to 900m, benthic	Fig. S7 (I)
Hexanchus sp. (OLL)	x	not known	down to 2500m	Fig. S7 (J)
Hexanchidae indet.	x	E1-E8, E17		
Hexanchidae symphyseal tooth	x	E17		Fig. S7 (P)
Raja sp.	x	E1-E8	litoral to neritic	Fig. S7 (R)
Squantinidae indet.	x	E1-E8	benthic	Fig. S7 (T)
Isurus sp.	x	E2	pelagic	Fig. S7 (L)
Alopias exigua	x	E17	pelagic	Fig. S7 (K)
Notorynchus primigenius	x	E17	deeper water	Fig. S7 (Q)
Carcharias acutissimus	x	E16	litoral to neritic	Fig. S7 (M)
Drag reduction denticle (OLL)	x			Fig. S7 (S)
Osteichthyes				
Diaphus sp.	xxx	E17	deeper water	Fig. S8 (F)
Diaphus aff. *kokeni*	xx	E17	deeper water	Fig. S8 (B, C, b, c)
Diaphus aff. *prisimetallis*	x	E17	deeper water	Fig. S8 (A, a)
Diaphus aff. *taaningi*	x	E17	deeper water	Fig. S8 (D, d)
aff. *Raniceps* aff. *coelorinchoides*	x	E17	deeper water	Fig. S8 (G, g)
Cf. *Coelorinchus*	x	E17	deeper water	Fig. S8 (H, h)

coarsening upward trend can be observed. Nevertheless, between the single gravel layers, fining upward trends from more gravelly sands to coarse sands occur. Gravel filled pockets can be identified again at the base of the layer LM19 (Fig. S1) as well as large unidentified burrows in LM20. Despite the occurrence of trace fossils throughout the Linz-Melk Formation, no faunal remains were observed. Generally, the clastic material is dominated by quartz, but accompanied by feldspar, which is often heavily weathered. Aside from the basal part, the grain sorting is quite well throughout the Linz-Melk Formation (Fig. 6).

4.1.2. Eferding Formation

The transition from the sandy facies of the Linz-Melk Formation towards the overlying strata is marked by an abrupt change to darker, grey-coloured deposits containing less quartz and feldspar towards a more pelitic, organic-rich matrix. However, this transition is not accompanied by an abrupt change in grain size. The granulometric data rather shows a transition from well sorted coarse sand to poorly sorted fine sand (Fig. 6), which is caused by a muddy matrix. Nevertheless, a marker horizon is recognized (E1), which is used as a mining floor due to its hardness. Abundant small plant particles and numerous wood fragments are present in this basal layer (E1; Fig. 4) at about 20 m within the profile. Some wood pieces are up to 50 cm long. Most of these wood fragments are heavily bored, in some cases only the refilled burrows remain. The most striking feature in E1 is the abundance of flat gypsum rosettes that precipitated within the wood fragments (Fig. S2) and the surrounding sediment. The sediment comprises a yellow-orange coloured coarse sand with abundant mica and glauconite, and is devoid of sedimentary structures. From the gypsum layer to 25 m upsection, a silty fine sand (E2, E3) with a homogeneous texture and low carbonate content can be observed. Especially in the lower part (E2), isolated trace fossils and skeletal fish remains are abundant. Mica, oxidized pyrite and glauconite are common minerals. From 25 to 25.8 m (E4) the

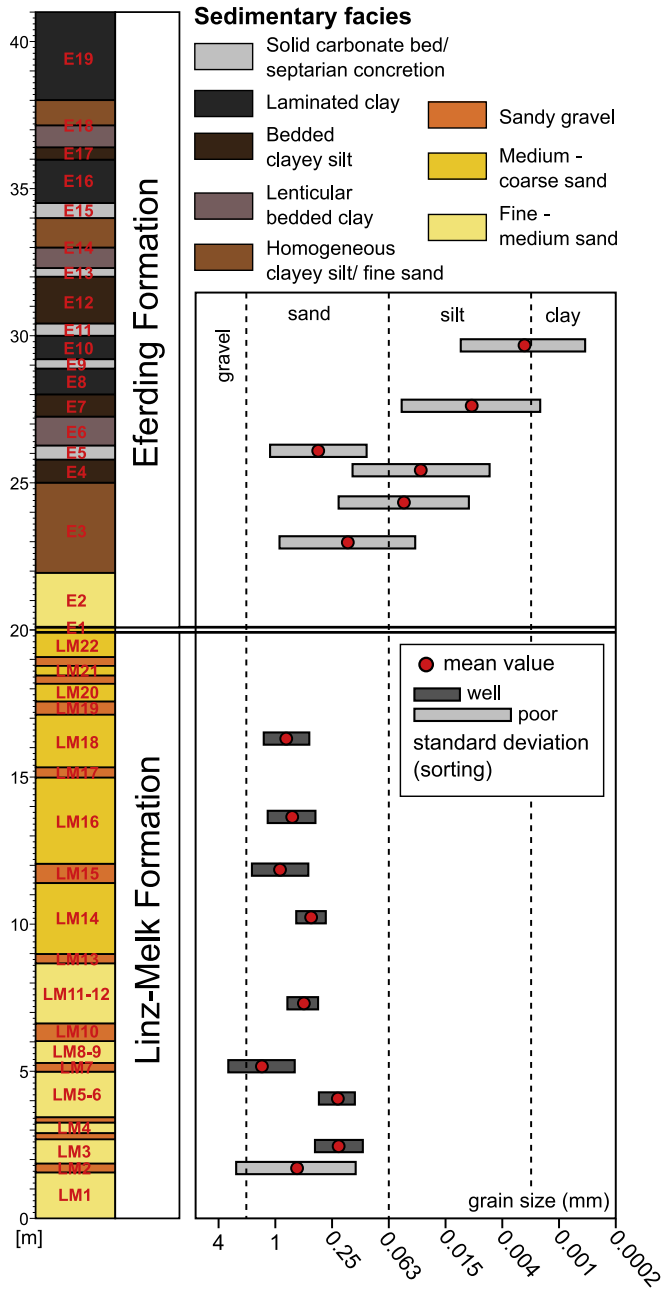

Fig. 6. Granulometry.
Results of the granulometric measurements. Bars represent standard deviation of mean grain size; the stratigraphic column represents the sedimentary facies of Unterrudling (see Fig. 4 for details)

homogeneous character changes into lenticular bedding with lenses of fine sand in a silty matrix (Fig. S2). E4 is interrupted by a 20 cm-thick, solid marlstone (E5; Fig. 4), which laterally intercalates with glauconitic sandstone (Fig. S2). This layer features several mollusc remains (Fig. 4) and plant seeds (Fig. S5), as well as trace fossils. Clayey silt with lenticular-bedded fine sand continues from 26 to 27 m (E6) in the section (Fig. S2), with a high abundance of well-preserved scales of unidentified bony fishes. The mica content in the lenticular-bedded part is very low, and concentrated in the sandy lenses. The lenticular bedding disappears in layer E7, the muddy sediment appears more homogeneous (Figs. 4, S2). Bedding is only visible due to horizontally arranged yellow phosphatic nodules (Fig. S2, compare Fig. 5), which are more frequent up section, but appear only as a few cm thick layer in E7 (Fig. 4). Fragments of mollusc shells are common. The bedding planes are well visible in bed E8 by thin silty interlayers within the clayey sediment (Fig. S2). This bed seems quite homogeneous. It is devoid of fossils and features only little mica. A solid carbonate layer (E9) follows with a thickness of about 20 cm (Fig. 4). This bed features occasional calcareous septarian concretions. Bed E10 is composed of thinly bedded, clayey silt with an increasing occurrence of phosphatic nodules (Fig. S2). Fish scales are also more frequent. In the following 50 cm calcareous concretions frequently occur in the laminated sediment (E11; Fig. S2). Granulometric samples are missing from the layer E11 upwards. However, a similar mean grain size distribution can be expected in the layers E12–E19 as the sedimentary facies does not change much. Sorting probably increases as layers with lenticular bedding are becoming sparse upsection. In bed E12, the silty sediment is thinly bedded and features abundant phosphatic nodules, fish scales and traces of agglutinated infaunal foraminifera (Figs. 4, S2; E12). In the uppermost part of this layer, phosphatic nodules are common and several small tectonic displacements are present (Fig. 4). E13 is a further solid marlstone bed, and the overlying bed E14 features sandy silt with lenticular bedding and some plant remains (Fig. S2). Bed E14 changes upwards into a massively bedded silty sediment, containing abundant plant remains and muscovite (Figs. 4, S2). At 34 m, a solid carbonate bed (E15; Fig. 2) is present, which is about 20 cm thick, can be traced laterally along the whole outcrop (Fig. 3) and can be considered as a marker bed of the section. Very large calcareous septarian concretions are common, often containing plenty of well-preserved fossils and calcite crystals in their centre. From this bed up to 36 m, a thinly bedded section of silty clay occurs (E16) with abundant scales of bony fishes, shark teeth, agglutinating foraminifera, and phosphatic nodules (Figs. 4, S2). Bed E17 is remarkable as it hosts a layer of well-preserved complete colonies of deep-sea corals in horizontal bedding (Fig. S2) and several associated bivalve species (Figs. S2, S6). Calcareous septarian concretions and wood fragments are also present in this layer (Fig. S1). Bed E17 varies laterally between laminated mud and glauconitic sand (Figs. 4, S2). In bed E18, the sandy silt shows lenticular bedding with isolated lenses of fine sand partially disturbed by bioturbation (Fig. 4). This bed also features traces of the foraminifera genus *Bathysiphon*, as well as plant particles. The uppermost bed E19 is typified by more uniform sedimentary fabrics (Fig. S2), consisting of rhythmic thin silty interlayers within muddy laminae featuring weathered pyrite, fish scales and traces of agglutinated foraminifera.

4.2. Petrography of phosphatic nodules

The phosphatic nodules are on average between 1 and 3 cm in size and exhibit varying morphologies. These include spherical to subspherical, angular, oval, and tubular shapes. Thin section analyses show that the nodules are composed almost entirely of cryptocrystalline phosphate (Fig. 5). The typical concretions feature no distinct core (Fig. 5A). Some feature accumulations of detrital quartz grains in the centre (Fig. 5C). A few exceptions reveal a hollow core in the centre and exhibit slight concentric growth rims with a lighter coloured cryptocrystalline phosphate matrix and a darker brownish rim (Fig. 5B). Detrital particles are mainly present as angular quartz grains measuring up to 500 μm in size, as well as occasional glauconite, pyrite, and iron oxihydroxides (Fig. 5C, D). Detrital and biogenic particles are randomly distributed in some nodules (Fig. 5A, B), while in most cases these particles have accumulated in the centre (Fig. 5C). Biogenic particles are present as shell fragments and planktonic foraminifera, whose carbonate shell rims are replaced by cryptocrystalline phosphate (Fig. 5D). Some nodules feature disseminated and framboidal pyrite, which partially grew within the test of foraminifera (Table 3). The phosphatic concretions are mainly composed of apatite (76 to 89 weight percentwt%), with traces of muscovite (1.9 to 8.6 wt%), quartz (3.8 to 7 wt%), dolomite (2.8 to 5.7 wt%), and calcite (1.4 to 4.1 wt%).

4.3. Trace fossils

4.3.1. Burrows

The trace fossil *Thalassinoides* sp. (Fig. S3A) descends from a discontinuity (LM10) down to 20 cm into LM9 (Fig. 4) and is filled with sand that is coarser than the host material. Density of the burrows decreases down the discontinuity. *Thalassinoides* Ehrenberg, 1944 is a crustacean burrow common in shallow marine deposits (Frey et al., 1984; Ekdale, 1992). Another crustacean burrow present is *Ophiomorpha* isp. (LM11; Fig. S3B). Its surface is smooth or covered with large, sparsely and irregularly distributed pellets. The wall is preferentially cemented and locally ferruginized. Moreover, *Ophiomorpha* cf. *annulata* (Książkiewicz, 1977) appears in the layer LM11 (Fig. S3C) and *Ophiomorpha* cf. *irregulaire* Frey et al., 1978 in the layer E2 (Fig. S3F). A longitudinal section of the latter shows a lumen, a wall, and irregular, drop-like protrusions from one side. *Ophiomorpha* Lundgren, 1891 is a dwelling and feeding burrow produced mainly by decapods (Frey et al., 1978).

Macaronichnus segregatis Clifton and Thompson, 1978 (LM11; Fig. S3D) is a feeding trace of polychaetes that segregate grains (e.g., Uchman et al., 2016). It occurs in fine- to medium-grained sand and is filled with lighter grains than in the surrounding. Locally, it is mantled with darker grains. *Piscichnus waitemata* Gregory, 1991 occurs in layer LM13 (Fig. S3E). It is a bowl-shaped depression with a circular to oval outline and filled with coarser material (very coarse pebbly sand) than the host sediment, which is the same as the overlying sand. *P. waitemata* is a ray fish feeding trace (e.g., Uchman et al., 2018).?*Teichichnus* isp. (E2; Fig. S3G) is visible in the vertical section as a single oval structure filled with fine sand and surrounded by muddy sand. At the base and at the top it shows a few stacked laminae, which are convex down or convex up. *Teichichnus* Seilacher, 1955 is a feeding burrow (Knaust, 2018). Tortuously branched, crowded, ferruginized burrows, about 4 mm in diameter are ascribed to *Bornichnus tortuosus* Bromley and Uchman, 2003, which is a polychaete dwelling-feeding burrow (LM7-LM12). Radiating tubes, up top 5 mm in diameter, wrapped up at their termination (LM7-LM12), belong to *Dactyloidites* cf. *peniculus* D'Alessandro and Bromley, 1986, which is a feeding burrow of probably polychaete origin (Uchman and Pervesler, 2007).

4.3.2. Wood borings

Wood borings were found in E1. Club-shaped *Teredolites clavatus* Leymerie, 1842 (Fig. S3H) produced by pholadid bivalves, *Apectoichnus longissimus* Kelly and Bromley, 1984 (Fig. S3H) produced by teredinid bivalves or isopods, and *A. lignummasticans* Melnyk et al., 2020 produced by isopods were identified. Additionally, one occurrence of tongue-shaped *Asthenopodichnium* isp. was found in E17 (Figs. 6L, S3I). One side of the tongue, 7 mm wide and covered with xenoglyphs of wood rings, shows a marginal, low ridge. *Asthenopodichnium* Thenius, 1979 can be produced by mayflies, wood rotting fungi (Genise et al., 2012) or gammarids (Uchman et al., 2007; Uchman, 2011). The large size and tongue-like shape of the specimen described herein suggest mayflies as the producers (cf. Thenius, 1979).

4.4. Pollen and leaves

A total number of 30 pollen taxa of 13 families were identified (Figs. S4, S5; Table 2) by analysing the phosphatic concretions and host sediment, including genera not previously described, from Typhaceae (*Spaganium*), Euphorbicaceae, Fagaceae (*Eotrigonobalanopsis*, *Trigonobalanopsis*), Platanaceae (*Platanus*), Sapotaceae (*Vitellariopsis*-type), and Styracaceae (*Rehderodendron* cf. *microcarpum*) (Figs. 7I, S5).

The pollen taxa reported within this work were assigned to their current geographical distribution and the Koeppen and Geiger classification (Kottek et al., 2006) of climate conditions (Table 2), reflecting mostly the Cfa (Humid subtropical), Cfb (Temperate oceanic), and Cwa (Monsoon-influenced humid subtropical) climate types.

Additionally, needles of Pinacae and various *Daphnogene* taxa were recovered from large septarian concretions and host sediment from lower and upper parts of the Eferding Formation (Fig. S5; E11, E15). These septarian concretions were described by Rupp and Ćorić (2015) as dolomite concretions. Through the previous described leaves from Kovar-Eder and Berger (1987) and newly found *Daphnogene* taxa (Fig. 7H), the following information emerges using CLAMP (Soysal et al., 2017): mean annual temperature (MAT), warm month and cold month mean (WMMT and CMMT), enthalpy (ENTHAL), growing season (GROWSEAS), growing season precipitation (GSP), precipitation during the three consecutive wettest and driest months (3-WET and 3-DRY), relative humidity (RH), and specific humidity (SH) (Table 2). Additionally, one fruiting body of Mycophyta gen. et sp. indet. was collected at E6. It should be emphasised that the exclusive occurrence of thick and leathery leaves, as well as wood fragments and the densely-walled fruiting body mentioned above, suggests a taphonomic bias of the fossil plant remains: only the parts most resistant to water transport and decay were preserved within the Eferding Formation.

4.5. Invertebrates

4.5.1. Anthozoa

Within bed E17, the scleractinian corals are confined to an approx. 5 cm thick lens of about 6–8 m in horizontal extent, which is composed of a slightly coarser matrix than the under- and overlying beds. The colonies are horizontally bedded, with several colonies stacked upon each other, and are preserved entirely apart from internal fracturing owing to diagenetic compaction of the sediment. Although surface details and the cups with the septa are preserved, the skeleton is very friable, thus indicating little or no neomorphism of the aragonitic skeleton. While a preliminary study suggests that the species may fall within the morphological range of variability of the modern deep-sea coral *Madrepora oculata* Linné, 1758 (A. Vertino, pers. comm. 2021), which today lives in depth between 200 and 3000 m (Cairns et al., 2009), a detailed analysis of the coral is beyond the scope of the present paper.

4.5.2. Echinodermata

Samples from the Eferding Formation from beds E17 and E18 yield disarticulated spines of unidentifiable cidaroid and spatangoid echinoids. Despite the apparent variability of ornamentation of the Eferding cidaroid spine fragments only a single taxon of cidaroids could be identified which is clearly different from those reported from other Cenozoic localities in the Paratethys (compare cidaroid material illustrated in Kroh, 2005). The fact that nearly smooth, as well as spines ornamented with sharp ridges bearing short thorns are present, is a result of variable preservation conditions. Based on the spiral pattern of perforations in the inner cylinder (see discussion in Schlüter et al., 2015), the second type of spines can be attributed to the order Spatangoida.

4.5.3. Bivalves

There are four bivalve species: gryphaeid *Neopycnodonte navicularis* (Brocchi, 1814), pectinid *Delectopecten vitreus* (Gmelin, 1791), propeamussiid *Propeamussium semiradiatum* (Mayer, 1861), and limid *Ctenoides* aff. *Eximia* (Giebel, 1864) (Fig. S6A–J). They all are members of the infraclass Pteriomorphia, characterized by calcite shells and an epibenthic mode of life (Carter, 1990). All species, except for the free living, carnivorous *P. semiradiatum* where identified from the coral interbed (E17). However, only the byssally attaching, suspension feeder *C.* aff. *eximia* is confined to the coral accumulation.

Neopycnodonte navicularis (Figs. 7B, S6A–D) is of small to moderate in size, with the largest specimens attaining 4 cm in length. *Propeamussium semiradiatum* was photographed directly at the outcrop (Fig. S6E) showing fragmented right valve attaining ~25 mm in length with around 6 prominent interior ribs reaching up to 3/4 of shell length.

Delectopecten vitreus specimens (Figs. 7C, S6G–H) are small-sized, weakly biconvex, with rounded disc outlines and thin and transparent

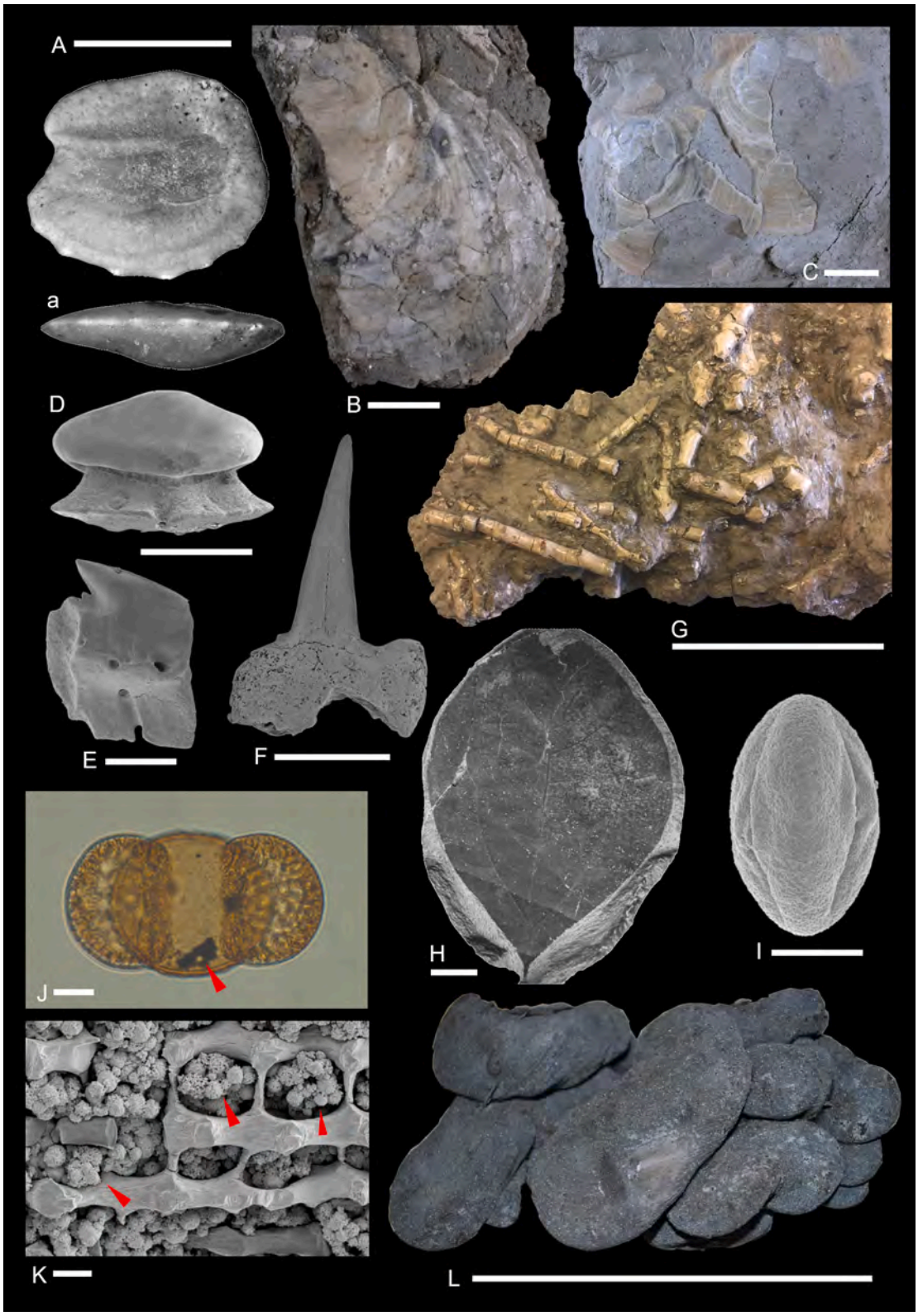

Fig. 7. Representative fossils of the Eferding Formation.
Representative fossils from the Eferding Formation at Unterrudling described in this study: (A,a) *Diaphus* aff. *kokeni,* right sagittae in inner and ventral view, scale: 1 mm; (B) *Neopycnodonte navicularis* left valve, scale: 5 mm; (C) *Delectopecten vitreus* left valve and right valve, scale: 5 mm; (D) *Raja* sp., scale: 400 μm; (E) *Etmopterus* sp. lower jaw, scale: 400 μm; (F) Dalatidae indet. upper jaw, scale: 1 mm; (G) *Madrepora* sp., scale: 10 cm; (H) *Daphnogene cinnamomifolia*, scale: 1 cm; (I) *Rehderodendron* cf. *microcarpum* equatorial view, scale: 10 μm; (J–K) Framboidal pyrite (red arrows): (J) in *Pinus* sp. pollen grain, scale: 10 μm, (K) in echinoid spine, scale 20 μm; (L) *Asthenopodichnium* isp., scale: 5 cm. (For interpretation of the references to colour in this figure legend, the reader is referred to the web version of this article.)

shell-walls. The exterior shell surfaces are smooth, except for thin scally riblets present on the right anterior ear and anterodorsal disc margin. Very fine incremental lines are observable with few minute nodes on the anterodorsal disc area, and *Camptonectes*-type microsculpture is present with long ears, anteriorly separated from the disc.

Ctenoides aff. *eximia* (Fig. S6I–J) is the most abundant bivalve in the section, and is found exclusively in the coral bed. It has a very thin and fragile, weakly convex shell with a height of about 20 mm and a rounded, drop shaped outline as feature. It is broadly rounded ventrally and truncated dorsally. The posterior ear shows a small depression which continues to disc outline. The anterior ear is missing. The surface shows up to 73 min slightly undulate and rarely scaly riblets with narrow interspaces, divaricating at the central disc axis which is a diagnostic feature for this genus (Mikkelsen and Bieler, 1989).

4.5.4. Foraminifera

The reevaluation of the analysed faunas of Rupp and Ćorić (2015) allowed calculating several palaeoenvironmental parameters for the Eferding Formation based on benthic foraminifera. All statistical results can be seen in Fig. 8 and the Supplementary Material (Table S1). The calculated salinity values vary from 34 to 36 PSU and indicate fully marine deposition throughout the whole section. Furthermore, all analysed samples are dominated by hyaline species (89–100%) that prefer muddy sediments as habitat with a general increase in muddy sediment dwellers up section (E1–E3: 60–70%, E4–E12: 87–87%, E13–E19: 89–96%).

Water depth calculations (Fig. 8D) after Hohenegger (2005) and Báldi and Hohenegger (2008) showed three shifts in the section. Samples from the layers E1–E3 were deposited within 50–60 m depth, the interval from sample E4–E12 was slightly deeper with depths of 60–110 m (deepest E11 and E12). Within this interval a sudden increase of water depth was recognized from sample E9–E10 (30 m). The deepest interval comprises samples E13–E19 and varies from 90 to 150 m. Thus, a general up section deepening can be observed. Water depth calculations based on the P/B ratio after Van der Zwaan et al. (1990) gives greater water depths for intervals E1–E3 (80–150 m) and E12–E19 (70–340 m), whereas the interval E4–E12 gives lower values (40–70 m) than the benthic calculations.

Calculated bottom water temperatures (Fig. 8E) in samples E1–E12 are rather constant and vary from 9 to 13 °C (11 °C mean temperature) and decrease slightly upsection (E13–E19) varying from 7 to 11 °C (9 °C mean temperature). Results indicated in Fig. 8C suggest comparably well oxygenated conditions for the interval E1–E3 with the highest amount of oxic indicators in sample E1. Bottom water conditions for the interval from E4–E19 can be characterized as sub-oxic (less than 12% oxic indicators). The feeding strategies and mode of life of foraminifera (Fig. 8A, B) as well as dissolved oxygen categories are shown (Fig. 8C). Deposit feeding infaunal species generally dominate the assemblages, but within the interval E1–E3 up to 27% of the species lived herbivore and 28–35% are epifaunal (vagile) and 20–30% epifaunal (sessile). Interval E4–E12 shows a high dominance of deposit feeding (91–96%) infaunal (68–87%) species, whereas herbivores and suspension feeders account for less than 5%, and epifaunal (vagile) species are represented by up to 26% (E11). The interval E13–E19 is also dominated by deposit feeders (89–95%) with up to 7% suspension feeders (E15); infaunal species are dominant (55–89%) but frequently accompanied by epifaunal (vagile) species (up to 21–41% from E14 and E17–19).

4.6. Vertebrates

4.6.1. Chondrichthyes

The elasmobranch teeth of the layer near the coral occurrences (E17) reveal a peculiar faunal composition of squalomorph sharks identified as *Etmopterus* sp. (Figs. 7E, S7A–B), *Palaeocentroscymnus*

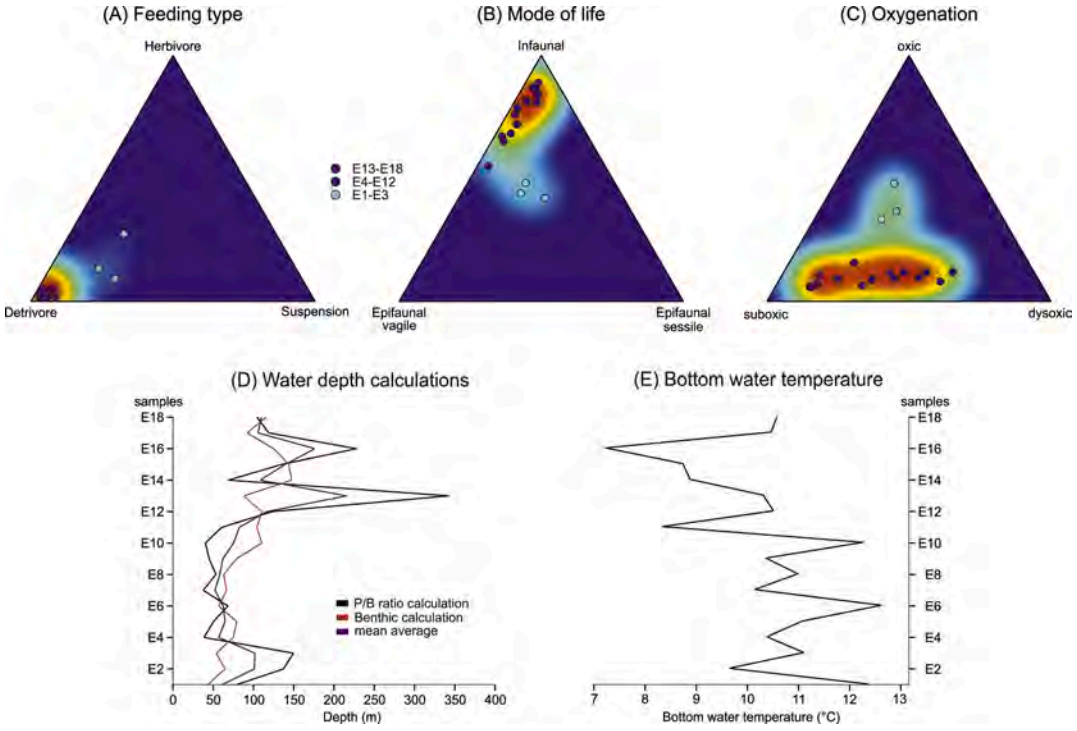

Fig. 8. Foraminifera.
Ternary diagrams with density map (violet = extremely low abundance, light blue = low abundance, green and yellow = moderate abundance, orange and red = high abundance) plotting percentages per sample regarding feeding type (A), mode of life (B) and oxygenation (C), light blue stands for samples E1–E3, dark blue stands for samples E4–E12 and green for samples E13–E18. Water depth (D - red line) and bottom water temperature (E) are based on the calculation using the formula of Hohenegger (2005) and Báldi and Hohenegger (2008). The black line in (D) displays depth values calculated with P/B ratios using the formula of Van der Zwaan et al. (1990), the blue line shows the mean average of both water depth calculations. The grey bar in (D) and (E) marks the confidence interval of the calculations. (For interpretation of the references to colour in this figure legend, the reader is referred to the web version of this article.)

horvathi (Underwood and Schlögl, 2013) (Figs. S7C-D), an undescribed dalatiid species (Figs. 7F, S7E-F), and *?Centroselachus* sp. (Fig. S7G–H). Additionally, to the majority of Squaliformes, scattered teeth of the order Hexanchiformes (*Heptranchias* sp. (Fig. S7N–O) and *Notorynchus primigenius* (Agassiz, 1835) (Fig. S7Q), Echinorhiniformes (*Echinorhinus schoenfeldi* Pfeil, 1983, and Lamniformes (*Alopias exigua* (Probst, 1879) (Fig. S7K)) accompanied the assemblage. Further teeth of various horizons of the section include a symphyseal tooth of a hexanchid (Fig. S7P), *Echinorhinus* sp. (Fig. S7I), *Isurus* sp. (Fig. S7L), *Carcharias acutissimus* (Agassiz, 1843) (Fig. S7M), *Raja* sp. (Figs. 7D, S7R), and dermal denticles of a drag reduction- and squatinid type (Fig. S7S–T).

4.6.2. Osteichthyes

The otolith assemblage comprises around 40 otoliths of *Diaphus*, two specimens of *Coelorinchus* sp., a single specimen of "aff. *Raniceps*" aff. *coelorinchoides* (Nolf and Brzobohatý, 1994) and several fragments and otoliths that are strongly corroded and unidentifiable. Among all *Diaphus* otoliths, only six were relatively well preserved (Figs. 7Aa, S8Aa–Ee). They were tentatively assigned at species level because each species was represented by only one or few otoliths, thus preventing an assessment of their intra- and interspecific variability. The remainder of the *Diaphus* otoliths was corroded and not identifiable (Fig. S8F).

Diaphus cf. *cahuzaci* Steurbaut is characterized by a relatively round shape, a relatively short rostrum, clear excisura and small antirostrum (Fig. S8E). In ventral view it is visible that the outer face is evenly convex and slightly thinning anteriorly (Fig. S8e). This otolith corresponds well to the drawings of *Diaphus cahuzaci* in Brzobohatý and Nolf (2000: pl. 5, figs. 1–6). *Diaphus* aff. *kokeni* (Prochazka) is the only species that is represented by more than one otolith in the material at hand (totally three otoliths, two shown on Fig. S8Bb–Cc). These otoliths correspond relatively well to the similarly-sized otoliths of *D. kokeni* depicted in Brzobohatý and Nolf (2000: pl. 2, figs. 1–6). They differ in their more rounded shape and an only finely undulating ventral margin (vs. clearly serrated ventral margin in *D. kokeni*). *Diaphus* aff. *pristimetallis* Nolf and Brzobohatý has a somewhat similar overall shape (Fig. S8A) and also a similar contour in ventral view (Fig. S8a) as seen in *D. pristimetallis* (see Nolf and Brzobohatý, 1994: pl. 4, figs. 9–14). However, it does not display the almost semi-circular ventral rim with multiple serrations that is typical for *D. pristimetallis*. *Diaphus* aff. *taaningi* Norman has an overall shape that conforms relatively well to the otoliths of *D. taaningi* shown in previous works (Brzobohatý and Nolf, 2000: pl. 2, figs. 7–12; Schwarzhans, 2013: pl. 4, figs. 7–15). The present otolith differs from *D. taaningi* as its ventral rim is only finely undulating (vs. clearly serrated in *D. taaningi*). "aff. *Raniceps*" aff. *coelorinchoides* is similar to the drawings of genus "aff. *Raniceps*" *coelorinchoides* in Nolf and Brzobohatý (1994: pl. 8, figs. 1–6) (see also Nolf, 2013: pl. 122), but its dorsal margin is clearly more elevated resulting in a high-triangular shape (vs. longish-triangular in "aff. *Raniceps*" aff. *coelorinchoides*).

Coelorinchus sp. (Fig. S8Hh) reveals an overall shape and sulcus similar to otoliths of *Coelorinchus*, but the outer face is almost smooth, in contrast to the ornamented face with lobes and bulges in typical *Coelorinchus*.

Most of the otoliths display strong corrosion or signs of etching and many otolith fragments are present. It is remarkable that several otoliths show well preserved outer faces, but strongly corroded inner faces, or vice versa. An example shown on Fig. S8G is the otolith of "aff. *Raniceps*" *coelorinchoides*: its outer face does not show any signs of corrosion (Fig. S8g), while the inner face is porous and overgrown by black, possibly phosphatic material (Fig. S8G).

5. Discussion

5.1. Biostratigraphy and palaeobiogeography

The new findings of bivalves, chondrichthyes teeth and otoliths from the Eferding Formation at Unterrudling provide a biostratigraphic frame (Fig. 2) and a better understanding of the palaeobiogeography of the NAFB.

The bivalve *Neopycnodonte navicularis* is the oldest record of this species previously thought to be confined to the Neogene (Mandic et al., 2020). The oldest occurrence of the genus is documented in the lowermost Oligocene of the North Sea Basin (Marquet et al., 2012). In the Central Paratethys, *N. navicularis* is common in the middle Miocene, in particular in the middle–upper Badenian deep-water sediments (Mandic et al., 2019a, 2019b). *Propeamussium semiradiatum* was already documented from the Eferding Formation of Unterrudling as *Propeamussium* (*P.*) sp by Schultz (2001). *P. semiradiatum*, originally described from the lower Oligocene of Häring in Tyrol (Löffler, 1999), was distributed throughout the Paratethys, found in related strata of the northern Hungary (Báldi, 1986), northern Bulgaria (Karagiuleva, 1964), and the southern Russia (Korobkov, 1939). Aside from the study site, its upper Oligocene record includes only central Slovenia, where *P. mojsisovici* (Bittner, 1884), originally described from the Govce Fm (Kuščer, 1967), represents its younger synonym (Báldi, 1986; this study). The collected *Delectopecten* specimens are highly similar with specimens living today off Iceland described by Dijkstra et al. (2009). Even the young adult specimen from Unterrudling (Fig. S6F) with increased ear height and a slightly coarser microsculpture corresponds well with the phenotypic variation documented by the latter study. This is the oldest known record of the species, and except for a questionable record from the upper lower Miocene of northern Italy reported by Sacco (1897), its stratigraphically oldest record by previous studies was from the middle Miocene of Central Paratethys (Studencka et al., 1998; Studencka, 2015). The oldest confident records from the Mediterranean (Ceregato et al., 2007) and the North Sea Basin (Marquet, 2002) date to the Pliocene. The last identified genus *Ctenoides* originated in the middle Eocene of the Paris Basin by *C. distropha* (Deshayes, 1860). In the early Oligocene it was present with *C. eximia* in the North Sea Basin (Koenen, 1883), proto-Mediterranean (Sacco, 1898), and eastern proto-Paratethys (Popov et al., 1993). Mikkelsen and Bieler (1989) demonstrated that *Ctenoides* have a highly variable outline and rib numbers, differing mostly by microsculptural features. Considering their stratigraphic difference, the found specimens presumably represent a different species. The comparison to the European Neogene record is not possible at the moment as stated above, yet the Miocene specimens appear distinctly larger (>3 cm height) (Sacco, 1898).

In addition, considering the palaeobiogeography and the stratigraphic occurrence of the most significant and newly described chondrichthyes species of the Eferding Formation, teeth of *Palaeocentroscymnus horvathi* were previously only documented from Miocene sediments (Pollerspöck et al., 2018) and are particularly common in sediments of the Ebelsberg Formation (upper Egerian, Aquitanian, lower Miocene). The undescribed dalatiid species has only been found in the Ebelsberg Formation of Wallern (Upper Austria, own data) so far and awaits description. Teeth of the genus *Etmopterus* are general rare within the fossil record and limited to a few localities, e.g., in France (Ledoux, 1972), Switzerland (Bolliger et al., 1995), Germany (Pollerspöck and Straube, 2017), Austria (Pollerspöck et al., 2018; Pollerspöck et al., 2020), and Slovakia (Underwood and Schlögl, 2013). None of the other known Oligocene faunas of the NAFB, e.g., Thalberg Beds (Reinecke et al., 2014), Schöneck Fm. (formerly "Fish Shale", Pfeil, 1981) or Miocene faunas of the upper Egerian Ebelsberg Formation, e.g., at Graben and Traunpucking (Pollerspöck et al., 2018) possess a similar domination of squalomorph sharks. In addition to the newly recorded squalomorphs, teeth of the lamniform *Alopias exigua* were to date unknown from the Oligocene deposits of the Eferding Formation (Schultz, 2001) but reported from equivalent sediments of the Thalberggraben in Germany (Reinecke et al., 2014).

For the findings of teleost remains the type of corrosion indicates that an etching process happened in situ at the location where the otoliths were embedded. If the corrosion would be related to transport, both sides of the otolith should be affected. Otoliths from Oligocene marine deposits of the Central Paratethys have previously been described from

the Eger Formation and the underlying Kiscell Formation near Eger (Hungary, Central Paratethys; Nolf and Brzobohatý, 1994). Both formations revealed a diverse marine fish fauna, pointing to an open marine, deep water environment. Moreover, the species composition was clearly different in each of the formations, with only three mutual species (Nolf and Brzobohatý, 1994).

In the Kiscell Formation, Myctophidae were represented with *Diaphus pristimetallis* (Nolf and Brzobohatý, 1994), which was the third most abundant species of the respective otolith assemblage (Nolf and Brzobohatý, 1994: table 1). A species that could be related to *D. pristimetallis* occurs in the material excavated from the layer near the coral-rich horizon (E17), but only a single otolith is present. Also, in the Eger Formation near Eger, Myctophids occurred in considerable numbers (about 50 otoliths); they were left in open nomenclature as *Diaphus* sp. by Nolf and Brzobohatý (1994). Two of those *Diaphus* sp. otoliths were illustrated (see Nolf and Brzobohatý , 1994: pl. 7, figs. 4–5); they differ in their very well-rounded dorsal margin from the here present *Diaphus*, which possesses a relatively flat dorsal margin. For a further comparison with the *Diaphus* otoliths from the Eger Formation near Eger, it would be necessary to inspect the entire material summarized as *Diaphus* sp. in Nolf and Brzobohatý (1994). From the early Miocene (Aquitanian), three nominal species of *Diaphus* have been reported in Brzobohatý and Nolf (2000), namely *D. cahuzaci* (Steurbaut, 1979), *D. regani* (Tåning, 1932) and *D. haereticus* (Brzobohatý and Schultz, 1978). Among those, only *D. cahuzaci* might be present in the material at hand. The other two species recognized in the material from the layer are similar to *D. taaningi* and *D. kokeni*, which have previously been described from the Burdigalian and Langhian (see Brzobohatý and Nolf, 2000).

In summary, the *Diaphus* species assemblage from the quarry seems to be different from previously reported *Diaphus* assemblages from the Oligocene or early Miocene. However, for an exact time allocation only an absolute dating can provide information on the age of the Eferding Formation.

5.2. Palaeoenvironment

5.2.1. Depositional environment

The facies of the Linz-Melk Formation at Unterrudling is characterized by a well-sorted sand, mainly composed of quartz and feldspar (Fig. 6). Gravel layers with a fining upwards tendency are intercalated periodically. The trace fossil *Macaronichnus,* which is often responsible for the obliteration of sedimentary structures (Pemberton et al., 2012), is very abundant. Thick units of reworked sand with *Macaronichnus segregatis* occur in well-oxygenated marine sediments of the upper foreshore environment (Pemberton et al., 2001; Bromley et al., 2009; Uchman et al., 2016). Consequently, only relics of sedimentary features are visible in a few beds (LM3, LM12, LM16, LM18) (Fig. 4), indicating large-scale cross-bedded submarine sandwaves. Similar nearshore facies of the Linz-Melk Formation were discussed in Roetzel et al. (1983) in the area between Krems and Melk and were interpreted as breakerzone deposits. In addition, large-scale cross-bedded sections, which are affected by bioturbation occur in the Linz-Melk Formation (Krenmayr and Roetzel, 2000a, 2000b) and were interpreted as submarine sandwaves in nearshore and shelf areas produced by high current velocities (Kulm et al., 1975). Such mega-scale bed forms also exist in the Molasse Basin of France (Kalifi et al., 2020) and are globally common in shelf environments (Bradshaw et al., 1991). Consequently, the observed sandwaves in Unterrudling are interpreted as deposited in foreshore to shoreface environments. This facies of the Linz-Melk Formation is comparable to high energy deposits described beneath the low water line by Freeman and Visher (1975). Waterdepths of 2 to 6 m can be expected (Reinecke and Singh, 1980).

The gravel layers interrupt normal sedimentation. Erosional surfaces at the base are common and are genetically different from the homogeneous medium to coarse grained sands described above. Observations along the North Sea coast suggest that gravel interlayers represent proximal deposits of storm events (Aigner and Reineck, 1982; Antia et al., 1994). A fining upwards trend, following the coarse-grained sedimentation and the re-establishment of benthic communities, indicated by trace fossils is typical for tempestites (Hunter and Clifton, 1982). Coarse sediments could have also been deposited in the basin by adjacent estuaries (Roetzel et al., 1983; Harzhauser and Mandic, 2001), inferring a riverine or deltaic depositional environment (Gingras et al., 2012). However, massive conglomerates, incised channels and brackish faunal communities are missing in Unterrudling, which would be expected in these environments (Gingras et al., 2012; Kalifi et al., 2020). Consequently, the high amount of sandy material in the Linz-Melk Formation and tempestite layers are indicative of a wave dominated shoreline (Swift et al., 1986; Anthony and Orford, 2002), strongly influenced by periodic storm events (Lin and Bhattacharya, 2020). The trace fossil *Ophiomorpha* in the bed LM11 indicates shallow marine conditions, as it is most abundant in the lower foreshore – upper shoreface zone (Frey et al., 1978, 1984; Pemberton et al., 2001). On the other hand, several specimens were identified related to the species *Ophiomorpha annulata* which is mostly known from deep-sea deposits (Uchman, 1998, 2001). Anyhow, the specimens found herein are larger and morphologically more similar to specimens described from Cretaceous shelf deposits (Howard and Frey, 1984; Frey and Howard, 1985). Consequently, those traces are described herein as *O.* cf. *annulata* and correlated to a shelf environment. *Piscichnus waitemata* (LM13, LM19) is interpreted as ray-fish feeding trace, it occurs mostly in the intertidal zone up to the fair-weather wave base (Uchman et al., 2018). *Thalassinoides* occurs in the bed LM9, it is common in deposits of variable, presumably shallow marine environments (Frey et al., 1984; Mángano and Buatois, 1991; Pemberton et al., 2001). It is produced mostly by scavenging and deposit-feeding crustaceans (Ekdale, 1992; Bromley, 1996; Schlirf, 2000). *Bornichnus tortuosus* originally described from tidal flat deposits (Bromley and Uchman, 2003) can occur also from shoreface to slope settings (Knaust, 2017). *Dactyloidites peniculus*, represented by *D.* cf. *peniculus* from the Linz-Melk Formation occurs typically in shoreface environments (Uchman and Pervesler, 2007). Other trace fossils (*Ophiomorpha*, *Thalassinoides*, *Piscichnus*, *Dactyloidites*, *Bornichnus*) can be ascribed with some caution to the impoverished proximal *Cruziana* ichnofacies, which is typical of the lower shoreface (Pemberton et al., 2001).

The mixed muddy-sandy and highly bioturbated lower part of the Eferding Formation (E2), rich in glauconite and pyrite, is similar to the sedimentary facies deposited in the transition zone of the inner shelf and foreshore in open oceanic conditions (Kulm et al., 1975; Reinecke and Singh, 1980). In open oceanic settings water depths of 8 to 30 m are typical for this zone (Nummedal et al., 2001). In contrast, the foraminifera data and depth indication of bivalves infers a slightly deeper environment. With increasing water depth in this zone, the wave energy is decreasing and the suspended terrigenous and pelitic material settles down (Longhitano, 2008; Schäfer, 2020). On the other hand, sandy material is washed in by currents and storms (Kulm et al., 1975). Bioturbation of the sandy material and intermixing with the predominantly muddy sediment sets in after storms calm down (Kulm et al., 1975; Schäfer, 2020). This fine-grained material (Fig. 6) produces the dark muddy matrix and the poor sorting, which typifies the Eferding Formation (Roetzel et al., 1983). In the lower part of the Eferding Formation a still quite shallow environment is indicated, but as *Teredolites clavatus* is produced by teredinid bivalves, which bore into wood, nut shells, peats and amber (Kelly and Bromley, 1984; Mayoral et al., 2020) and is common in shallow-marine transgressive deposits (Savrda et al., 1993). The trace fossil *Teichichnus* found in the bed E2 is a typical feeding structure in several marine facies, common in calmer, lagoonal environments (Knaust, 2018).

The muddy deposits from the layer E3 upwards, with lenticular bedding and lamination indicate decreasing current velocities, which is best interpreted as an environment beneath the storm wave base (Reinecke and Singh, 1980), where sedimentation rates are low and fine

material dominates (Schäfer, 2020). This facies indicates a greater distance to the coast (Fig. 1B) and water depths ranging from 130 to more than 200 m (Reinecke and Singh, 1980; Schäfer, 2020). However, following the calculations from the foraminifera water depths of 50 to 130 m are expected in these layers. The silty lenticular bedding also reveals input from proximal regions by storm events or tidal currents (Aigner and Reineck, 1982; Bradshaw et al., 1991). According to Kulm et al. (1975) fine sand and silt is held in suspension in a mid-water layer and can thereby be transported far onto the shelf. The rather restricted palaeogeographic conditions in the NAFB are often difficult to compare to open oceans and large shelf areas in terms of sedimentation. Consequently, it is beneficial to use ecological preferences of faunal elements for detailed bathymetric reconstruction. For instance, the foraminiferal assemblages and shark species clearly show a shelf environment for the Eferding Formation (Rupp and Ćorić, 2015; Feichtinger et al., 2019a). The uppermost part of the Unterrudling section is dominated by a rhythmic lamination of clay, silty interlayers are absent. These bedding types indicate ongoing deepening and less turbulent conditions. In today's oceans laminated muddy sediment occurs on the outer shelf, close to the shelf break, where density layering is dominant (Schäfer, 2020). A deeper depositional environment can be excluded, as the carbonate content is very high and typical slope or deep-sea sediments, such as turbidites and oozes, are absent (Veeken, 2007). The rather homogeneous appearance of the sediment is only disturbed by large (>1 m) calcareous concretions and marlstone beds (Fig. S2). These concretions are generally very common in the Eferding Formation (Rupp and Ćorić, 2015) and in equivalent Oligocene deposits of the NAFB (Roetzel et a., 1983). Large calcareous concretions of various shapes and sizes are common throughout the Phanerozoic (Coleman, 1993; Coleman and Raiswell, 1995; Seilacher, 2001). They are most common in sandstones and mudstones where they protrude from host deposits, which are usually softer and less well cemented than the concretions themselves (Marshall and Pirrie, 2013). The concretions from the Eferding Formation are likely formed as an early diagenetic product after sedimentation of the fine-grained muds (Selles-Martinez, 1996; Seilacher, 2001). Evidence for an early diagenetic formation of the calcareous concretions from the Eferding Formation comes from the exceptionally well-preserved fossils, such as plant fossils (Roetzel et al., 1983; Kovar-Eder and Berger, 1987). Moreover, continued concretion growth requires a constant influx of solutes towards the locus of carbonate precipitation (Raiswell and Fisher, 2004; Mozley and Davis, 2005). Concretions from the Eferding Formation most likely started to form shortly after sediment deposition, triggered by constant flux of saturated pore waters and microbial degradation of organic matter within the sediments.

5.2.2. Terrestrial environment and climate

The assemblage of the encountered pollen taxa is similar to the microfloras described previously by Klaus (1971) and Hochuli (1978) from the middle and upper layers of the Eferding Formation. The new results of this study corroborate the hypothesis of Klaus (1971), Hochuli (1978), Kovar-Eder and Berger (1987), and Utescher et al. (2020) in which the surrounding area was most likely covered by an evergreen and deciduous mixed forest composed of woody and herbaceous gymnosperms (e.g., *Ephedra*, *Pinus*, *Picea*, *Cathaya*, *Tsuga* cf. *diversifolia*) and angiosperms (e.g., *Trigonobalanopsis*, *Quercus*, *Betula*, *Carpinus*, *Engelhardia*) during the late Oligocene. However, the recent discoveries allow a deeper insight into the prevailing conditions. Surrounding areas with a mid to high altitude can be assumed based on the findings of the gymnosperms *Tsuga*, *Abies*, *Picea*, and *Cathaya* (Jiménez-Moreno et al., 2008). In addition, the pollen from *Eotrigonobalanopsis* sp. and *Fagus* sp. are also an important indicator for prevailing mixed mesophytic forests of the Paleogene in Europe (Denk et al., 2012; Özer et al., 2017). On the other hand, *Sparganium* sp., as a representative of the aquatic, marsh, and swamp plant family Typhaceae indicates a proximity to freshwater. *Sparganium* are commonly found in temperate and tropical regions of the world (IPNI, 2020; Soysal et al., 2017). Since there is no other taxon indicative of such an environment throughout the profile, it is assumed that storm events washed these types of pollen grains, leaves, and other plant materials into the depositional site. Such freshwater environments with coastal brackish settings developed at that time along the western coast in Bavaria (Lower Freshwater Molasse), in the Gallneukirchen Basin and south of the Horn Basin (Doppler et al., 1996; Nehyba and Roetzel, 2010). The genus *Rehderodendron* is a genus with a restricted recent distribution in Asia (China, Vietnam and Myanmar; IPNI, 2020) comprising five species of small deciduous trees (Fritsch et al., 2001). The fossil pollen taxon found within the Eferding Formation is most similar to pollen of the extant *Rehderodendron* cf. *microcarpum*, which thrives in a warm temperate humid climate with dry winters and hot to warm summers (Cfa, Cwb after Kottek et al., 2006). The *Vitellariopsis*-type pollen (Sapotaceae) and Oleaceae pollen (cf. *Fraxinus* and *Phillyrea*), also indicate a warmer climate since their modern equivalents occur in warm-temperate to tropical zones of Eurasia and Africa (IPNI, 2020). Woody semi shrubs, shrubs, and trees of the family Euphorbiaceae are found in the subtropics and tropics as well, while the herbaceous plants of this family occur worldwide in temperate to tropical zones (POWO, 2019).

The CLAMP analysis of the fossil leaves described by Kovar-Eder and Berger (1987) are gymnosperms, such as Pinaceae, and angiosperms, such as *Dicotylophyllum*, *Myrica lignitum*, aff. *Quercus sprengeli*, *Platanus neptuni*, Lauraceae gen. et sp. indet, and *Daphnogene,* together with our newly found specimens of *Daphnogene* sp., and Mycophyta gen. et. sp. indet (Fig. S5H–K). This suggests that the area was surrounded by a mixed forest with an annual mean temperature (MAT) of 15–22 °C (20.6 °C mean temperature) and a mean precipitation (GSP) of 150–250 mm (169.3 mm). These results are similar to conditions found in South-East Asia today (Cfa, Cfb, Cwb, Cwa; after Kottek et al., 2006). The calculated continental climate during the Oligocene corresponds with the global developments in Europe and fits with higher temperatures of the latest Chattian (Zachos et al., 2001a, 2001b; Mosbrugger et al., 2005). Precipitation was quite high throughout the Oligocene with mean annual values of 1500 mm (Mosbrugger et al., 2005). Noteworthy is the rising seasonality with an annual variation of 20 °C since the closure of the Tethys Ocean and the concomitant subsidence of the NAFB. However, it should be emphasised that the leaves mentioned are all thick, leathery and robust, thus this selection was probably taphonomically biased. Nevertheless, the distribution of today's relatives of the newly identified genera (*Spaganium*, *Eotrigonobalanopsis*, *Platanus*, *Vitellariopsis* and *Rehderodendron* cf. *microcarpum*.) suggests climatic conditions and a floral composition similar to other Oligocene sites (cf. Özer et al., 2017; Utescher et al., 2020) and makes an attribution of the Eferding Formation to the upper Oligocene/lower Miocene most likely.

5.2.3. Phosphogenesis and eutrophication

Today, phosphogenesis is a common process in upwelling regions, where it is observed close to the sediment-water interface in suboxic to anoxic sediments (Föllmi, 1996). In the present case, phosphogenesis is manifested by the formation of small phosphatic nodules. The phosphatic precipitates from layers E7, E10, E12, and E16 are addressed as nodules herein due to their variety of irregular shapes and small size, yet their occurrence and relation to the host sediments are similar to those of larger phosphatic concretions (Scasso and Castro, 1999). Phosphatic nodules, albeit less common in the geologic record than carbonate nodules and concretions, have been reported by numerous studies and typically form as in situ precipitates during early diagenesis (Scasso and Castro, 1999; Fazio et al., 2007; Hall and Savdra, 2008). Such nodules require very specific environments for growth. Phosphorus concentrations in the oceans are very low, and its high mobility in marine sediments allows it to accumulate only under specific conditions (Glenn et al., 1994; Föllmi, 1996). Eutrophic conditions as suggested by the undisturbed sedimentation, with only little bioturbation and high organic carbon content in the Eferding Formation would have provided ideal conditions for phosphorus accumulation in pore waters, where

organic matter is the main source of phosphorus (cf. Arning et al., 2009). Organic remains in the form of fish debris and plant debris are abundant, often accompanied by mica-rich sandy sediment. This lithology occurs in particular in those layers that feature phosphatic nodules. Such deposits of mobilized terrestrial debris are often observed after storm events (West et al., 2011), when coastal sediments are reworked (Goodwin et al., 2020). The wood fragment found in the Layer E17 even shows the boring *Asthenopodichnium* isp. (Fig. S3), which is a fresh-water boring produced in wood by mayflies (Thenius, 1979). Therefore, it can be assumed that reworking of terrestrial sediments and coastal runoff of organic-rich material into the nearshore marine environment was high. Probably, logs infested by mayflies were transported to the sea by rivers, and the borings were filled with sand and preserved as casts after deposition and coalification. Inundation of forested coastal plains is expected in transgressive conditions. Furthermore, the layers E5, E9, E11, E13, E15, E17 often feature lithified areas of glauconitic sandstone or marlstone beds. Glauconite is often correlated with transgressive phases, where its formation is facilitated, among other factors, by the decay of organic matter related to microbial sulphate reduction (McRae, 1972; Baldermann et al., 2013). Microbial activity is important in liberating phosphorus from organic matter in suboxic to anoxic conditions (Benitez-Nelson, 2000). The low oxygen concentrations in bottom waters of the Eferding Formation, as suggested by the distribution of foraminifera and shark species, would have favoured organic matter preservation, phosphorus delivery to sediments, and the possible proliferation of anaerobic microbial communities. Although sulphide-oxidizing bacteria are key agents of phosphorite formation in upwelling zones today (Schulz and Schulz, 2005; Goldhammer et al., 2010), there is no evidence for sulphide oxidation in the phosphatic nodules or the host sediments such as body fossil remains of Beggiatoacea. Without such evidence, only the occurrence of framboidal pyrite within the nodules (Fig. 5D) may suggest a dependence of phosphogenesis on the sulphur cycle, with microbial sulphate reduction as a catalyst for liberating phosphorus from sedimentary organic matter (Alsenz et al., 2015).

Phosphogenesis is intimately linked to the sedimentary sulphur cycle, where the interaction of bacterial sulphide oxidation and sulphate reduction have been shown to promote the precipitation of phosphate minerals in marine, organic matter-rich sediments (Arning et al., 2009). Organoclastic sulphate reduction is a ubiquitous process in modern marine sediments, capable of accumulating phosphorus and precipitating phosphorite minerals such as apatite (Van Cappellen and Berner, 1991; Berndmeyer et al., 2012). The presence of dolomite in the phosphatic nodules agrees with an early diagenetic environment typified by pronounced microbial sulphate reduction (cf. Vasconcelos et al., 1995). Interestingly, beds of early diagenetic dolomite occur in the Miocene Monterey Formation (USA), which is also known for its abundant phosphorites (Hoffmann-Sell et al., 2011). The low sedimentation rates of terrigenous material for the shelf environment above layer E3, as suggested by fine-grained, muddy deposits, would have also favoured the accumulation of phosphorus on a high-productivity shallow marine shelf (Filippelli, 2011). It is therefore feasible that sulphate-reducing bacteria degraded the preserved organic matter, liberated phosphorus to solution, and enabled the formation of phosphatic nodules and the precipitation of pyrite in the Eferding Formation. In addition, the pollen grains extracted from the phosphatic nodules show both internal residues of authigenic pyrite and traces of bacteria on external sculptures (compare Fig. 7J, K).

Whether eutrophication in the photic zone, which enabled the formation of phosphatic nodules, was caused by upwelling, by organic carbon input from coastal runoff, or a combination of both is a matter of discussion. Nutrient-rich waters are common in oceanic basins with a positive water balance, where evaporation is compensated by freshwater input and humid climate, which are both confirmed for the NAFB during the Egerian (Pippèrr, 2011). Coastal discharge and efficient input of nutrients would have stimulated primary productivity and the drawdown of oxygen in the shallow nearshore shelf environment (Rosenberg et al., 1990). Therefore, high primary productivity and eutrophic conditions are not necessarily caused by upwelling (Pippèrr and Reichenbacher, 2010). However, in the NAFB, eutrophic conditions in an upwelling regime have been suggested for different formations (Roetzel et al., 2006; Grunert et al., 2010a, 2010b). On the other hand, these upwelling-related deposits are typically accompanied by blooms of siliceous organisms (Roetzel et al., 2006; Grunert et al., 2010a, 2010b), which are not present in Unterrudling. Additionally, the mountainous regions surrounding the Paratethys at the time (Alps, Bohemian Massif, Carpathians) would have functioned as wind barriers, causing cold, nutrient rich water from the deep to rise to shallower depths (Kovác et al., 2017). Upwelling conditions have been shown to evolve even during storm events (Swift et al., 1986). The sedimentological interpretation and the ecological data of the foraminifera assemblages clearly show strong wave action and storm events along the coast. Therefore, the eutrophic conditions in Unterrudling may have been caused by conditions similar to upwelling, yet the strong coastal discharge of organic matter appears to have been the major cause for eutrophication. Phosphogenesis in the Eferding Formation may be linked to numerous coeval phases of phosphogenesis, related to global carbon-cycle dynamics between the late Oligocene warming and the middle Miocene so-called Monterey Event (Auer et al., 2016 and references therein). The organic-rich deposits from Unterrudling may represent a beginning pulse of enhanced productivity in the late Oligocene, leading up to the middle Miocene greenhouse, followed in turn by the middle Miocene climate transition and the extant icehouse conditions (cf. Zachos et al., 2001b).

5.3. Palaeoecology

By combining the palaeontological and sedimentological results, a deeper insight into the marine conditions and oceanic zonation is possible. The Eferding Formation in Unterrudling yielded a rich and diverse fossil fauna, which reveals that a transgression from the Linz-Melk Formation to the upper part of the Eferding Formation took place. The granulometric data (Fig. 6) demonstrate a fining upwards sequence throughout the whole section, which is indicating a rising sea level. As mentioned above, the assemblage of foraminifera throughout the Eferding Formation amplifies a deepening trend throughout the section from middle to outer neritic/uppermost bathyal settings. A distinct difference between water depth calculations using benthic foraminifera and the P/B ratio could be observed. On the one hand, calculations using P/B ratios work well in the open ocean (e.g., Kouwenhoven and Van der Zwaan, 2006) but tend to show large offsets due to restricted conditions in marginal areas (see Pippèrr, 2011 and Kranner et al., 2021). On the other hand, calculations based on benthic foraminifera could lead to a slight underestimation of water depth due to allochthonous faunal elements (as interpreted by Rupp and Ćorić, 2015). To take in account both calculations and their differences, both are illustrated in Fig. 8. The calculations using only benthic foraminifers indicate middle neritic settings for sample E1–E3 (40–60 m), slightly deeper conditions for E4–E12 still within the middle to outer neritic (60–110 m) and deep middle neritic to outer neritic conditions (90–150 m) for samples E13–E18. Calculations using the P/B ratio indicate deeper conditions for sample E1–E3 (80–150 m) and a shallowing within the samples E4–E12 (40–60 m) contradict the calculations using the transfer equation (Eq. 1). The interval of samples E13–E18 correlate to the deepening indicated by Eq. 1 but indicates deeper outer neritic to bathyal conditions (100–340 m).Nevertheless, taking in account the benthic and P/B ratio results supports a general deepening trend up section with minor fluctuations within the middle part (E4–E12). Also, the benthic foraminifera indicate a strong decrease in bottom water oxygenation from low oxic within section E1–E3 (mean values of 39% oxic, 37% suboxic and 24% dysoxic indicators) to sub-dysoxic in section E4–E12 (mean values of 46% suboxic accompanied by 44% of dysoxic indicators) and a slight shift to more suboxic conditions in E13–E18 (71% suboxic and 20% dysoxic indicators; Fig. 8C). These general low

oxic conditions within E4–E18 further promote abundances of infaunal foraminifera (77%; Fig. 8B) with a detritivore lifestyle (93%; Fig. 8A). Within samples E1–E3 the fauna is still dominated by detritivore (63%) infauna (45%) species but the high number of epifaunal sessile (24%) and suspension feeding species (20%, Fig. 8) can point to increased bottom current movements (Grunert et al., 2010a, 2010b). Lenticular bedding in the Eferding Formation and the coarse sediment at the base, as well as the washed in plant material supports at least periodically higher current velocities. Furthermore, the time equivalent Linz-Melk Formation is clearly showing signs of storm events. The reconstructed bottom water temperature is rather constant throughout the section with a mean of 10 °C. Considering the deepening throughout the section, the variation from mean 11 °C (E1–E12) to 9 °C (E13–E18) is rather small but might still reflect the deepening trend. Moreover, the observed decreasing water temperature throughout the section (Fig. 8) correlates with the global isotope curve from Zachos et al. (2001a, 2001b) (Fig. 2). Consequently, the decreasing bottom water temperature either reflect the distinct deepening or the global signal of the late Oligocene cooling phase is indicated in Unterrudling. Combining all indications and calculations of foraminifera leads to fully marine (34–36 PSU) relatively cool, sub-dysoxic, middle neritic to uppermost bathyal conditions with high nutrient input.

Furthermore, the findings of echinoids and bivalves in the Eferding Formation allow also a deeper insight into oceanic zonations and conditions. The fossil echinoid fauna within the Eferding Formation (Tables 1, 3) is typically found in fossil and modern sublittoral to deep water habitats (compare Kroh, 2005; Schlüter et al., 2015). The bivalves of the Eferding Formation (Table 1, Fig. S6), found in two different horizons, allows a closer insight to their depositional environment and sedimentary processes. The bivalve assemblage of bed E17, associated with cold-water corals, comprises *Neopycnodonte navicularis*, *Delectopecten vitreus*, and *Ctenoides* aff. *eximia*. Yet, *Ctenoides* is a cosmopolitan thermophilic genus restricted today to the peri-equatorial belt of Atlantic and Indo-Pacific domains. Caribbean *C. mitis*, very similar to the species studied herein, is a shallow-water dweller at maximum depth of about 50 m, although empty shells have been found down to 500 m water depths (Mikkelsen and Bieler, 1989). It lives there byssally attached to some sort of rubbly substratum, e.g., under or among rocks, sponges or coral and especially in crevices of reefs and ledges. Only single shells of *C.* aff. *Eximia* were detected in the coral bed of Unterrudling, pointing to their redeposition by storm currents from a shallow water environment. Still living, *D. vitreus* dwell in deep sublittoral to abyssal environments throughout the Atlantic Ocean and the Mediterranean Sea at depths from 50 to 4255 m. It is a suspension feeder, found at current-swept bottoms, byssally attached on dead and living deep-water coral colonies, their skeletons, or other secondary hardgrounds on soft mud bottoms (Dijkstra and Goud, 2002; Dijkstra et al., 2009; Mastrototaro et al., 2010; Rueda et al., 2019). *Neopycnodonte* is a cosmopolitan, hard ground cementing genus, living today in strictly steno- and euhaline oceanic waters at temperatures of 12° to 14 °C and depths of 27 to 1500 m (Stenzel, 1971). *Neopycnodonte cochlear*, a direct descendant of the studied species, lives today in the Mediterranean and NE Atlantic as a suspension-feeder in the euphotic zone between 45 and 250 m (Poppe and Goto, 1993; Wisshak et al., 2009). *Neopycnodonte navicularis* is described from deep-water muddy sediments of the Paratethys, associated there with cold-water corals (Mandic et al., 2019a, 2019b). This correlates well with its co-occurrence with the accumulation of skeletal remains by *Madrepora* cf. *oculata* at Unterrudling, representing apparently an autochthonous assemblage. In the Mediterranean Sea both, *N. cochlear* as well as *D. vitreus* dwell in habitats formed by the cold-water corals *M. oculata* and *Lophelia pertusa* (Rueda et al., 2019). In contrast to the latter assemblage, the record of *Propeamussium* is confined to the glauconitic sands of the lowermost Eferding Formation (Fig. 4). Living species of the genus *Propeamussium* are carnivorous active swimmers, free-living at the sea bottom and preying on small crustaceans (Dijkstra and Janssen, 2013). They show a cosmopolitan distribution and an extraordinary depth-range of 100–5000 m (Dijkstra and Beu, 2018). Along with *Propeamussium semiradiatum*, the assemblage of the basal Eferding Formation includes *N. navicularis* and *D. vitreus*, pointing together to a cold-water environmental condition at a minimum depth of 100 m.

In addition, the vertebrate composition of equivalent strata of the NAFB (e.g., Pfeil, 1981; Reinecke et al., 2014; Pollerspöck et al., 2018) contrasts significantly due to the presence of a conspicuous majority of squalomorph sharks (87%). Shark species related to living taxa such as *Etmopterus*, *Heptranchias*, *Echinorhinus* and *Centroselachus* are primarily bottom water-dwelling deepwater inhabitants of the continental and insular slopes (Ebert et al., 2013). They range in depth down to more than 2000 m, but usually dwell at 100 m (*Heptranchias*) or 200 m (*Etmopterus*, *Centroselachus*) (Ebert et al., 2013). Consequently, the faunal assemblage reported in this study contrasts with the nearby deposits of Kriechbaum (Upper Austria), which are supposed to represent sediments from the same age. The Kriechbaum fauna is characterized by elasmobranch species of coastal environments, such as *Carcharias*, *Araloselachus*, *Galeocerdo*, *Notorynchus*, *Carcharhinus*, as well as by benthic rajid species. Merely few teeth of deep-water taxa (*Hexanchus agassizi*, *Scyliorhinidae*) and planktivorous sharks (*Nanocetorhinus*) were collected at this site (Feichtinger et al., 2019a, 2019b, 2020). Based on vertebrates present, we conclude that in particular the coral layer (E17) of Unterrudling represents a deep-water habitat, which was situated in a depth of approximately 200–300 m or more. Even though the slightly coarser material deposited in the coral layer (Fig. 4) could indicate a temporary shallowing. Nevertheless, this coarse sediment is rather caused by a storm event, as above the layer E17 the laminated muddy sedimentation continues. Furthermore, the lack of benthic shark species such as *Squatina* or bathomorph elasmobranchs possibly indicates the presence of a temporal oxygen depletion, which was previously suggested for the Ebelsberg Formation at Pucking (Grunert et al., 2010a, 2010b). Beside the majority of deep-water inhabitants, teeth of pelagic sharks, such as *Alopias exigua,* are rare elements within these sediments.

Considering the accompanied otolith assemblage, which comprises four species of Myctophidae (lantern fishes), one species of Ranicipitidae (tadpole cods), and one species of Macrouridae (deep-sea grenadiers), a possible predator-prey relationship can be interpreted. The majority of otoliths belong to the lantern fishes (Myctophidae), which are exclusively preyed by some squalimorph sharks such as *Centroscyllium*, *Deania*, *Etmopterus*, and *Squalus* (Ebert et al., 2013). This conspicuous interrelationship between the dominance of squalomorph sharks (87%) and otoliths of their preferred prey (93% lantern fish otoliths) within the coral layer point towards a vital predator-prey interaction, similar to modern representatives.

5.4. Palaeogeography

Most striking in the section Unterrudling is the facies change from the Linz-Melk Formation towards the Eferding Formation. One of the major factors is the transgressive phase documented in the Egerian (Roetzel et al., 1983; Piller et al., 2007; Rupp and Ćorić, 2015). The Eferding Formation at Unterrudling is dated by Rupp and Ćorić (2015) with an age of 24.3–23.4 Ma, and can therefore be correlated with the sequence Ch-3 (Piller et al., 2007) (Fig. 9). The faunal communities, as well as the facies development analysed in this study suggest a sea-level rise of about 200–300 m from the Linz-Melk Formation to the Eferding Formation, and thus correlates with the transgressive part of the sequence Ch-3. This transgression was probably triggered by global events (Haq et al., 1988), but also by regional tectonic subsidence induced by the ongoing Alpine Orogeny during the Oligocene (Roetzel et al., 1983; Kuhlemann and Kempf, 2002). Due to the propagation of the thrust front and the simultaneous deepening in the south, parts of the Eferding Formation were imbricated (Wagner, 1998), suggesting palaeogeographic changes in the eastern NAFB during this transgressive period. Nehyba and Roetzel (2010) showed that tectonic subsidence is a

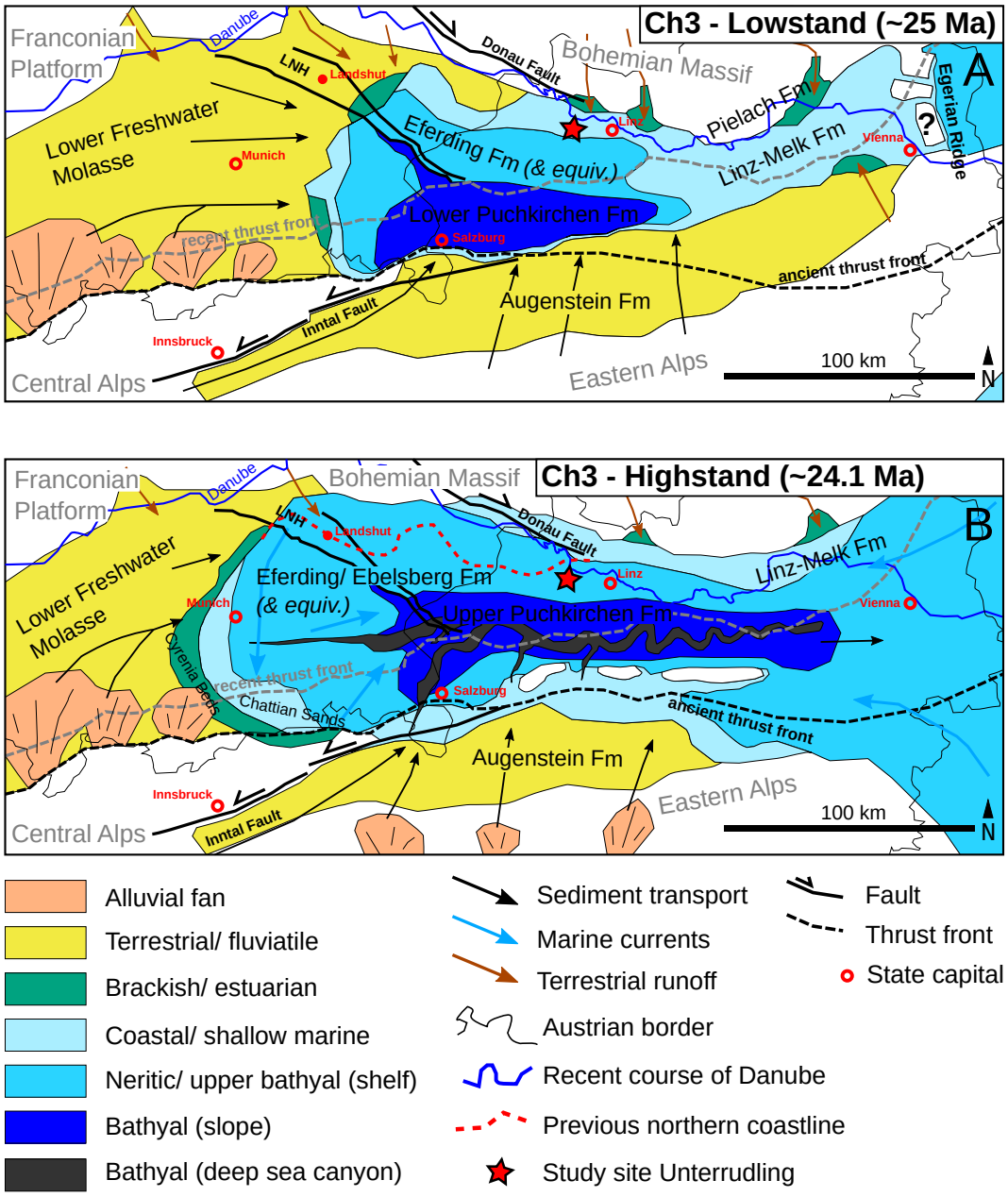

Fig. 9. Palaeogeographic reconstructions.
Palaeogeographic reconstruction of the transgressive phase during the late Chattian in the Central Paratethys. (A) Sea level lowstand of the sequence Ch-3, deposition of the Linz-Melk- Formation in Unterrudling. (B) Transgression and deposition of the Eferding- Formation in Unterrudling, re-opening towards the Central Paratethys. Reconstructions from the following authors are taken into account: Fuchs et al. (1980), Jiricek and Seifert (1990), Doppler et al. (1996), Knierzinger et al. (2019), Ortner and Stingl (2001), Kuhlemann and Kempf (2002), Roetzel et al. (1983), Wagner (1998), De Ruig and Hubbard (2006) and Nehyba and Roetzel (2010). The tectonic structure of the Landshut-Neuötting-High (LNH) according to Lemcke (1973), ancient and recent thrust front according to Kuhlemann and Kempf (2002). Previously reconstructed northern coastline by Doppler et al. (1996).

controlling factor for the formation of palaeovalleys inside the Bohemian Massif on the external passive margin of the NAFB. Moreover, subsidence allowed for development of the fluvial St. Marein-Freischling Formation and the brackish Pielach Formation during the Egerian.

During the sea level lowstand of sequence Ch-3 in the middle Egerian the marine part of the NAFB was isolated towards the west (Doppler et al., 2005), and the palaeocoastline probably reached up to present-day Landshut, about 150 km west of Unterrudling (Fig. 9) (Kuhlemann and Kempf, 2002). Whereas the Landshut-Neuötting High, a SE-NW aligned fault system (Lemcke, 1973), which underwent significant subsidence (Hofmayer et al., 2019). It was responsible for a slightly deeper area at its western margin (Fig. 9) (Lemcke, 1973). Partial basin isolation eastwards by the so-called Egerian Ridge in the area of today's Waschberg Unit has been postulated (Knierzinger et al., 2019). In the nearshore Linz-Melk Formation along the Bohemian Massif brackish deposits and only few sedimentological evidence for tidal influence have been observed (Roetzel et al., 1983). Nevertheless, the presence of the trace fossil *Macaronichnus*, as described here, responsible for destroying of sedimentary structures, hints towards a lacking preservation potential of such structures. In the regions west of Unterrudling and around the town of Melk, 100 km east of Unterrudling, mega-scale cross-bedding is observed in the Linz-Melk Formation. These mainly several metres thick sets are interpreted as submarine sandwaves on a shelf environment, showing tidal flood currents coming from the east (Krenmayr and

Roetzel, 2000a). This indicates tidal influence in the east, adjacent to the Egerian Ridge and a decrease of tidal current velocity to the west. In addition, the narrowing of the NAFB in the crystalline area around Amstetten might have contributed to a reinforcement of tidal currents in the east. Moreover, no complete isolation of the NAFB is likely, as marine deposition continues throughout the Oligocene (Doppler et al., 1996). Consequently, a seaway, or small strait must have existed through the Egerian Ridge (Krenmayr and Roetzel, 2000a).

During the transgressive phase of sequence Ch-3 this narrow seaway was flooded (Knierzinger et al., 2019) together with large areas to the south and west, as well as to the north. The sea expanded to present-day Munich and Salzburg (Doppler et al., 1996; De Ruig and Hubbard, 2006). Assuming a sea level rise in the order of 200 m (this study) the palaeocoastline shifted several kilometres further north than previously postulated (Figs. 1B, 9; Doppler et al., 1996). The former terrestrial realm in the west and south provided vast amounts of siliciclastic material (Lower Freshwater Molasse, Augenstein Formation) (Frisch et al., 2001; Doppler et al., 2005), which was eroded and transported through feeder channels into the basin (Fig. 9; De Ruig and Hubbard, 2006; Knierzinger et al., 2019). The result was a positive sedimentary budget in the NAFB (Goodwin et al., 2020). At the same time the seaway to the east expanded and the Egerian Ridge disappeared, which enabled sedimentary discharge eastwards to the Central Paratethys (Knierzinger et al., 2019). This palaeogeographic change is archived in the Puchkirchen Formation, which changed from deep sea turbidites (Lower Puchkirchen Formation) to an east-west oriented deep sea channel with high sedimentation rates (Upper Puchkirchen Formation) (De Ruig and Hubbard, 2006). Additionally, the connection to the Central Paratethys re-established oceanic currents westwards (Fig. 9). Furthermore, migratory shark species documented in the Eferding Formation at the locality Kriechbaum (Feichtinger et al., 2020), indicating open seaways to the Mediterranean Sea. The effects of the transgression on the northern coast of the NAFB are quite similar. Here estuaries persisted at the confluence of big rivers from the north along the Bohemian Massif (Harzhauser and Mandic, 2001; Nehyba and Roetzel, 2010), archived by the Pielach Formation (Wagner, 1998). This predominantly muddy facies consists of organic material and reworked sediments from the deeply weathered kaolinitic crust on the crystalline of the Bohemian Massif, developed in the Eocene tropical conditions (Fuchs, 1972; Roetzel et al., 1999). These sediments are released into the basin during the transgressive phase of the sequence Ch-3 (Goodwin et al., 2020). Furthermore, the mineralogical inventories of the Eferding Formation and Pielach Formation show a high amount of kaolinite (Wimmer-Frey et al., 2013), which also points to a weathered crystalline basement as a source area.

6. Conclusions

Summarizing the new available data we conclude that: (1) The granulometric data and analysed fossil groups reveal a transgressive sequence, which can be correlated to the sequence Ch-3. This transgression led from a partial isolation to the re-opening of the NAFB to the Central Paratethys and a subsequent sedimentary discharge eastwards. (2) In addition, the sedimentological analysis together with the present trace fossils, the shark teeth, and the revised foraminifera data from Rupp and Ćorić (2015) enabled a detailed reconstruction of the depositional environment: The Linz-Melk Formation was deposited in a foreshore to shoreface environment with water depths less than 10 m and dominant wave action. Material was washed into the sea from estuaries and coastal runoff and was reworked by periodic storm events. The lowermost part of the Eferding Formation represents the transition zone of an inner shelf to foreshore environment. Water depths of less than 30 m are inferred, strong bioturbation is apparent and muddy sediment indicates decreasing wave energy. The laminated muddy sediment in the upper part of the Eferding Formation is typical for an outer shelf to bathyal environment. The collected vertebrates (shark, fish) and invertebrates (bivalves, corals), as well as the calculated values from the foraminifera indicate maximum water depths of 200–300 m. (3) Several faunal elements such as *Delectopecten vitreus*, *Neopycnodonte navicularis*, *Palaeocentroscymnus horvathi, Alopias exigua* are newly recorded within the middle Egerian of the NAFB. (4) Using previously described and newly found plant material, the reconstructed climate is characterized by mean annual temperatures of 20.6 °C and a mean annual precipitation of 170 mm, which is similar to today's South-East Asia. (5) A bottom water temperature of about 10 °C is inferred from calculations based on benthic foraminifera. (6) Scarce bioturbation structures within the upper parts of the Eferding Formation, as well as the peculiar shark and foraminifera assemblages indicate oxygen depletion in the Eferding Formation. These conditions were caused by the high input of organic matter, such as plant material, which led to the consumption of oxygen due to the degradation of organic matter by heterotrophs, including microbes. This was leading to the liberation of phosphorus to pore waters and the early diagenetic formation of phosphatic nodules, which are known today from upwelling regions, which are characterized by eutrophic conditions. (7) Distinct ecological relationships are observed in this environment as a predator-prey relationship was reconstructed. Several shark species were exclusively preying on the present fish species.

Supplementary data to this article can be found online at https://doi.org/10.1016/j.palaeo.2021.110527.

Declaration of competing interest

The authors declare that they have no known competing financial interests or personal relationships that could have appeared to influence the work reported in this paper.

Acknowledgements

We warmly thank Franz Zeitlinger (Kriechbaum, OÖ) for assistance during fieldwork and the Quarzsande GmbH for permission to enter the quarry and assistance while working. We also thank Christa Hofmann and Reinhard Zetter for palaeobotanical advice and Leyla Seyfullah (all University of Vienna) for language advice, and Anna Weinmann (NHM Vienna) for assistance during the field trips. Additionally, we express our gratitude to Francesca Bosellini and Agostina Vertino for help with the identification of corals and further work on these. We warmly thank both reviewers for their comments to improve this work.

Appendix 1

Kingdom	Class	Order	Family	Genus	Species/Element	Inventory Numbers
Animalia	Anthozoa	Scleractinia	Oculinidae	*Madrepora*	sp.	NHMW/2020/0140/0001
Animalia	Echinodea	Spatangoida	indet.			NHMW/2020/0140/0004a
Animalia	Echinodea	Cidardoida	indet.			NHMW/2020/0140/0004b
Animalia	Bivalvia	Pectinida	Pectinidae	*Delectopecten*	sp.	NHMW/2020/0140/0003
Animalia	Bivalvia	Ostreida	Gryphaeidae	*Neopycnodonte*	*navicularis*	NHMW/2020/0140/0050

(*continued on next page*)

(*continued*)

Kingdom	Class	Order	Family	Genus	Species/Element	Inventory Numbers
Animalia	Bivalvia	Ostreida	Gryphaeidae	*Neopycnodonte*	*navicularis*	NHMW/2020/0140/0051
Animalia	Bivalvia	Ostreida	Gryphaeidae	*Neopycnodonte*	*navicularis*	NHMW/2020/0140/0052
Animalia	Bivalvia	Ostreida	Gryphaeidae	*Neopycnodonte*	*navicularis*	NHMW/2020/0140/0053
Animalia	Bivalvia	Ostreida	Gryphaeidae	*Neopycnodonte*	*navicularis*	NHMW/2020/0140/0057
Animalia	Bivalvia	Pectinida	Pectinidae	*Delectopecten*	*vitreus*	NHMW/2020/0140/0054
Animalia	Bivalvia	Pectinida	Pectinidae	*Delectopecten*	*vitreus*	NHMW/2020/0140/0059
Animalia	Bivalvia	Limida	Limidae	*Ctenoides*	aff. *eximia*	NHMW/2020/0140/0055
Animalia	Bivalvia	Limida	Limidae	*Ctenoides*	aff. *eximia*	NHMW/2020/0140/0056
Animalia	Bivalvia	Limida	Limidae	*Ctenoides*	aff. *eximia*	NHMW/2020/0140/0058
Animalia	Bivalvia	Limida	Limidae	*Ctenoides*	aff. *eximia*	NHMW/2020/0140/0060
Animalia	Bivalvia	Limida	Limidae	*Ctenoides*	aff. *eximia*	NHMW/2020/0140/0061
Animalia	Bivalvia	Limida	Limidae	*Ctenoides*	aff. *eximia*	NHMW/2020/0140/0062
Animalia	Chondrichthyes	Lamniformes	Lamnidae	indet.		NHMW/2020/0140/0005
Animalia	Chondrichthyes	Lamniformes	Lamnidae	indet.		NHMW/2020/0140/0006
Animalia	Chondrichthyes	Squaliformes	Etmopteridae	*Etmopterus*	sp.	NHMW/2020/0140/0007
Animalia	Chondrichthyes	Squaliformes	Etmopteridae	*Etmopterus*	sp.	NHMW/2020/0140/0008
Animalia	Chondrichthyes	Squaliformes	Somniosidae	*Palaeocentroscymnus*	sp.	NHMW/2020/0140/0009
Animalia	Chondrichthyes	Squaliformes	Somniosidae	*Palaeocentroscymnus*	sp.	NHMW/2020/0140/0010
Animalia	Chondrichthyes	Squaliformes	Dalatidae	indet.		NHMW/2020/0140/0011
Animalia	Chondrichthyes	Squaliformes	Dalatidae	indet.		NHMW/2020/0140/0012
Animalia	Chondrichthyes	Squaliformes	Dalatidae	indet.		NHMW/2020/0140/0013
Animalia	Chondrichthyes	Squaliformes	Somniosidae	?*Centroselachus*	sp.	NHMW/2020/0140/0014
Animalia	Chondrichthyes	Hexanchiformes	Hexanchidae	*Heptranchias*	sp.	NHMW/2020/0140/0015
Animalia	Chondrichthyes	Hexanchiformes	Hexanchidae	*Heptranchias*	sp.	NHMW/2020/0140/0016
Animalia	Chondrichthyes	Squaliformes	Echinorhinidae	*Echinorhinus*	sp.	NHMW/2020/0140/0017
Animalia	Chondrichthyes	Squaliformes	Echinorhinidae	*Echinorhinus*	sp.	NHMW/2008/0266/0001
Animalia	Chondrichthyes	Hexanchiformes	Hexanchidae	indet.	symphyseal tooth	NHMW/2020/0140/0018
Animalia	Chondrichthyes	Rajiformes	Rajidae	*Raja*	sp.	NHMW/2020/0140/0019
Animalia	Chondrichthyes	Squatiniformes	Squantinidae	indet.	denticle	NHMW/2020/0140/0020
Animalia	Chondrichthyes	Squaliformes	Etmopteridae	*Etmopterus*	sp.	NHMW/2020/0140/0021
Animalia	Chondrichthyes	Squaliformes	Etmopteridae	*Etmopterus*	sp.	NHMW/2020/0140/0022
Animalia	Chondrichthyes	Squaliformes	Etmopteridae	*Etmopterus*	sp.	NHMW/2020/0140/0023
Animalia	Chondrichthyes	Squaliformes	Somniosidae	*Palaeocentroscymnus*	sp.	NHMW/2020/0140/0024
Animalia	Chondrichthyes	Squaliformes	Somniosidae	*Palaeocentroscymnus*	sp.	NHMW/2020/0140/0025
Animalia	Chondrichthyes	Squaliformes	Etmopteridae	cf. *Etmopterus*		NHMW/2020/0140/0026
Animalia	Chondrichthyes	Squaliformes	indet.			NHMW/2020/0140/0027
Animalia	Chondrichthyes			indet.	drag reduction denticle	NHMW/2020/0140/0028
Animalia	Chondrichthyes	Hexanchiformes	Hexanchidae	indet.	isolated cusp	NHMW/2020/0140/0029
Animalia	Chondrichthyes	Lamniformes	Lamnidae	*Isurus*	sp.	NHMW/2018/0144/0001
Animalia	Chondrichthyes	Lamniformes	Alopiidae	*Alopias*	*exigua*	NHMW/2020/0140/0035
Animalia	Chondrichthyes	Hexanchiformes	Hexanchidae	*Notorynchus*	primigenius	NHMW/2020/0140/0036
Animalia	Chondrichthyes	Lamniformes	Odontaspididae	*Carcharias*	acutissminus	NHMW/2020/0140/0037
Animalia	Chondrichthyes	Hexanchiformes	Hexanchidae	*Heptranchias*	sp.	NHMW/2020/0140/0038
Animalia	Chondrichthyes	Squaliformes	Somniosidae	?*Centroselachus*	upper jaw	NHMW/2020/0140/0039
Animalia	Chondrichthyes	Squaliformes	Somniosidae	?*Centroselachus*	lower jaw	NHMW/2020/0140/0040
Animalia	Chondrichthyes	Squaliformes	Etmopteridae	*Etmopterus*	sp.	NHMW/2020/0140/0041
Animalia	Chondrichthyes	Squaliformes	Somniosidae	*Palaeocentroscymnus*	sp.	NHMW/2020/0140/0042
Animalia	Chondrichthyes	Squaliformes	Dalatidae	indet.		NHMW/2020/0140/0043
Animalia	Chondrichthyes	Squaliformes	Etmopteridae	*Etmopterus*	sp.	OLL 2020/87
Animalia	Chondrichthyes	Squaliformes	Somniosidae	*Plaeocentroscymnus*	sp.	OLL 2020/88
Animalia	Chondrichthyes	Squaliformes	Dalatidae	indet.		OLL 2020/89
Animalia	Chondrichthyes	Squaliformes	Dalatidae	indet.		OLL 2020/90
Animalia	Chondrichthyes				drag reduction denticle	OLL 2020/91
Animalia	Chondrichthyes	Hexanchiformes	Hexanchidae		*Hexanchus* remains	OLL 2020/92
Animalia	Actinopterygii	Myctophiformes	Myctophidae	*Diaphus*	cf. *cahuzaci*	NHMW/2018/0144/0001
Animalia	Actinopterygii	Myctophiformes	Myctophidae	*Diaphus*	aff. *kokeni*	NHMW/2020/0140/0032
Animalia	Actinopterygii	Myctophiformes	Myctophidae	*Diaphus*	aff. *pristimetallis*	NHMW/2020/0140/0033
Animalia	Actinopterygii	Myctophiformes	Myctophidae	*Diaphus*	aff. *taaningi*	NHMW/2020/0140/0034
Animalia	Actinopterygii	Gadiformes	Gadidae	aff. *Raniceps*	aff. *coelorinchoides*	NHMW/2020/0140/0070
Animalia	Actinopterygii	Gadiformes	Macrouridae	cf. *Coelorinchus*		NHMW/2020/0140/0071
Plantae	Pinopsida	Pinales	Pinaceae	*Pinus*	sp.	PIUW
Plantae	Pinopsida	Pinales	Pinaceae	*Pinus*	sp.	PIUW
Plantae	Pinopsida	Pinales	Pinaceae	*Picea*	sp.	PIUW
Plantae	Pinopsida	Pinales	Pinaceae	*Cathaya*	sp.	PIUW
Plantae	Pinopsida	Pinales	Pinaceae	*Tsuga*	sp.	PIUW
Plantae	Pinopsida	Pinales	Cupressaceae	indet.		PIUW
Plantae	Monocots	Poales	Thypaceae	*Sparganium*	sp.	PIUW
Plantae	Eudicots	Proteales	Platanaceae	*Platanus*	sp.	PIUW
Plantae	Eudicots	Rosales	Ulmaceae	*Ulmus*	sp.	PIUW
Plantae	Eudicots	Rosales	Ulmaceae	*Zelkova*	sp.	PIUW
Plantae	Eudicots	Fagales	Fagaceae	*Eotrigonobalanopsis*	sp.	PIUW
Plantae	Eudicots	Fagales	Fagaceae	*Quercus*	sp.	PIUW
Plantae	Eudicots	Fagales	Fagaceae	*Trigonobalanopsis*	sp.	PIUW
Plantae	Eudicots	Fagales	Betulaceae	*Carpnius*	sp.	PIUW
Plantae	Eudicots	Fagales	Betulaceae	*Betula*	sp.	PIUW
Plantae	Eudicots	Fagales	Juglandaceae	*Engelhardia*	sp.	PIUW

(*continued on next page*)

(*continued*)

Kingdom	Class	Order	Family	Genus	Species/Element	Inventory Numbers
Plantae	Eudicots	Fagales	Juglandaceae	*Carya*	sp.	PIUW
Plantae	Eudicots	Malpighiales	Euphorbiaceae	indet.		PIUW
Plantae	Eudicots	Ericales	Styricaceae	*Rhederodendron*	sp.	PIUW
Plantae	Eudicots	Ericales	Sapotaceae	indet.	sp.	PIUW
Plantae	Eudicots	Ericales	Symplocaceae	*Symplocos*	sp.	PIUW
Plantae	Eudicots	Lamiales	Oleaceae	indet.		PIUW
Plantae	Magnoliopsida	Laurales	Lauraceae	*Daphnogene*	*cinnamomifolia*	OLL 2020/93
Plantae	Magnoliosida	Laurales	Lauraceae	*Daphnogene*	sp.	PIUW
	Mycophyta			indet.		PIUW

References

Adegoke, A.K., Abdullah, W.H., Yandoka, B.M.S., 2017. Provenance and paleoenvironment of organic matter within the Fika sediments in Chad (Bornu) Basin, northeastern Nigeria: an integrated organic geochemical and palynofacies approach. Int. J. Coal Geol. 173, 94–109. https://doi.org/10.1016/j.coal.2017.02.007.

Aigner, T., Reineck, H.E., 1982. Proximality trends in modern storm sands from the Helgoland Bight (North Sea) and their implications for basin analysis. Senckenberg. Marit. 14, 183–215.

Alsenz, H., Illner, P., Ashckenazi-Polidova, S., Meilijson, A., Abramovich, S., Feinstein, S., Almogi-Labin, A., Berner, Z., Püttmann, W., 2015. Geochemical evidence for the link between sulfate reduction, sulfide oxidation and phosphate accumulation in a Late Cretaceous upwelling system. Geochem. Trans. 16 https://doi.org/10.1186/s12932-015-0017-1.

Altenbach, A.V., Lutze, G.F., Schiebel, R., Schönfeld, J., 2003. Impact of interrelated and interdependent ecological controls on benthic foraminifera: an example from the Gulf of Guinea. Palaeogeogr. Palaeoclimatol. Palaeoecol. 197, 213–238. https://doi.org/10.1016/S0031-0182(03)00463-2.

Anthony, E.J., Orford, J.D., 2002. Between wave- and tide-dominated coasts: the Middle Ground revisited. J. Coast. Res. 36, 8–15. https://doi.org/10.2112/1551-5036-36.sp1.8.

Antia, E., Flemming, B., Wefer, G., 1994. Transgressive facies sequence of a high energy, wave-tide-storm-influenced shoreface: a case study of the East Frisian barrier islands (southern North Sea). Facies 30, 15–24. https://doi.org/10.1007/BF02536887.

Arning, E.T., Birgel, D., Brunner, B., Peckmann, J., 2009. Bacterial formation of phosphatic laminites off Peru. Geobiology 7, 295–307.

Auer, G., Hauzenberger, C.A., Reuter, M., Piller, W.E., 2016. Orbitally paced phosphogenesis in Mediterranean shallow marine carbonates during the middle Miocene Monterey event. Geochem. Geophys. Geosyst. 17, 1492–1510.

Bachmann, G.H., Müller, M., 1992. Sedimentary and structural evolution of the German Molasse Basin. Eclogae Geol. Helv. 85, 519–530 doi:0012-9402/92 030519-11.

Baldermann, A., Warr, L.N., Grathoff, G.H., Dietzel, M., 2013. The rate and mechanism of deep-sea glauconite formation at the Ivory Coast – Ghana marginal ridge. Clay Clay Miner. 61, 258–276.

Báldi, T., 1986. Mid-Tertiary Stratigraphy and Paleogeographic Evolution of Hungary. Akadémiai Kiadó, Budapest, 201 p.

Báldi, K., Hohenegger, J., 2008. Paleoecology of benthic foraminifera of the Baden-Sooss section Badenian, Middle Miocene, Vienna Basin, Austria. Geol. Carpath. 59, 411–424.

Báldi, T., Seneš, J., 1975. Chronostratigraphy Und Neostratotypen, Miozän der Zentralen Paratethys, Band 5, OM Egerian. Die Egerer, Pouzdraner, Puchkirchener Schichtengruppe und die Bretkaer Formation, Schweizerbart, 580 p.

Benitez-Nelson, C.R., 2000. The biogeochemical cycling of phosphorus in marine systems. Earth-Sci. Rev. 51, 109–135.

Berger, J.-P., Reichenbacher, B., Becker, D., Grimm, M., Grimm, K., Picot, L., Storni, A., Pirkenseer, C., Schaefer, A., 2005. Eocene-Pliocene time scale and stratigraphy of the Upper Rhine Graben (URG) and the Swiss Molasse Basin (SMB). Int. J. Earth Sci. 94, 711–731. https://doi.org/10.1007/s00531-005-0479-y.

Berggren, W.A., Kent, D.V., Swisher, C.C., Aubry, M.-P., 1995. A revised Cenozoic geochronology and chronostratigraphy. SEPM Special Publ. 54, 129–212. https://doi.org/10.2110/pec.95.04.0129.

Berndmeyer, C., Birgel, D., Brunner, B., Wehrmann, L.M., Jöns, N., Bach, W., Arning, E. T., Föllmi, K.B., Peckmann, J., 2012. The influence of bacterial activity on phosphorite formation in the Miocene Monterey Formation, California. Palaeogeogr. Palaeoclimatol. Palaeoecol. 317–318, 171–181.

Bittner, A., 1884. Die Tertiär-Ablagerungen von Trifail und Sagor. Jahrbuch der geologischen Reichsanstalt 34, 433–600.

Böhme, M., 2003. The Miocene Climate Optimum: evidence from ectothermic vertebrates of Central Europe. Palaeogeogr. Palaeoclimatol. Palaeoecol. 195, 389–401. https://doi.org/10.1016/s0031-0182(03)00367 -5.

Böhme, M., Bruch, A.A., Selmeier, A., 2007. The reconstruction of Early and Middle Miocene climate and vegetation in Southern Germany as determined from the fossil wood flora. Palaeogeogr. Palaeoclimatol. Palaeoecol. 253, 91–114. https://doi.org/10.1016/j.palaeo.2007.03.035.

Bolliger, T., Kindlimann, R., Wegmüller, U., 1995. Die marinen Sedimente (jüngere OMM, St. Galler-Formation) am Südwestrand der Hörnlischüttung (Ostschweiz) und die palökologische Interpretation ihres Fossilinhaltes. Eclogae Geol. Helv. 88, 885–909. https://doi.org/10.5169/seals-167709.

Bradshaw, B.E., Healy, T.R., Dell, P.M., Bolstad, W.M., 1991. Inner shelf dynamics on a storm-dominated coast, East Coromandel, New Zealand. J. Coast. Res. 7, 11–30.

Brinkmann, I., Pippèrr, M., Reichenbacher, B., 2019. A new well-preserved ostracod fauna from the middle Burdigalian (lower Miocene) of the North Alpine Foreland Basin. Geobios. https://doi.org/10.1016/j.geobi os.2019.07.005.

Brocchi, G.V., 1814. Conchiologia Fossile Subapennina Con Osservazioni Geologiche Sugli Apennini e sul Suolo Adiacente. Tomo secondo, Stamperia Reale, Milano. https://doi.org/10.5962/bhl.title.11569, 712 p.

Bromley, R.G., 1996. Trace Fossils. Biology, Taphonomy and Applications, Second ed. Chapman & Hall. https://doi.org/10.1017/S0016756897316987. 361 p.

Bromley, R.G., Knaust, D. (Eds.), 2012. Trace Fossils as Indicators of Sedimentary Environments. Developments in Sedimentology, 64. Elsevier, Amsterdam, 960 p.

Bromley, R.G., Uchman, A., 2003. Trace fossils from the Lower and Middle Jurassic marginal-marine deposits of the Sorthat Formation, Bornholm, Denmark. Bull. Geol. Soc. Den. 52, 185–208.

Bromley, R.G., Uchman, A., Milàn, J., Hansen, K.S., 2009. Rheotactic *Macaronichnus*, and human and cattle trackways in Holocene beachrock, Greece: reconstruction of palaeoshoreline orientation. Ichnos 16, 103–117. https://doi.org/10.1080/10420940802470987.

Brzobohatý, R., Nolf, D., 2000. *Diaphus* otoliths from the European Neogene (Myctophidae, Teleostei). Bull. Inst. R. Sci. Nat. Belg. Sci. Terre 70, 185–206.

Brzobohatý, R., Schultz, O., 1978. Die Fischfauna des Badeniens. In: Papp, A., Cicha, I., Seneš, J., Steininger, F. (Eds.), Chronostratigraphie und Neostratotypen, 6. SAV Press, pp. 441–465.

Buatois, L.A., Mángano, M.G., 2011. Ichnology: Organism-Substrate Interactions in Space and Time. Cambridge University Press, Cambridge, 358 pp.

Cairns, S.D., Jaap, W.C., Lang, J.C., 2009. Scleractinia (Cnidaria) of the Gulf of Mexico. In: Felder, D.L., Camp, D.K. (Eds.), Gulf of Mexico – Origins, Waters, and Biota. Biodiversity. Texas A&M University Press, College Station, Texas, pp. 333–347. https://hdl.handle.net/10088/19157.

Carter, J.G., 1990. Evolutionary significance of shell microstructure in the Palaeotaxodonta, Pteriomorphia and Isofilibranchia. In: Carter, J.G. (Ed.), Skeletal Biomineraliztion, Patterns, Processes and Evolutionary Trends. Van Nostrand Reinhold and Co, New York, pp. 135–412.

Ceregato, A., Raffi, S., Scarponi, D., 2007. The circalittoral/bathyal paleocommunities in the Middle Pliocene of Northern Italy: the case of the Korobkovia oblonga–Jupiteria concava paleocommunity type. Geobios 40, 555–572. https://doi.org/10.1016/j.geobios.2006.08.004.

Chábera, S., Huber, K.H., 2000. Ein Beitrag zur Frage der Oberen Moldau im Tertiär. Jahrbuch des oberösterreichischen Musealvereins 145 (1), 339–367.

Cicha, I., Rögl, F., Rupp, C., Ctyrokya, J., 1998. Oligocene-Miocene Foraminifera of the Central Paratethys. Abh. Senckenb. Naturforsch. Ges. 549, 1–325.

Coleman, M.L., 1993. Microbial processes: Controls on the shape and composition of carbonate concretions. Mar. Geol. 113, 127–140.

Coleman, M.L., Raiswell, R., 1995. Source of carbonate and origin of zonation in pyritiferous carbonate concretions; evaluation of a dynamic model. Am. J. Sci. 295, 282–308.

Ćorić, S., Roetzel, R., Krenmayr, H.G., Gebhardt, H., 2013. Exkursion E2 – Fazies und Stratigrafie der oligzänen und miozänen Sedimente in der alpinen Vortiefe auf den Blättern 55 Ober-Grafendorf und 56 St. Pölten. In: Gebhardt, H., (Red) (Eds.), Arbeitstagung 2013 der Geologischen Bundesanstalt. Geologie der Kartenblätter 55 Ober-Grafendorf und 56 St. Pölten, pp. 236–269.

D'Alessandro, A., Bromley, R.G., 1986. Trace fossils in Pleistocene sandy deposits from Gravina area southern Italy. Riv. Ital. Paleontol. Stratigr. 92, 67–102.

De Ruig, M.J., Hubbard, S.M., 2006. Seismic facies and reservoir characteristics of a deep-marine channel belt in the Molasse foreland basin, Puchkirchen Formation, Austria. Am. Assoc. Pet. Geol. Bull. 90, 735–752. https://doi.org/10.1306/10210505018.

Denk, T., Grímsson, F., Zetter, R., 2012. Fagaceae from the early Oligocene of Central Europe: persisting new world and emerging old world biogeographic links. Rev. Palaeobot. Palynol. 169, 7–20. https://doi.org/10.1016/j.revpalbo.2011.09.010.

Deshayes, G.-P., 1860. Description des Animaux sans Vertèbres découverts dans le Bassin de Paris. In: Tome Premier. Mollusques Acéphalés Dimyaires. Texte et Atlas - (Baillière et Fils) Paris-Londres-New-York, 912 p.

Dijkstra, H.H., Beu, A.G., 2018. Living scallops of Australia and adjacent waters (Mollusca: Bivalvia: Pectinoidea: Propeamussiidae, Cyclochlamydidae and

Pectinidae). Rec. Aust. Mus. 70, 113–330. https://doi.org/10.3853/j.2201-4349.70.2018.1670.
Dijkstra, H.H., Goud, J., 2002. Pectinoidea (Bivalvia, Propeamussiidae & Pectinidae) collected during the Dutch CANCAP and MAURITANIA expeditions in the south-eastern region of the North Atlantic Ocean. Basteria 66, 31–82.
Dijkstra, H.H., Janssen, R., 2013. Bathyal and abyssal Pectionoidea from the Red Sea and Golf of Aden. Archiv für Molluskenkunde 142 (2), 181–214.
Dijkstra, H.H., Warén, A., Gudmnundsson, G., 2009. Pectinoidea (Mollusca: Bivalvia) from Iceland. Mar. Biol. Res. 5, 207–243. https://doi.org/10.1080/17451000802425643.
Dohmann, L., Braunstein, R., 1993. Unteroligozäne Fischschiefer in Süddeutschland und Österreich. Zitteliana 20, 403–409.
Doppler, G., Schwerd, K., Unger, H.J., 1996. Gesteinsfolgen des Molassebeckens und der inneralpinen Tertiärbecken. In: Landesamt, Bayerisches Geologisches (Ed.), Erläuterungen zur Geologischen Karte von Bayern 1:500.000. - 4. Auflage.
Doppler, G., Heissig, K., Reichenbacher, B., 2005. Die Gliederung des Tertiärs im süddeutschen Molassebecken. Newsl. Stratigr. 41, 359–375. https://doi.org/10.1127/0078-0421/2005/0041-0359.
Ebert, D.A., Fowler, S., Compagno, L.J.V., 2013. Sharks of the World – A Fully Illustrated Guide. Wild Nature Press. ISBN 978–0–9573946–0–5, 528pp.
Ehrenberg, K., 1944. Ergänzende Bemerkungen zu den seinerzeit aus dem Miozäan von Burgschleinitz beschrieben Gangkernen und Bauten dekapoder Krebse. Paläontol. Z. 23, 354–359.
Ekdale, A.A., 1992. Muckraking and mudslinging: The joys of deposit-feeding. In: Maples, C.G., West, R.R. (Eds.), Trace Fossils. Short Courses in Paleontology, 5. The Paleontological Society, Knoxville, Tennessee, pp. 145–171.
Faupl, P., Roetzel, R., 1990. Die Phosphoritsande und Fossilreiche Grobsande: Gezeitenbeeinflußte Ablagerungen der Innviertler Gruppe (Ottnangien) in der oberösterreichischen Molassezone. Jahrb. Geol. Bundesanst. 133 (2), 157–180.
Fazio, A.M., Scasso, R.A., Castro, L.N., Carey, S., 2007. Geochemistry of rare earth elements in early-diagenetic Miocenephosphatic concretions of Patagonia, Argentina: phosphogenetic implications. Deep-Sea Res. II 54, 1414–1432.
Feichtinger, I., Kranner, M., Rupp, C., Harzhauser, M., 2019a. A new outer neritic elasmobranch assemblage from the Egerian (late Oligocene) of the North Alpine Foreland Basin (Austria). Neues Jahrb. Geol. Palaontol. Abh. 293, 19–35. https://doi.org/10.1127/njgpa/2019/0828.
Feichtinger, I., Kranner, M., Zeitlinger, F., Pollerspöck, J., Harzhauser, M., 2019b. New data on the elasmobranch fauna of the Eferding Formation (Egerian, North Alpine Foreland Basin) of Austria. In: 25. Jahrestagung ÖPG Bad Vöslau (11.–13.10.2019).
Feichtinger, I., Pollerspöck, J., Harzhauser, M., 2020. A new species of the enigmatic shark genus *Nanocetorhinus* (Chondrichthyes) from the Oligocene of Austria with palaeoceanographic implications. Aust. J. Earth Sci. 113, 229–236. https://doi.org/10.17738/ajes.2020.0014.
Filippelli, G.M., 2011. Phosphate rock formation and marine phosphorus geochemistry: the deep time perspective. Chemosphere 84, 759–766.
Föllmi, K.B., 1996. The phosphorus cycle, phosphogenesis and marine phosphate-rich deposits. Earth-Sci. Rev. 40, 55–124.
Freeman, W.E., Visher, G.S., 1975. Stratigraphic analysis of the Navajo Sandstone. J. Sediment. Petrol. 45, 651–668.
Frey, R.W., Howard, J.D., 1985. Trace fossils from the Panther Member, Star Point Formation (Upper Cretaceous), Coal Creek Canyon, Utah. J. Paleontol. 59, 370–404.
Frey, R.W., Howard, J.D., Pryor, W.A., 1978. *Ophiomorpha*: its morphologic, taxonomic, and environmental significance. Palaeogeogr. Palaeoclimatol. Palaeoecol. 23, 199–229.
Frey, R.W., Curran, A.H., Pemberton, G.S., 1984. Trace making activities of crabs and their environmental significance: the ichnogenus *Psilonichnus*. J. Paleontol. 58, 333–350.
Frisch, W., Kuhlemann, J., Székely, B., Dunkl, I., 2001. The elevated plateaus in the Calcareous Alps - 35 Million years old land surfaces. Gmundner Geo-Studien 2, 181–190.
Fritsch, P.W., Morton, C.M., Chen, T., Meldrum, C., 2001. Phylogeny and biogeography of the Styracaceae. Int. J. Plant Sci. 162, 95–116. https://doi.org/10.1086/323418.
Fuchs, W., 1972. Tertiär und Quartär am Südostrand des Dunkelsteiner Waldes. Jahrb. Geol. Bundesanst. 115, 205–245.
Genise, J.F., Garrouste, R., Nel, P., Grandcolas, Maurizot, P., Cluzel, D., Cornette, R., Fabre, A.-C., Nel, A., 2012. *Asthenopodichnium* in fossil wood: different trace makers as indicators of different terrestrial palaeoenvironments. Palaeogeogr. Palaeoclimatol. Palaeoecol. 365–366, 184–191. https://doi.org/10.1016/j.palaeo.2012.09.025.
Gradstein, F.M., Ogg, J.G., Schmitz, M., Ogg, G., 2020. Geological Time Scale 2020, 1. Elsevier, p. 1390.
Giebel, C., 1864. Die Fauna der Braunkohlenformation von Latdorf bei Bernburg. Abhandlungen der Naturforschenden Gesellschaft zu Halle 8, 183–275.
Gingras, M.K., MacEachern, J.A., Dashtgard, S.E., Zonneveld, J.-P., Schoengut, J., Ranger, M.J., Pemberton, S.G., 2012. Estuaries. Dev. Sedimentol. 64, 467–497. https://doi.org/10.1016/B978-0-444-53813-0.00016-2.
Glenn, C.R., Föllmi, K.B., Riggs, S.R., Baturin, G.N., Grimm, K.A., Trappe, J., Abed, A.M., Galli-Olivier, C., Garrison, R.E., Ilyin, A.V., Jehl, C., Rohrlich, V., Sadaqah, R.M.Y., Schildowksi, M., Sheldon, R.E., Siegmund, H., 1994. Phosphorus and phosphorites: Sedimentology and environments of formation. Eclogae Geol. Helv. 87, 747–788.
Gmelin, J.F., 1791. Caroli a Linné Sytema Naturae, Tom. 1, Pars 6, pp. 3021–3910. Lipsiae (Georg Emanuel Beer).
Goodwin, I.D., Ribó, M., Mortlock, T., 2020. Coastal sediment compartments, wave climate and centennial-scale sediment budget: The South-eastern Australian example. In: Jackson, D., Short, A.D. (Eds.), Sandy Beach Morphodynamics, pp. 615–640. https://doi.org/10.1016/B978-0-08-102927-5.00025-4.
Grunert, P., Harzhauser, M., Rögl, F., Sachsenhofer, R., Gratzer, R., Soliman, A., Piller, W.E., 2010a. Oceanographic conditions as a trigger for the formation of an Early Miocene (Aquitanian) Konservat-Lagerstätte in the Central Paratethys Sea. Palaeogeogr. Palaeoclimatol. Palaeoecol. 292, 425–442. https://doi.org/10.1016/j.palaeo.2010.04.001.
Grunert, P., Soliman, A., Harzhauser, M., Müllegger, S., Piller, W., Roetzel, R., Rögl, F., 2010b. Upwelling conditions in the Early Miocene Central Paratethys Sea. Geol. Carpath. 61, 129–145. https://doi.org/10.2478/v1009 6-010-0006-3.
Grunert, P., Soliman, A., Ćorić, S., Roetzel, R., Harzhauser, M., Piller, W.E., 2012. Facies development along the tidal-influenced shelf of the Burdigalian Seaway: an example from the Ottnangian stratotype (Early Miocene, middle Burdigalian). Mar. Micropaleontol. 84–85, 14–36. https://doi.org/10.1016/j.marmi cro.2011.11.004.
Grunert, P., Hinsch, R., Sachenhofer, R., Ćorić, S., Harzhauser, M., Piller, W.E., Sperl, H., 2013. Early Burdigalian infill of the Puchkirchen Trough (North Alpine Foreland Basin, Central Paratethys): facies development and sequence stratigraphy. Mar. Pet. Geol. 39, 164–186.
Grunert, P., Tzanova, A., Harzhauser, M., Piller, W.E., 2014. Mid-Burdigalian Paratethyan alkenone record reveals link between orbital forcing, Antarctic ice-sheet dynamics and European climate at the verge to Miocene Climate Optimum. Glob. Planet. Chang. 123, 36–43. https://doi.org/10.1016/j.gloplacha.2014.10.011.
Grunert, P., Auer, G., Harzhauser, M., Piller, W.E., 2015. Stratigraphic constraints for the upper Oligocene to lower Miocene Puchkirchen Group (North Alpine Foreland Basin, Central Paratethys). Newsl. Stratigr. 48, 111–133. https://doi.org/10.1127/nos/2014/0056.
Halbritter, H., Ulrich, S., Grímsson, F., Weber, M., Zetter, R., Hesse, M., Buchner, R., Svojtka, M., Frosch-Radivo, A., 2018. Illustrated Pollen Terminology, Second ed. Springer, Vienna.
Hall, J.T., Savdra, C.E., 2008. Ichnofossils and ichnofabrics in syngenetic phosphatic concretions in siliciclastic shelf deposits, Ripley Formation, Cretaceous, Alabama. Palaios 23, 233–245.
Hammer, Ø., Harper, D.A.T., Ryan, P.D., 2001. PAST: Paleontological Statistics software package for education and data analysis. Palaeontol. Electron. 4 (1), 9.
Haq, B.U., Hardenbol, J., Vail, P.R., 1988. Mesozoic and Cenozoic chronostratigraphy and cycles of sea-level change. Soc. Econ. Paleontol. Mineral. Spec. Publ. 42, 71–107.
Harzhauser, M., Mandic, O., 2001. Late Oligocene gastropods and bivalves from the Lower and Upper Austrian Molasse Basin. In: Piller, W.E., Rasser, M.W. (Eds.), Paleogene of the Eastern Alps. Österreichische Akademie der Wissenschaften, 14. Schriftenreihe der Erdwissenschaftliche Komission, pp. 671–795.
Harzhauser, M., Mandic, O., 2008. Neogene lake systems of Central and South-Eastern Europe: Faunal diversity, gradients and interrelations. Palaeogeogr. Palaeoclimatol. Palaeoecol. 260, 417–434. https://doi.org/10.1016/j.palaeo.2007.12.013.
Harzhauser, M., Piller, W.E., 2007. Benchmark data of a changing sea – palaeogeography, palaeobiogeography and events in the Central Paratethys during the Miocene. Palaeogeogr. Palaeoclimatol. Palaeoecol. 253, 8–31. https://doi.org/10.1016/j.palae o.2007.03.031.
Harzhauser, M., Mandic, O., Kern, A.K., Piller, W.E., Neubauer, T.A., Albrecht, C., Wilke, T., 2013. Explosive demographic expansion by dreissenid bivlaves as a possible result of astronomical forcing. Biogeosciences 10, 8423–8431. https://doi.org/10.5194/bg-10-8423-2013.
Hesse, M., Halbritter, H., Zetter, R., Weber, M., Buchner, R., Frosch-Radivo, A., Ulrich, S., 2009. Pollen Terminology – An Illustrated Handbook. Springer, Wien.
Hilgen, F., Lourens, L.J., Van Dam, J.A., 2012. The Neogene Period. In: Gradstein, F.M., Ogg, J.G., Schmitz, M.D., Ogg, G.M. (Eds.), The Geological Time Scale 2012, vol. 1. Elsevier, pp. 923–978.
Hochuli, P.A., 1978. Palynologische Untersuchungen im Oligozän und Untermiozän der Zentralen Paratethys. Beitr. Paläontol. Österr. 4, 1–132.
Hoffmann-Sell, L., Birgel, D., Arning, E.T., Föllmi, K.B., Peckmann, J., 2011. Archaeal lipids in Neogene dolomites (Monterey and Sisquoc Formations, California) – Planktic versus benthic archaeal sources. Org. Geochem. 42, 593–604.
Hofmayer, F., Kirscher, U., Sant, K., Krijgsman, W., Fritzer, T., Jung, D., Weissbrodt, V., Reichenbacher, B., 2019. Three-dimensional geological modeling supports a revised Burdigalian chronostratigraphy in the North Alpine Foreland Basin. Int. J. Earth Sci. 108, 2627–2651. https://doi.org/10.1007/s00531-019-01780-0.
Hohenegger, J., 2005. Estimation of environmental paleogradient values based on presence/absence data: a case study using benthic foraminifera for paleodepth estimation. Palaeogeogr. Palaeoclimatol. Palaeoecol. 217, 115–130. https://doi.org/10.1016/j.palaeo.2004.11.020.
Holcová, K., Brzobohatý, R., Kopecká, J., Nehyba, S., 2015. Reconstruction of the unusual Middle Miocene (Badenian) palaeoenvironment of the Carpathian Foredeep (Lomnice/Tisnov denudational relict, Czech Republic). Geol. Quarter. 59, 654–678. https://doi.org/10.7306/gq.1249.
Holcová, K., Doláková, N., Nehyba, S., Vacek, F., 2018. Timing of Langhian bioevents in the Carpathian Foredeep and northern Pannonian Basin in relation to ocean o graphic, tectonic and climatic processes. Geol. Quarter. 62, 3–17. https://doi.org/10.7306/gq.1399.
Houben, A.J.P., Van Mourik, C.A., Montanari, A., Coccioni, R., Brinkhuis, H., 2012. The Eocene-Oligocene transition: changes in sea-level, temperature or both? Palaeogeogr. Palaeoclimatol. Palaeoecol. 335–336, 75–83. https://doi.org/10.1016/j.palaeo.2011.04.008.
Howard, J.D., Frey, R.W., 1984. Characteristic trace fossils in nearshore to offshore sequences, Upper Cretaceous of east-central Utah. Can. J. Earth Sci. 21, 200–219.
Hülscher, J., Fischer, G., Grunert, P., Auer, G., Bernhardt, A., 2019. Selective recording of tectonic forcings in an Oligocene/Miocene Submarine Channel System: insights from new age constraints and sediment volumes from the Austrian Northern Alpine Foreland Basin. Front. Earth Sci. 7, 302.

Hunter, R.E., Clifton, H.E., 1982. Cyclic deposition and hummocky cross-stratification of probable storm origin in Upper Cretaceous rocks of the Sebastian area, southwestern Oregon. J. Sediment. Petrol. 52, 127–143. https://doi.org/10.1306/212F7EF5-2B24-11D7-8648000102C1865D.
IPNI, 2020. International Plant Names Index. Published on the Internet https://www.ipni.org. The Royal Botanic Gardens, Kew, Harvard University Herbaria & Libraries and Australian National Botanic Gardens [Retrieved 10.23.2020].
Jiménez-Moreno, G., Fauquette, S., Suc, J.P., 2008. Vegetation, climate and palaeoaltitude reconstructions of the Eastern Alps during the Miocene based on pollen records from Austria, Central Europe. J. Biogeogr. 35, 1638–1649. https://doi.org/10.1111/j.1365-2699.2008.01911.x.
Jiricek, R., Seifert, P.H., 1990. Palaeogeography of the Neogene in the Vienna Basin and the adjacent part of the foredeep. In: Minariková, D., Lobitzer, H. (Eds.), Thirty Years of Geological Cooperation between Austria and Czechoslovakia. Geological Survey, Prague, pp. 89–105.
Kaiho, K., 1994. Benthic foraminiferal dissolved-oxygen index and dissolved-oxygen levels in the modern ocean. Geology 22, 719–722. https://doi.org/10.1130/00917613.
Kalifi, A., Sorrel, P., Leloup, P.-H., Spina, V., Huet, B., Galey, A., Rubino, J.-L., Pittet, B., 2020. Changes in hydrodynamic process dominance (wave, tide or river) in foreland sequences: the subalpine Miocene Molasse revisited (France). Sedimentology 67, 2455–2501. https://doi.org/10.1111/sed.12708.
Kälin, D., Kempf, O., 2009. High-resolution stratigraphy from the continental record of the Middle Miocene Northern Alpine Foreland Basin of Switzerland. In: Neues Jahrbuch für Geologie und Paläontologie Abhandlungen, 254, pp. 177–235. https://doi.org/10.1127/0077-7749/2009/0010.
Kaminski, M.A., Gradstein, F.M., 2005. Atlas of Paleogene cosmopolitan deep-water agglutinated foraminifera. Grzybowski Found. Special Publ. 10, 547 pp.
Karagiuleva, J.D., 1964. Les Fossiles de Bulgarie. In: 6a, Palèogene Mollusca. Bulgarian Academy of Sciences, Sofia, 270 p.
Kelly, S.R.A., Bromley, R.G., 1984. Ichnological nomenclature of clavate borings. Palaeontology 27, 793–807.
Klaus, W., 1971. Shape and preservation of fossil pollen grains in coprolites and phosphorites. Neues Jahrbuch der Geologischen Bundesanstalt Monatsheft 9, 537–551.
Knaust, D., 2017. Atlas of Trace Fossils in Well Core: Appearance, Taxonomy and Interpretation. Springer. https://doi.org/10.1007/978-3-319-49837-9_1, 271 pp.
Knaust, D., 2018. The ichnogenus *Teichichnus* Seilacher, 1955. Earth Sci. Rev. 177, 386–403.
Knierzinger, W., Wagreich, M., Palzer-Khomenko, M., Gier, S., Meszar, M., Lee, E.Y., Koukal, V., Strauss, P., 2019. Provenance and palaeogeographic evolution of Lower Miocene sediments in the eastern North Alpine Foreland Basin. Swiss J. Geosci. 112, 269–286. https://doi.org/10.1007/s00015-018-0312-9.
Kocsis, L., Vennemann, T.W., Fontignie, D., Baumgartner, C., Montanari, A., Jelen, B., 2008. Oceanographic and climatic evolution of the Miocene Mediterranean deduced from Nd, Sr, C, and O isotope composition of marine fossils and sediments. Palaeoceanography 23. https://doi.org/10.1029/2007PA001540.
Koenen, A.v., 1883. Das Norddeutsche Unter-Oligocän und seine Mollusken-Fauna. Abhandlungen zur geologischen Specialkarte von Preussen und Thüringischen Staten 10 (5), 1005–1248.
Korobkov, I.A., 1939. Mollusken des Unteren Oligozäns des Nord-Kaukasus (Zone Variamussium fallax Korobkov). Abhandlungen des Geologischen Erdöl-Instituts, Leningrad-Moskva, Ser. A 113, 3–94 (in Russian with German abstract).
Kottek, M., Grieser, J., Beck, C., Rudolf, B., Rubel, F., 2006. World Map of the Köppen-Geiger climate classification updated. Meteorol. Z. 15, 259–263. https://doi.org/10.1127/0941-2948/2006/0130.
Kouwenhoven, T.V., Van der Zwaan, G.J., 2006. A reconstruction of late Miocene Mediterranean circulation patterns using benthic foraminifera. Palaeogeogr. Palaeoclimatol. Palaeoecol. 238, 373–385. https://doi.org/10.1016/j.palaeo.2006.03.035.
Kovác, M., Hudácková, N., Halásová, E., Kovácová, M., Holcová, K., Oszczypko-Clowes, M., Báldi, K., Less, G., Nagymarosy, A., Ruman, A., Kluciar, T., Jamrich, M., 2017. The Central Paratethys palaeoceanography: a water circulation model based on microfossil proxies, climate, and changes of depositional environment. Acta Geol. Slov. 9, 75–114.
Kovar-Eder, J., Berger, J.-P., 1987. Die oberoligozäne Flora von Unter-Rudling bei Eferding in Oberösterreich. Ann. Naturhist. Mus. Wien 89, 57–93.
Kovar-Eder, J., Jechorek, H., Kvacek, Z., Parashiv, V., 2008. The integrated plant record: an essential tool for reconstructing Neogene Zonal Vegetation in Europe. Palaios 23, 97–111.
Kranner, M., Harzhauser, M., Mandic, O., Strauss, P., Siedl, W., Piller, W.E., 2021. Early and middle Miocene paleobathymetry of the Vienna Basin (Austria). Mar. Pet. Geol. 132, 105187. https://doi.org/10.1016/j.marpetgeo.2021.105187.
Krenmayr, H.-G., Roetzel, R., 2000a. Mega-scale cross stratification in tide-influenced Egerian sands of the Austrian Molasse. Mitteilungen der Gesellschaft der Geologie- und Bergbaustudenten in Österreich 43, 1–156.
Krenmayr, H.-G., Roetzel, R., 2000b. Die lithostratigraphische Formalisierung der Melker- und Linzer Sande: die “Linz-Melk-Formation”. Berichte des Instituts für Geologie und Paläontologie der Universität Graz 2, 10.
Kroh, A., 2005. Catalogus Fossilium Austriae. Band 2. Echinoidea Neogenica, 210 pp.
Kuhlemann, J., Kempf, O., 2002. Post-Eocene evolution of the North Alpine Foreland Basin and its response to Alpine tectonics. Sediment. Geol. 152, 45–78. https://doi.org/10.1016/S0037-0738(01)00285-8.
Kuhlemann, J., Frisch, W., Szekely, B., Dunkl, I., Kazmer, M., 2002. Post-collisional sediment budget history of the Alps: tectonic versus climatic control. Int. J. Earth Sci. 91, 818–837. https://doi.org/10.1007/s00531-002-0266-y.
Kulm, L.D., Roush, R.C., Harlett, J.C., Neudeck, R.H., Chambers, D.M., Runge, E.J., 1975. Oregon continental shelf sedimentation: interrelationship of facies distribution and sedimentary processes. J. Geol. 83 (2), 145–175. https://doi.org/10.1086/628080.
Kuščer, D., 1967. Teriary formations of Zagorje. In: Geologija, Razprave in Poročila, 10, pp. 5–86.
Ledoux, J.-C., 1972. Les Squalidae (Euselachii) miocènes des environs d'Avignon (Vaucluse). Documents des Laboratoires de Geologie de la Facult des Sciences de Lyon, Notes et Mémoires 52, 133–175.
Lemcke, K., 1973. Die Lagerung der jüngsten Molasse im nördlichen Alpenvorland. Bulletin der Vereinigung Schweizer Petroleum-Geologen und Ingenieure 39 (95), 29–41.
Lemcke, K., 1988. Geologie von Bayern 1: Das bayerische Alpenvorland vor der Eiszeit – Erdgeschichte, Bau, Bodenschätze. Schweizerbart 5-65, 125–135.
Leymerie, M.A., 1842. Suite de mémoire sur le terrain Crétacé du département de l'Aube. Mémoire de la Société géologique de France 5, 1–34.
Lin, W., Bhattacharya, J.P., 2020. Depositional facies and the sequences stratigraphic control of a mixed-process influenced clastic wedge in the Cretaceous Western Interior Seaway: the Gallup System, New Mexico, USA. Sedimentology 67, 920–950. https://doi.org/10.1111/sed.12667.
Löffler, S.-B., 1999. Systematische Neubearbeitung und Paläoökologische Aspekte der unteroligozänen Molluskenfauna aus den Zementmergeln von Bad Häring (Unterinntal, Tirol). Tübinger Geowissenschaftliche Arbeiten, A 54, 1–207.
Longhitano, S.G., 2008. Sedimentary facies and sequence stratigraphy of coarse-grained Gilbert-type deltas within Pliocene thrust-top Potenza Basin (Southern Apennines, Italy). Sediment. Geol. 210, 87–110. https://doi.org/10.1016/j.sedgeo.2008.07.004.
Mandic, O., Rundic, L.J., Ćorić, S., Pezelj, D., Theobalt, D., Sant, K., Krijgsman, W., 2019a. Age and mode of the middle Miocene marine flooding of the Pannonian Basin - constraints from central Serbia. Palaios 34, 71–95. https://doi.org/10.2110/palo.2018.052.
Mandic, O., Sant, K., Kallanxhi, M.-E., Ćorić, S., Theobalt, D., Grunert, P., De Leeuw, A., Krijgsman, W., 2019b. Integrated bio-magnetostratigraphy of the Badenian reference section Ugljevik in southern Pannonian Basin - implications for the Paratethys history (middle Miocene, Central Europe). Glob. Planet. Chang. 172, 374–395. https://doi.org/10.1016/j.glopl acha.2018.10.010.
Mandic, O., Schneider, S., Harzhauser, M., Danninger, W., 2020. Bivalves from the Innviertel Group of Allerding in the North Alpine Foreland Basin (lower Miocene, Upper Austria). N. Jb. Geol. Paläont. 297, 47–100. https://doi.org/10.1127/njgpa/2020/0914.
Mángano, M.G., Buatois, L.A., 1991. Discontinuity surfaces in the Lower Cretaceus of the High Andes (Mendoza, Argentina): trace fossils and environmental implications. J. S. Am. Earth Sci. 4, 215–299.
Marquet, R., 2002. The Neogene Amphineura and Bivalvia (Protobranchia and Pteriomorphia) from Kallo and Doel (OostVlaanderen, Belgium). Paleontos 2, 1–99.
Marquet, R., Lenaerts, J., Laporte, J., 2012. A systematic study of the Bivalvia (Mollusca) from the Grimmertingen Sand Member and from the Klimmen Member (Early Oligocene) in Belgium and the Netherlands. Palaeontos 22, 1–118.
Marshall, J.D., Pirrie, D., 2013. Carbonate concretions – explained. Geol. Today 29, 53–62.
Martini, E., 1971. Standard Tertiary and Quaternary calcareous nanoplankton zonation. In: Ferinacci, A. (Ed.), Proceeding of 2nd Planktonic Conference, Roma 1970, pp. 739–785.
Marx, F.G., Albers, J., Berning, B., 2011. Lost in translation – a history of systematic confusion and comments on the type species of *Squalodon* and *Patriocetus* (Cetacea, Odontoceti). Palaeontology 54, 303–307. https://doi/10.1111/j.1475-4983.2010.01018.
Masalimova, L.U., Lowe, D.R., McHargue, T., Derksen, R., 2015. Interplay between an axial channel belt, slope gullies and overbank deposits in the Puchkirchen-Formation in the Molasse Basin, Austria. Sedimentology 62, 1717–1748. https://doi.org/10.1111/sed.12201.
Mastrototaro, F., D'Onghia, G., Corriero, G., 2010. Biodiversity of the white coral ecosystem off Cape Santa Maria di Leuca (Mediterranean Sea): an update. Deep-Sea Res. II 57, 412–430. https://doi.org/10.1016/j.dsr2.2009.08.021.
Mayer, M.C., 1861. Description de Coquilles fossiles des tertiaires inférieurs. Journal de Conchyliologie, 9 (Ser. 5, tome 1) 52–68.
Mayoral, E., Santos, A., Gámez-Vintaned, J.A., Wisshak, M., Neumann, C., Uchman, A., Nel, A., 2020. Bivalve bioerosion in Cretaceous-Neogene amber around the globe, with implications for the ichnogenera *Teredolites* and *Apectoichnus*. Palaeogeogr. Palaeoclimatol. Palaeoecol. 538, 109410. https://doi.org/10.1016/j.palaeo.2019.109410.
McRae, S.G., 1972. Glauconite. Earth Sci. Rev. 8, 397–440.
Melnyk, S., Packer, S., Zonneveld, J.-P., Gingras, M.K., 2020. A new marine woodground ichnotaxon from the Lower Cretaceous Mannville Group, Saskatchewan, Canada. J. Paleontol. 1–8. https://doi.org/10.1017/jpa.2020.63.
Mikkelsen, P.M., Bieler, R., 1989. Biology and comparative anatomy of Divariscintilla yoyo and D. troglodytes, two new species of Galeommatidae Bivalvia from Stomatopod burrows in Eastern Florida. Malacologia 31, 175–195.
Milker, Y., Schmiedl, G., 2012. A taxonomic guide to modern benthic shelf foraminifera of the western Mediterranean Sea. Palaeontol. Electron. 15, 1–134. https://palaeo-electronica.org/content/pdfs/271.pdf.
Miller, W. (Ed.), 2007. Trace Fossils Concepts, Problems, Prospects. Elsevier, Amsterdam, 611 pp.
Mosbrugger, V., Utescher, T., Dilcher, D.L., 2005. Cenozoic continental climatic evolution of Central Europe. Proc. Natl. Acad. Sci. 102, 14964–14969. https://doi.org/10.1073/pnas.0505267102.
Mozley, P.S., Davis, J.M., 2005. Internal structure and mode of growth of elongate calcite concretions: evidence for small-scale, microbially induced, chemical heterogeneity in groundwater. Geol. Soc. Am. Bull. 117, 1400–1412.

Murray, J.W., 1991. Ecology and Paleoecology of Benthic Foraminifera. Longman Scientific and Technical, 365 p. https://doi.org/10.1017/S0025315400053650.
Murray, J.W., 2006. Ecology and Applications of Benthic Foraminifera. Cambridge University Press. https://doi.org/10.1017/CBO9780511535529, 438 p.
Nebelsick, J.H., Rasser, M., Höltke, O., Thompson, J.R., Bieg, U., 2019. Turritelline mass accumulations from the Lower Miocene of southern Germany: implications for tidal currents and nutrient transport within the North Alpine Foreland Basin. Lethaia 53 (2). https://doi.org/10.1111/let.12356.
Nehyba, S., Roetzel, R., 2010. Fluvial deposits of the St. Marein-Freischling Formation - insights into initial depositional processes on the distal external margin of the Alpine-Carpathian Foredeep in Lower Austria. Aust. J. Earth Sci. 103 (2), 50–80.
Nolf, D., 2013. The Diversity of Fish Otoliths, Past and Present. Royal Belgian Institute of Natural Sciences, Brussels.
Nolf, D., Brzobohatý, R., 1994. Fish otoliths from the Late Oligocene (Eger and Kiscell Formations) in the Eger area (northeastern Hungary). Bull. Inst. R. Sci. Nat. Belg. Sci. Terre 64, 225–252.
Nummedal, D., Cole, R., Young, R., Shanley, K., Boyles, M., 2001. Book Cliffs sequence stratigraphy: The Desert and Castlegate Sandstones. In: 2001 Annual Convention of the American Association of Petroleum Geologists, GJGS/SEPM Field Guide Trip 15. Oomkens, E. & Terwindt, J. H. J, Denver, Colorado, pp. 1–81.
Ortner, H., Stingl, V., 2001. Facies and basin development of the Oligocene in the Lower Inn Valley, Tyrol/Bavaria. In: Piller, W.E., Rasser, M.W. (Eds.), Paleogene of the Eastern Alps. Österreichische Akademie der Wissenschaften. Schriftenreihe der Erdwissenschaftliche Komission, 14, pp. 153–196.
Özer, M.S., Sancay, R.H., Şen, Ş., Sözeri, K., Métais, G., Ayyıldız, T., Varol, B., 2017. Paleoenvironment of the Late Oligocene from the Kağızman-Tuzluca Basin (northeastern Anatolia) based on the micro- and macrofloras. Turk. J. Earth Sci. 26, 227–248. https://doi.org/10.3906/yer-1612-26.
Palzer-Khomenko, M., Wagreich, M., Knierzinger, W., Meszar, M., Gier, S., Kallanxhi, M.-E., Soliman, A., 2018. A calcite crisis unravelling Early Miocene (Ottnangian) stratigraphy in the North Alpine-Carpathian Foreland Basin: a litho- and chemostratigraphic marker for the Rzehakia Lake System. Geol. Carpath. 69, 315–334. https://doi.org/10.1515/geoca-2018-0019.
Pemberton, G.S., Spila, M., Pulham, A.J., Saunders, T., MacEachern, J.A., Robbins, D., Sinclair, I.K., 2001. Ichnology & Sedimentology of shallow to marginal marine systems: Ben Nevis & Avalon Reservoirs, Jeanne D'Arc Basin. In: Geological Association of Canada, Short Course Notes, 15, 343 pp.
Pemberton, S.G., MacEachern, J.A., Dashtgard, S.E., Bann, K.L., Gingras, M.K., Zonneveld, J.-P., 2012. Shorefaces. In: Knaust, D., Bromley, R.G. (Eds.), Developments in Sedimentology, 64. Elsevier, pp. 563–603. https://doi.org/10.1016/B978-0-444-53813-0.00019-8.
Pfeil, F.H., 1981. Eine nektonische Fischfauna aus dem unteroligozänen Schönecker Fischschiefer des Galon-Grabens in Oberbayern. Geol. Bavarica 82, 357–388.
Piller, W.E., Harzhauser, M., Mandic, O., 2007. Miocene Central Paratethys stratigraphy – current status and future directions. Stratigraphy 4, 151–168.
Pippèrr, M., 2011. Characterisation of Ottnangian (middle Burdigalian) palaeoenvironments in the North Alpine Foreland Basin using benthic foraminifera - a review of the Upper Marine Molasse of southern Germany. Mar. Micropaleontol. 79, 80–99. https://doi.org/10.1016/j.marmi cro.2011.02.002.
Pippèrr, M., Reichenbacher, B., 2010. Foraminifera from the borehole Altdorf (SE Germany): proxies for Ottnangian (early Miocene) palaeoenvironments of the Central Paratethys. Palaeogeogr. Palaeoclimatol. Palaeoecol. 289, 62–80. https://doi.org/10.1016/j.palaeo.2010.02.009.
Pippèrr, M., Reichenbacher, B., 2017. Late Early Miocene palaeoenvironmental changes in the North Alpine Foreland Basin. Palaeogeogr. Palaeogeogr. Palaeoecol. 468, 485–502. https://doi.org/10.1016/j.palaeo.2017.01.002.
Pippèrr, M., Reichenbacher, B., Kirscher, U., Sant, K., Hanebeck, H., 2018. The middle Burdigalian in the North Alpine Foreland Basin (Bavaria, SE Germany) – a lithostratigraphic re-evaluation. Newsl. Stratigr. 51, 285–309. https://doi.org/10.1127/nos/2017/0403.
Pirkenseer, C., Rauber, G., Roussé, S., 2018. A revised Palaeogene lithostratigraphic framework for the northern Swiss Jura and the southern Upper Rhine Graben and its relationship to the North Alpine Foreland Basin. Riv. Ital. Paleontol. Stratigr. 124, 163–246.
Pollerspöck, J., Straube, N., 2017. A new deep-sea elasmobranch fauna from the Central Paratethys (Neuhofener Beds, Mitterdorf, near Passau, Germany, Early Miocene, Middle Burdigalian). Zitteliana 90, 27–54.
Pollerspöck, J., Flammensbeck, C.K., Straube, N., 2018. *Palaeocentroscymnus* (Chondrichthyes: Somniosidae), a new sleeper shark genus from Miocene deposits of Austria (Europe). Paläontol. Z. 92, 443–456. https://doi.org/10.1007/s12542-017-0398-9.
Pollerspöck, J., Güthner, T., Straube, N., 2020. Re-evaluation of the Lower Miocene (Burdigalian, Ottnangian) elasmobranch fauna (Elasmobranchii, Neoselachii) from Upper Austria (Allerding, near Schärding, Austria) with comments on the paleogeographic distribution of the recorded squaliform sharks. Annalen des Naturhistorischen Museums in Wien, Serie A 122.
Popov, S.V., Voronina, A.A., Goncharova, I.A., 1993. Oligocene-Lower Miocene stratigraphy and bivalves of the Eastern Paratethys. Trudy Paleontologicheskogo instituta Moskva 256, 1–206 (in Russian).
Poppe, G.T., Goto, Y., 1993. European Seashells. Scaphopoda, Bivalvia, Cephalopoda. Verlag Christa, Wiesbaden, 221, p.
Pytlak, L., Gross, D., Sachsenhofer, R.F., Bechtel, A., Linzer, H.-G., 2017. Gas accumulations in Oligocene-Miocene reservoirs in the Alpine Foreland Basin (Austria): evidence for gas mixing and gas degradation. Int. J. Earth Sci. 106, 2171–2188. https://doi.org/10.1007/s00531-016-1421-1.
Raiswell, R., Fisher, Q.J., 2004. Rates of carbonate cementation associated with sulphate reduction in DSDP/ODP sediments: implications for the formation of concretions. Chem. Geol. 211, 71–85.
Rasmussen, T.L., 2005. Systematic paleontology and ecology of benthic foraminifera from the Plio-Pleistocene Kallithea Bay section, Rhodes, Greece. Cushman Found. Spec. Publ. 39, 53–157.
Ratschbacher, L., Dingeldey, C., Miller, C., Hacker, B.R., McWilliams, M.O., 2004. Formation, subduction, and exhumation of Penninic oceanic crust in the Eastern Alps: time constraints from 40Ar/39Ar geochronology. Tectonophysics 394, 155–170. https://doi.org/10.1016/j.tecto.2004.08.003.
Reichenbacher, B., 1993. Mikrofaunen, Paläogeographie und Biostratigraphie der miozänen Brack- und Süßwassermolasse in der westlichen Paratethys unter besonderer Berücksichtigung der Fisch-Otolithen. Senckenb. Lethaea 73, 277–374.
Reichenbacher, B., 1999. Preliminary otolith-zonation in continental Tertiary deposits of the Paratethys and adjacent areas. Neues Jahrb. Geol. Palaontol. Abh. 214, 375–390. https://doi.org/10.1127/njgpa/214/1999/375.
Reinecke, H.-E., Singh, I.B., 1980. Depositional Sedimentary Environments – With Reference to Terrigenous Clastics. Springer, 4pp.
Reinecke, T., Balsberger, M., Beaury, B., Pollerspöck, J., 2014. The elasmobranch fauna of the Thalberg Beds, early Egerian (Chattian, Oligocene), in the Subalpine Molasse Basin near Siegsdorf, Bavaria, Germany. Palaeontos 26, 1–127.
Reitner, H., Malecki, G., Roetzel, R., 2005. SedPacWin – SedpacMac – Characterization of Sediments by Grainsize Analysis. Geophysical Research Abstracts 7, EGU General Assembly Vienna 2005. SRef-ID: 1607-7962/gra/EGU05-A-04297.
Roetzel, R., Hochuli, P., Steininger, F., 1983. Die Faziesentwicklung des Oligozän in der Molassezone zwischen Krems und Wieselburg (Niederösterreich). Jahrb. Geol. Bundesanst. 126, 129–179.
Roetzel, R., Mandic, O., Steininger, F.F., 1999. Lithostratigraphie und Chronostratigraphie der tertiären Sedimente im westlichen Weinviertel und angrenzenden Waldviertel. In: Arbeitstagung der Geologischen Bundesanstalt 1999 Retz-Hollabrunn, pp. 38–54.
Roetzel, R., Ćorić, S., Galovic, I., Rögl, F., 2006. Early Miocene (Ottnangian) coastal upwelling conditions along the southeastern scarp of the Bohemian Massif (Parisdorf, Lower Austria, Central Paratethys). Beiträge zur Paläonol. 30, 387–413.
Roetzel, R., de Leeuw, A., Mandic, O., Márton, E., Nehyba, S., Kuiper, K.F., Scholger, R., Wimmer-Frey, I., 2014. Lower Miocene (Upper Burdigalian, Karpatian) volcanic ash-fall at the south-eastern margin of the Bohemian Massif in Austria - new evidence from $^{40}Ar/^{39}Ar$-dating, palaeomagnetic, geochemical and mineralogical investigations. Aust. J. Earth Sci. 107, 2–22.
Rögl, F., 1996. Stratigraphic correlation of the Paratethys Oligocene and Miocene. Mitteilungen der Gesellschaft der Geologie- und Bergbaustudenten Österreich 41, 65–73.
Rögl, F., 1998. Palaeogeographic Considerations for Mediterranean and Paratethys Seaways (Oligocene to Miocene). Ann. Naturhist. Mus. Wien 99, 279–310.
Rögl, F., Spezzaferri, S., 2003. Foraminiferal paleoecology and biostratigraphy of the Mühlbach section. Gaindorf Formation, Lower Badenian, Lower Austria. Ann. Naturhist. Mus. Wien 104A, 23–75.
Rögl, F., Steininger, F., 1969. Miogypsina (Miogypsinoides) formosensis Yabe & Hanzawa, 1928 (Foraminiferida) aus den Linzer Sanden (Egerien-Oberoligozän) von Plesching bei Linz, Oberösterreich. Mitteilungen der Geologischen Gesellschaft 62, 46–54.
Rögl, F., Steininger, F.F., 1983. Vom Zerfall der Tethys zu Mediterran und Paratethys – Die neogene Paläogeographie und Palinspastik des zirkum-meditarranen Raumes. Ann. Naturhist. Mus. Wien 85, 135–163.
Rosenberg, R., Elmgren, R., Fleischer, S., Jonsson, P., Persson, G., Dahlin, H., 1990. Marine Eutrophication Case Studies in Sweden. Ambio 19, 102–108.
Rueda, J.L., Urra, J., Aguilar, R., Angeletti, L., Bo, M., García-Ruiz, C., González-Duarte, M.M., López, E., Madurell, T., Maldonado, M., Mateo-Ramírez, Á., Megina, C., Moreira, J., Moya, F., Ramalho, L.V., Rosso, A., Sitjà, C., Taviani, M., 2019. Cold-water coral associated fauna in the Mediterranean Sea and adjacent areas. In: Orejas, C., Jiménez, C. (Eds.), Mediterranean Cold-Water Corals: Past, Present and Future. Coral Reefs of the World, 9, pp. 295–333.
Rupp, C., Ćorić, S., 2012. Zur Ebelsberg-Formation. Jahrb. Geol. Bundesanst. 152, 67–100.
Rupp, C., Ćorić, S., 2015. Zur Eferding-Formation. Jahrb. Geol. Bundesanst. 155, 33–95.
Rupp, C., Linner, M., Mandl, G.W., 2011. Geologie der Österreichischen Bundesländer. Erläuterungen zur Geologischen Karte von Oberösterreich 1:200.000. Geologische Bundesanstalt.
Sacco, F., 1897. I Molluschi dei terreni terziarii del Piemonte e della Liguria. In: Parte XXIV (Pectinidae). Torino, Carlo Clausen, 71 p.
Sacco, F., 1898. I Molluschi dei terreni terziarii del Piemonte e della Liguria. In: Parte XXVI (Arcidae, Pectunculidae, Limopsidae, Nuculidae, Ledidae e Malletidae). Torino, Carlo Clausen, 92 p.
Sachsenhofer, R.F., Leitner, B., Linzer, H.-G., Bechtel, A., Ćorić, S., Gratzer, R., Reischenbacher, D., Soliman, A., 2010. Deposition, erosion and hydrocarbon source potential of the Oligocene Eggerding Formation (Molasse Basin, Austria). Aust. J. Earth Sci. 103, 76–99.
Sant, K., Kirscher, U., Reichenbacher, B., Pippèrr, M., Jung, D., Doppler, G., Krijgsman, W., 2017. Late Burdigalian Sea retreat from the North Alpine Foreland Basin: new magnetostratigraphic age constraints. Glob. Planet. Chang. 152, 38–50. https://doi.org/10.1016/j.gloplacha.2017.02.002.
Savrda, C.E., Ozalas, K., Demko, T.H., Huchison, R.A., Scheiwe, T.D., 1993. Loggrounds and the ichnofossil *Teredolites* in transgressive deposits of the Clayton Formation (Lower Paleocene), western Alabama. Palaios 8, 311–324.
Schäfer, A., 2020. Klastische Sedimente - Fazies und Sequenzstratigraphie, 2. edition. Springer.

Schlirf, M., 2000. Upper Jurassic trace fossils from the Boulonnais (northern France). Geol. Palaeontol. 34, 145–213.
Schlunegger, F., Melzer, J., Tucker, G.E., 2001. Climate, exposed source-rock lithologies, crustal uplift and surface erosion: a theoretical analysis calibrated with data from the Alps/North Alpine Foreland Basin system. Int. J. Earth Sci. 90, 484–499. https://doi.org/10.1007/s005310100174.
Schlüter, N., Wiese, F., Reich, M., 2015. Systematic assessment of the Atelostomata (Spatangoida and Holasteroida; irregular echinoids) based on spine microstructure. Zool. J. Linnean Soc. 175, 510–524. https://doi.org/10.1111/zoj.12291.
Schneider, S., Prieto, J., 2011. First record of an autochthonous community of fluviatile freshwater molluscs from the Middle/Late Miocene Upper Freshwater Molasse (southern Germany). Archiv für Molluskenkunde 140, 1–18. https://doi.org/10.1127/arch.moll/1869-0963/140/001-018.
Schultz, O., 2001. Bivalvia neogenica. 1. Nuculacea-Unionacea, pp. 1-379 [2001]; 2. Lucinoidea-Mactroidea, pp. 381–690 [2003]; 3. Solenoidea-Clavagelloidea, pp. 691–1212 [2005]. In: Piller W.E. (Ed.), Catalogus Fossilium Austriae. Vol. 1 (Verlag der Österreichischen Akademie der Wissenschaften) Wien.
Schulz, H.N., Schulz, H.D., 2005. Large sulfur bacteria and the formation of phosphorite. Science 307, 416–418. https://doi.org/10.1126/science.1103096.
Schwarzhans, W., 2013. A comparative morphological study of the recent otoliths of the genera *Diaphus*, *Idiolychnus* and *Lobianchia* (Myctophidae). Palaeo-Ichthyologica 13, 41–82. https://doi.org/10.13140/2.1.2872.3843.
Seilacher, A., 1955. Spuren und Fazies im Unterkambrium. In: Schindewolf, O.H., Seilacher, A. (Eds.), Beiträge zur Kenntnis des Kambriums in der Salt Range (Pakistan). Akademie der Wissenschaften und der Literatur in Mainz. Abhandlungen der mathematisch-naturwissenschaftlichen Klasse, 10, pp. 373–399.
Seilacher, A., 2001. Concretion morphologies reflecting diagenetic and epigenetic pathways. Sediment. Geol. 143, 41–57.
Selles-Martinez, 1996. Concretion morphology, classification and genesis. Earth Sci. Rev. 41, 177–210.
Sen Gupta, B., Smith, L.E., Machain-Castillo, M.L., 2009. Foraminifera of the Gulf of Mexico. In: Gulf of Mexico–Origins, Waters, and Biota. Biodiversity. Texas A and M Press, College Station, Texas, pp. 87–129.
Sgarrella, F., Moncharmont Zei, M., 1993. Benthic foraminifera of the Gulf of Naples (Italy): systematics and autoecology. Boll. Soc. Paleontol. Ital. 32, 145–264.
Sharman, G.R., Hubbard, S.M., Covault, J.A., Hinsch, R., Linzer, H.-G., Graham, S.A., 2018. Sediment routing evolution in the North Alpine Foreland Basin, Austria: Interplay of transverse and longitudinal sediment dispersal. Basin Research 30, 426–447.
Soysal, E., Wang, J., Jiang, M., Wu, Y., Pakhomov, S., Liu, H., Xu, H., 2017. CLAMP–a toolkit for efficiently building customized clinical natural language processing pipelines. J. Am. Med. Inform. Assoc. 25, 331–336. https://doi.org/10.1093/jamia/ocx132.
Spezzaferri, S., Tamburini, F., 2007. Paleodepth variations on the Eratosthenes Seamount Eastern Mediterranean: sea level changes or subsidence? Earth Discuss. 2, 115–132. https://doi.org/10.1029/2004PA001071.
Steininger, F.F., 1999. The continental European Miocene. Chronostratigraphy, Geochronology and Biochronology of the Miocene "European Land Mammal Mega - Zones" (ELMMZ) and the Miocene "Mammal - Zones (MN - Zones)". In: Rössner, G., Heissig, K. (Eds.), The Miocene Land Mammals of Europe. Pfeil, pp. 9–24.
Steininger, F.F., Wesseley, G., 2000. From the Tethys Ocean to the Paratethys Sea: Oligocene to Neogene stratigraphy, paleogeography and paleobiogeography of the circum-Mediterranean region and the Oligocene to Neogene Basin evolution in Austria. Mitteilungen der Österreichischen Geologischen Geselleschaft 92, 95–116.
Stenzel, H.B., 1971. Oysters. In: Treatise on Invertebrate Paleontology, Part, Bivalvia, 3, pp. 953–1224.
Steurbaut, E., 1979. Les otolithes de téléostéens des Marnes de Saubrigues (Miocène; Aquitaine méridionale, France). In: Palaeontographica. Abteilung A. Paläozoologie, Stratigraphie, 166, pp. 50–91.
Studencka, B., 2015. Middle Miocene bivalves from the Carpathian Foredeep Basin: the Busko (Młyny) PIG-1 and Kazimierza Wielka (Donosy) PIG-1 boreholes – stratigraphy and taxonomy. Biuletyn Państwowego Instytutu Geologicznego 461, 95–114. https://doi.org/10.1515/agp-2016-0017.
Studencka, B., Gontsharova, I.A., Popov, S.V., 1998. The bivalve faunas as a basis for reconstruction of the Middle Miocene history of the Paratethys. Acta Geol. Pol. 48, 285–342.
Swift, D.J., Han, G., Vincent, C.E., 1986. Fluid processes and sea-floor responses on a modern storm-dominated shelf: middle Antlantic shelf of North America. Part 1: The storm-current regime. In: Knight, R.J., McLean, J.R. (Eds.), Shelf Sands and Sandstones. Canadian Society of Petroleum Geologists, 2, pp. 99–119.
Székely, S.F., Bindiu-Haitonic, R., Filipescu, S., Bercea, R., 2017. Biostratigraphy and paleoenvironmental reconstruction of the marine lower Miocene Chechiș Formation in the Transylvanian Basin based on foraminiferal assemblages. Carnets de géologie 17, 11–37. https://doi.org/10.4267/2042/62041.
Tåning, A.V., 1932. Notes on Scopelids from the Dana Expeditions. I. Videnskabelige Meddelelser fra Dansk Naturhistorisk Forening, 94, pp. 125–146.
Taviani, M., Freiwald, A., Zibrowius, H., 2005. Deep-coral growth in the Mediterranean Sea: An overview. In: Freiwald, A., Roberts, J.M. (Eds.), Deep-Water Corals and Ecosystems. Springer-Verlag, Berlin Heidelberg, pp. 137–156.
Teschner, C., Reichenbacher, B., 2017. Otolith-based age determination of mid-Burdigalian marine sediments in the North Alpine Foreland Basin. Bull. Geosci. 92, 143–152. https://doi.org/10.3140/bull.geosc i.1659.
Thenius, E., 1979. Lebensspuren von Ephemeropteren-Larven aus dem Jung-Tertiär des Weiner Beckens. Ann. Naturhist. Mus. Wien 82, 177–188.
Uchman, A., 1998. Taxonomy and ethology of flysch trace fossils: a revision of the Marian Książkiewicz collection and studies of complementary material. Ann. Soc. Geol. Pol. 68, 105–218.
Uchman, A., 2001. Eocene flysch trace fossils from the Hecho Group of the Pyrenees, northern Spain. Beringeria 28, 3–41.
Uchman, A., 2011. Recent freshwater wood borings from the Vistula River in Poland. In: Carreiro-Silva, M., Ávila, S.P. (Eds.), 7th International Bioerosion Workshop, Faial, Azores, pp. 18–23 (September 2011: 30).
Uchman, A., Krenmayr, H.-G., 2004. Trace fossils, Ichnofabrics and sedimentary facies in the shallow marine Lower Miocene Molasse of Upper Austria. Jahrb. Geol. Bundesanst. 44, 233–251.
Uchman, A., Pervesler, P., 2007. Palaeobiological and palaeonvironmental significance of the Pliocene trace fossil *Dactyloidites peniculus*. Acta Palaeontol. Pol. 52, 799–808.
Uchman, A., Gaigalas, A., Melešytė, M., Kazauskas, V., 2007. Trace fossil *Asthenopodichnium lithuanicum* isp. nov. from the Late Neogene brown-coal deposits, Lithuania. Geol. Quarter. 50, 437–446.
Uchman, A., Johnson, M.E., Rebelo, A.C., Melo, C., Cordeiro, R., Ramalho, R., Ávila, S.P., 2016. Vertically-oriented trace fossil *Macaronichnus segregatis* from Neogene of Santa Maria Island (Azores; NE Atlantic) records a specific palaeohydrological regime on a small oceanic island. Geobios 49, 229–241. https://doi.org/10.1016/j.geobios.2016.01.016.
Uchman, A., Torres, P., Johnson, M.E., Berning, B., Ramalho, R.S., Rebelo, A.C., Melo, C. S., Baptista, L., Madeira, P., Cordeiro, R., Avila, S.P., 2018. Feeding traces of recent ray fish and occurences of the trace fossil *Piscichnus waitemata* from the Pliocene of Santa Maria Island, Azores (Northeast Atlantic). Palaios 33, 361–375. https://doi.org/10.2110/palo.2018.027.
Underwood, C.J., Schlögl, J., 2013. Deep-water chondrichthyans from the Early Miocene of the Vienna Basin (Central Paratethys, Slovakia). Acta Palaeontol. Pol. 58, 487–509. https://doi.org/10.4202/app.2011.0101.
Utescher, T., Erdei, B., François, L., Henrot, A.-J., Mosbrugger, V., Popova, S., 2020. Oligocene vegetation of Europe and western Asia: diversity change and continental pattern reflected by plant functional types. Geol. J. 56, 1–22. https://doi.org/10.1002/gj.3830.
Vakarcs, G., Hardenbol, J., Abreu, V.S., Vail, P.R., Várnai, P., Tari, G., 1998. Oligocene - Middle Miocene depositional sequences of the Central Paratethys and their correlation with regional stages. SEPM Spec. Publ. 60, 219–231.
Van Cappellen, P., Berner, R.A., 1991. Fluorapatite crystal growth from modified seawater solutions. Geochim. Cosmochim. Acta 55, 1219–1234.
Van der Boon, A., Beniest, A., Ciurej, A., Gázdzicka, E., Grothe, A., Sachsenhofer, R.F., Langereis, C.G., Krijgsman, W., 2018. The Eocene-Oligocene transition in the North Alpine Foreland Basin and subsequent closure of a Paratethys gateway. Glob. Planet. Chang. 162, 101–119. https://doi.org/10.1016/j.gloplacha.2017.12.009.
Van der Zwaan, G.J., Jorissen, F.J., Stigter, H.C., 1990. The depth dependency of planktonic/benthic foraminiferal ratios: constrains and applications. Mar. Geol. 95, 1–16. https://doi.org/10.1016/0025-3227(90)90016-D.
Vasconcelos, C., McKenzie, J.A., Bernasconi, S., Grujic, D., Tien, A.J., 1995. Microbial mediation as a possible mechanism for natural dolomite formation at low temperatures. Nature 377, 220–222.
Veeken, P.C.H., 2007. Seismic Stratigraphy, Basin Analysis and Reservoir Characterisation. Handbook of Geophysical Exploration, 37 p.
Voss, M., Berning, B., Reiter, E., 2016. A taxonomic and morphological re-evaluation of *"Halitherium" cristolii* Fitziniger, 1842 (Mammalia, Sirenia) from the late Oligocene of Austria, with the description of a new genus. Eur. J. Taxon. 256, 1–32. https://doi.org/10.5852/ejt.2016.256.
Wagner, L., 1996. Die tektonisch-stratigraphische Entwicklung der Molasse und deren Untergrundes in Oberösterreich und Salzburg. In: Egger, H., Hofmann, T., Rupp, C. (Eds.), Ein Querschnitt durch die Geologie Oberösterreichs. Wandertagung Österreichische Geologische Gesellschaft, pp. 36–65. " 7–11. Oktober 1996 in Wels 16.
Wagner, L.R., 1998. Tectono-stratigraphy and hydrocarbons in the Molasse Foredeep of Salzburg, Upper and Lower Austria. Geol. Soc. Spec. Publ. 134, 339–369. https://doi.org/10.1144/GSL.SP.1998.134.01.16.
West, A.J., Lin, C.-W., Lin, T.-C., Hilton, R.G., Liu, S.-H., Chang, C.-T., Lin, K.-C., Galy, A., Sparkes, R.B., Hovius, N., 2011. Mobilization and transport of coarse woody debris to the oceans triggered by an extreme tropical storm. Limnol. Oceanogr. 56, 77–85. https://doi.org/10.4319/lo.2011.56.1.0077.
Wimmer-Frey, I., Ćorić, S., Peresson, M., Rabeder, J., 2013. Mineralogische und korngrößenmäßige Untersuchungen an quartären und miozänen Sedimenten auf den Kartenblättern 55 Ober-Grafendorf und 56 St. Pölten. Arbeitstagung der Geologischen Bundesanstalt 2013 - Melk, pp. 138–141.
Wisshak, M., López Correa, M., Gofas, S., Salas, C., Taviani, M., Jakobsen, J., Freiwald, A., 2009. Shell architecture, element composition, and stable isotope signature of the giant deep-sea oyster *Neopycnodonte zibrowii* sp. n. from the NE Atlantic. Deep-Sea Res. I 66, 374–407.
Zachos, J., Pagani, M., Sloan, L., Thomas, E., Billups, K., 2001a. Trends, rhythms, and aberrations in global climate 65 Ma to present. Science 292. https://doi.org/10.1126/science.1059412, 686-69.
Zachos, J.C., Shackleton, N.J., Revenaugh, J.S., Pälike, H., Flower, B.P., 2001b. Climate response to orbital forcing across the oligocenemiocene boundary. Science 292, 274–278. https://doi.org/10.1126/science.1058288.
Zetter, R., 1998. Palynological investigations from the early Miocene lignite opencast mine Oberdorf (N Voitsberg, Styria, Austria). Jahrb. Geol. Bundesanst. 140, 461–468.
Zibrowius, H., 1980. Les scléractiniaires de la Méditerranée et de l'Atlantique nord-oriental. Mémoires de l'Institut Océanographique, Monaco 11, 284 p.
Plants of the World Online. Facilitated by the Royal Botanic Gardens, Kew. Published on the Internet, 2019–. (Accessed 21 March 2021).